RESEARCH MEMORANDUM

THEORETICAL INVESTIGATION OF THE ATTACK PHASE OF AN AUTOMATIC INTERCEPTOR SYSTEM AT SUPERSONIC SPEEDS WITH PARTICULAR ATTENTION TO AERODYNAMIC AND DYNAMIC REPRESENTATION OF THE INTERCEPTOR

By Windsor L. Sherman and Albert A. Schy

Langley Aeronautical Laboratory
Langley Field, Va.

NATIONAL ADVISORY COMMITTEE FOR AERONAUTICS

WASHINGTON

January 25, 1957

NATIONAL ADVISORY COMMITTEE FOR AERONAUTICS

RESEARCH MEMORANDUM

THEORETICAL INVESTIGATION OF THE ATTACK PHASE OF AN AUTOMATIC INTERCEPTOR SYSTEM AT SUPERSONIC SPEEDS WITH PARTICULAR ATTENTION TO AERODYNAMIC AND DYNAMIC REPRESENTATION OF THE INTERCEPTOR

By Windsor L. Sherman and Albert A. Schy

SUMMARY

This paper presents the results of a theoretical investigation of the attack phase of an automatically controlled interceptor. The specific objectives of this study were to investigate the dynamic representation of the airplane, the flight behavior of the airplane when it is a part of an interceptor system, and the effect of nonlinear aerodynamics on the airplane flight maneuvers. In order to conduct this study, a modern high-speed interceptor, a dynamically perfect radar-controlled director-type guidance system for a lead-collision course and a velocity-type automatic pilot were simulated on a large analog computer. Radar noise and gust effects were neglected. The results are presented as time histories of the airplane and system motions.

The basic flight maneuver encountered is a 5g climbing turn with roll and acceleration commands applied simultaneously. The use of a linear representation for the airplane caused errors in the airplane motion and, in addition, caused large errors to appear in the miss distances. The principal effect of the nonlinear aerodynamics was to change the elevator and aileron motions. Secondary effects appeared in the longitudinal motions and sideslip and yawing velocities.

INTRODUCTION

The concept of automatically controlled interception of hostile aircraft was established when it became apparent that interception missions would have to be carried out in all types of weather and that the operational problems of modern interceptor aircraft were making the performance of the interceptor mission increasingly difficult for the

unassisted pilot. The philosophy of the automatic interceptor weapon system requires that the entire interceptor mission, from take-off through landing, be accomplished under automatic control. Several military contracts for the development of operating interceptor systems have resulted in system stability studies in which the airplane is considered as a linear component of the system. None of the published studies, however, have investigated the effects on system response of the nonlinear dynamic terms and nonlinear aerodynamic forces in the equations of motion of the airplane. The present study is primarily concerned with these effects.

The attack phase was selected for this investigation because violent maneuvers may be required of the airplane. The effects of nonlinear terms in the airplane representation would naturally be most evident for such large motions. The objectives of the investigation were as follows:

(a) To determine if significant errors are introduced in the airplane motions and system response when a linear representation is assumed for an airplane and to determine the simplest set of nonlinear equations that can be used to represent the airplane in the interceptor system herein considered.

(b) To study the effect of nonlinear aerodynamics on the airplane motions and system response.

(c) To study the flight behavior of the airplane during an automatically controlled attack run for a system where gravity corrections are omitted from the roll command.

In order to investigate the attack problem, a target, fire-control radar, fire-control and guidance computer, automatic pilot, and the airplane were simulated. This required the use of a large analog computer, and through the cooperation of the U. S. Navy, the Typhoon Computer at the U. S. Naval Air Development Center, Johnsville, Pa., was made available for this study. The use of this computing facility permitted the simulation of an advanced high-speed interceptor by the six-degree-of-freedom rigid-body equations of motion. In addition, aerodynamics that were nonlinear functions of the angle of attack and linear functions of Mach number were included in the airplane simulation. Radar noise and gust effects were neglected in this study.

The attack run, which starts when the radar locks on the target and ends with the discharge of the interceptor's armament, was made by an interceptor flying at a Mach number of 2.2 against a target that had a Mach number of 1.4. This paper presents a description of the interceptor system assumed, results that illustrate typical interceptor motions, and the effects of changes in the dynamic and aerodynamic representation of

the interceptor on the motions of the airplane during the attack run. A summary of some of the more important results was previously presented in reference 1.

SYMBOLS

a_z	normal acceleration
b	wing span
$\bar{c}$	mean aerodynamic chord
$D = \frac{d}{dt}$	
E_a, E_e	unfiltered azimuth and elevation steering errors
F_X, F_Y, F_Z	forces along interceptor body X-, Y-, and Z-axes
g	acceleration of gravity
I_X, I_Y, I_Z	moments of inertia about X, Y, and Z principal body axes
$K_1 \ldots K_{20}$	constants
L	rolling moment
l_i, m_i, n_i	direction cosines between space axes and airplane principal body axes
M	pitching moment
M_a, M_e	azimuth and elevation miss distances in airplane principal body axes
M*	Mach number
m	mass
N	yawing moment
n	interceptor normal acceleration, g units
n_T	target normal acceleration, g units

p	airplane rolling velocity in principal body axes
q	airplane pitching velocity in principal body axes
q_s	local sonic dynamic pressure
R	range
R_X, R_Y, R_Z	range components in principal body axes
r	airplane yawing velocity in principal body axes
S	wing area
t	time
t_f	time of flight, interceptor
t_g	time to go; time from present to firing point
u	interceptor velocity along X body axis
V_f	interceptor velocity
V_m	missile velocity relative to interceptor
V_s	velocity of sound, free stream
V_T	target velocity
v	interceptor velocity along Y body axis
W	weight
w	interceptor velocity along Z body axis
X,Y,Z	right-hand cartesian coordinate system
α	angle of attack
β	angle of sideslip
γ	flight-path angle

Δ when associated with variable, indicates perturbation in variable

$\delta_a, \delta_e, \delta_r$ aileron, elevator, and rudder deflector angles, respectively

$\epsilon = \sqrt{\epsilon_a^2 + \epsilon_e^2}$

ϵ_a, ϵ_e filtered azimuth and elevation steering errors in body axes

$\hat{\epsilon}_e$ g-limited flight-path command

θ Euler angle (interceptor pitch)

θ_a, θ_e azimuth and elevation radar gimbal angles

ρ air density

τ time of flight of rocket

τ_{fl} filter time constant

τ_{SA} aileron servomotor time constant

τ_{SE} elevator servomotor time constant

τ_{SR} rudder servomotor time constant

Φ Euler angle (interceptor bank)

ψ Euler angle (interceptor yaw)

C_X X-force coefficient, $\frac{2F_X}{\rho S V_f^2}$

C_Y Y-force coefficient, $\frac{2F_Y}{\rho S V_f^2}$

C_Z Z-(normal) force coefficient, $\frac{2F_Z}{\rho S V_f^2}$

C_l rolling-moment coefficient, $\frac{2L}{\rho S V_f^2 b}$

C_m pitching-moment coefficient, $\frac{2M}{\rho S V_f^2 \bar{c}}$

C_n yawing-moment coefficient, $\frac{2N}{\rho S V_f^2 b}$

$C_{X_{\delta_e}} = \frac{\partial C_X}{\partial \delta_e}$

$C_{Y_\beta} = \frac{\partial C_Y}{\partial \beta}$

$C_{Y_{\delta_r}} = \frac{\partial C_Y}{\partial \delta_r}$

$C_{Z_{\delta_e}} = \frac{\partial C_Z}{\partial \delta_e}$

$C_{l_\beta} = \frac{\partial C_l}{\partial \beta}$

$C_{l_{\delta_a}} = \frac{\partial C_l}{\partial \delta_a}$

$C_{l_{\delta_r}} = \frac{\partial C_l}{\partial \delta_r}$

$C_{l_p} = \frac{\partial C_l}{\partial \frac{pb}{2V_f}}$

$C_{l_r} = \frac{\partial C_l}{\partial \frac{rb}{2V_f}}$

$$C_{m_q} = \frac{\partial C_m}{\partial \frac{q\bar{c}}{2V_f}}$$

$$C_{n_\beta} = \frac{\partial C_n}{\partial \beta}$$

$$C_{n_{\delta_r}} = \frac{\partial C_n}{\partial \delta_r}$$

$$C_{n_p} = \frac{\partial C_n}{\partial \frac{pb}{2V_f}}$$

$$C_{n_r} = \frac{\partial C_n}{\partial \frac{rb}{2V_f}}$$

Subscripts:

b	principal body-axes coordinate system
c	command, that is, Φ_c signifies roll command
cr	indicates critical value of variable
i	numerical subscript values 1, 2, 3
l	indicates limiting value of variable
o	indicates initial condition
s	indicates space coordinate system

Dot indicates differentiation with respect to time.

All angles measured in radians unless otherwise stated.

SIMULATION OF THE ATTACK PHASE OF THE AUTOMATIC INTERCEPTOR SYSTEM

This study was made on the Typhoon Computer at the U. S. Naval Air Development Center, Johnsville, Pa. Reference 2 is a detailed description of the Typhoon computer, whereas reference 3 discusses the simulation of this problem and presents a discussion of the interceptor system used. Appendix A of this paper summarizes the equations used to simulate the automatic interceptor attack problem for this study.

Basic Assumptions

The principal assumptions made in setting up this system are as follows:

(a) The dynamics of the radar, computers, and flight data sensing instruments, such as rate gyros, are neglected.

(b) Radar noise and gust effects are neglected.

(c) Rocket ballistics are neglected.

(d) Changes of atmospheric density with altitude are neglected, the value assumed being that for the altitude of the target as given by the NACA standard atmosphere (ref. 4).

(e) The angles α and β are small angles

$$\sin \alpha \approx \alpha \qquad \sin \beta \approx \beta$$

$$\cos \alpha \approx 1 \qquad \cos \beta \approx 1$$

(f) The angle ϵ, the angle between the body reference system and principal axis, was small ($\epsilon = 1.2^{\circ}$) and was assumed zero. Thus, the body reference system was assumed to be coincident with the principal axes.

(g) $V_f = \sqrt{u^2 + v^2 + w^2} \approx \frac{2u}{2 - \alpha^2}$

(h) Control surface servomotors are represented as first-order systems.

Components Simulated

Figure 1 is a generalized block diagram of the interceptor system simulated for this investigation. The components of the system are target, radar, fire-control computer, filters, command computer, autopilot, and airplane. The principal information flow routes have been indicated on the block diagram.

The target.- The target was programmed to fly a straight-line course at an altitude of 50,000 feet. The target Mach number was 1.4, which corresponds to an airspeed of 1,529 feet per second. Provisions were incorporated so that, if desired, the target could make a ±2g vertical plane maneuver that started at radar lock-on.

The radar and fire-control computer.- The radar, which is mounted in the interceptor, tracks the target and supplies range, range rate, antenna gimbal angles, and the angular velocities of the line of sight to the fire-control computer. Since a perfect radar was assumed, the kinematic relations, equations (A1) to (A4) of appendix A, were used to determine the required information. The geometry on which these kinematics were based is presented in figure 2. The fire-control computer was a director-type computer with first-order prediction that solved the equations of a lead collision rocket-firing course for the miss distance parameters $\frac{M_a}{t_g + \tau}$ and $\frac{M_e}{t_g + \tau}$. Equations (A5) of appendix A were used to represent this computer. In deriving these equations it was assumed that the interceptor was armed with unguided rockets. For this study the rocket had an average velocity of 2,000 feet per second relative to the interceptor, and the time of rocket flight was 1.5 seconds.

The command computer.- The miss-distance parameters, which were the output of the fire-control computer, were fed to the command computer. The command computer converts this miss-distance information to autopilot commands. The miss-distance parameters are first converted to steering errors by equations (A6), then filtered and corrected for cross-roll effects by equations (A7). These filtered steering errors are then converted to autopilot commands $\hat{\epsilon}_e$ and ϕ_c by equations (A8) to (A10), where $\hat{\epsilon}_e$ is the normal-acceleration limited flight-path command and ϕ_c is the roll command. Both of these commands are uncompensated for the effects of gravity.

The automatic pilot.- The automatic pilot was composed of two velocity control loops, one for roll and one for the flight path. The roll control system is described in reference 5 and the flight-path control system is described in reference 6. Figures 3 and 4 show the block diagrams of the lateral and flight-path control systems, respectively. The values

of the gains used are presented in appendix A as are the equations that describe figures 3 and 4 for simulation (eqs. (A11) and (A12)).

The roll control automatic pilot was the primary lateral control loop for the interceptor and was not changed during the course of the investigation. Two auxiliary regulators were considered for rudder control. The first was a yaw rate feedback to the rudder for controlling the Dutch roll mode and the second was a $\dot{\beta}$ feedback that, in addition to providing Dutch roll damping, tends to reduce the sideslip during maneuvers.

As indicated in reference 6, a low-gain longitudinal control system was satisfactory for tracking a nonmaneuvering target, whereas a high-gain control system was required to track a maneuvering target. In this study the low- and high-gain flight-path control system were used against nonmaneuvering targets in order to determine how the gain in the flight-path control system affected the airplane response when nonlinear aerodynamics was included in the airplane simulation.

In accordance with assumption (g), all servomotors in the automatic control system were represented by first-order equations, so that $\frac{\delta_o}{\delta_i} = \frac{1}{1 + \tau_S D}$ with $\tau_S = 0.03$ for all servomotors.

The roll control system had an acceleration feedback of $\dot{p}$. This feedback was included to alleviate control-surface rate-limiting oscillations and is discussed in detail in reference 5.

Appendix B presents the modifications in the airplane effective damping and inertia characteristics introduced by the automatic pilot.

The airplane.- The airplane was represented by the six-degree-of-freedom rigid-body equations of motion referenced to principal body axes (see eqs. (A13)). The terms in the brackets are the nonlinear cross-product terms normally neglected in the linear analysis of small motions. These terms were programmed so that they could be deleted from the equations in order to study the effects introduced by representing the airplane by linear equations. The interceptor was assumed to be in trimmed straight and level flight at a Mach number of 2.2, $V_f = 2{,}136$ feet per second, at radar lock-on. This flight condition determined the initial conditions for the equations of motion and the direction cosine computation. The direction cosines are functions of the airplane angular velocities and were computed by equations (A14). The direction cosines were used to obtain the correct distribution of gravity forces in the airplane equations and in the radar simulation for the coordinate transformation between space axes and interceptor body axes.

The right-hand sides of the equations of motions (eqs. (A13)) are the forces and moments acting on the airplane. Equations (A15) and (A16) are the control-surface forces and moments, and equations (A17) and (A18) are the other aerodynamic forces and moments. The parameters α, angle of attack, β, angle of sideslip, and M*, Mach number, required in the computation of the forces and moments were computed by equations (A19). All stability derivatives were functions of Mach number. The pitching-moment coefficient C_m and the stability derivatives C_{l_β}, C_{n_β}, C_{l_p}, and C_{n_p} were nonlinear functions of the angle of attack in addition to being functions of Mach number. The stability derivatives were computed by equations (A20) and (A21), using servo multipliers.

The analog for the airplane was prepared so that any of the following forms of the stability derivatives could be used:

(a) constant derivatives

(b) derivatives that vary with Mach number

(c) derivatives that vary nonlinearly with angle of attack

(d) derivatives that vary with Mach number and nonlinearly with angle of attack.

The nonlinear angle-of-attack variations in C_m, C_{l_β}, C_{l_p}, C_{n_β}, and C_{n_p} could be added to the problem singly or in any combination. As the estimates of the stability derivatives showed that $C_{m_{\dot{\alpha}}}$ was very small and, when compared with C_{m_q} and C_{m_α}, would have practically no influence on the pitching-moment equation, it was omitted from the simulation. In the case of $C_{Y_{\dot{\beta}}}$, $C_{l_{\dot{\beta}}}$, and $C_{n_{\dot{\beta}}}$, no estimates or wind-tunnel results were available; therefore, these stability derivatives were neglected. Aerodynamic cross-coupling terms such as C_{m_β} were omitted from the simulation.

Initial Conditions

Five initial conditions were used in this study. (See fig. 5(a).) Of these five initial conditions, two (I and II) were bow attacks and three (III, IV, and V) were beam attacks. All of these initial conditions except V result in forward hemisphere attacks on the target. In initial condition V the interceptor starts as a beam attack that degenerates into a tail chase that came in 30° off the tail of the target. Figure 5(a)

presents a sketch which shows the variables that define the initial conditions. The specific values of these parameters are given in the table of figure 5(a). Figure 5(b) is presented to clarify the lock-on orientation of the target and interceptor for each initial condition. This figure shows the lock-on condition as it would be seen by an observer in an airplane that is above and on the right rear quarter of the target.

In these attack runs it was assumed that the radar had been tracking the target long enough so that the fire-control computer had completely charged the filters before commands were fed to the automatic pilot. This was accomplished by putting the following initial condition on the filter:

$$\left.\begin{aligned} \epsilon_a(0) &= E_a(0) \qquad \dot{\epsilon}_a(0) = 0 \\ \epsilon_e(0) &= E_e(0) \qquad \dot{\epsilon}_e(0) = 0 \end{aligned}\right\} \tag{1}$$

Because many combinations of autopilots, equations of motion, and aerodynamics were used, the different basic system configurations have been defined in table I. All configurations used will be referred to by the numbers given in table I. When nonlinear cross-product terms and aerodynamics that vary nonlinearly with α are used, it will be stated, together with the configuration number to which the addition applies.

RESULTS AND DISCUSSION

All data-gathering runs were made with the target and guidance equipment included as part of the closed-loop system. Time histories of the airplane and fire-control variables were recorded from the time of radar lock-on to the firing time, $t_g = 0$.

Variables Used in the Analysis of Results

Before discussing the results of this study, a brief discussion of some of the variables used in the analysis is in order.

The direction cosines, which relate the interceptor body axes to space axes, determine the interceptor angular orientation. The direction cosines may be computed in two ways: by integrating the angular velocities of the interceptor as was done in this study (eqs. (A14)) or as trigonometric functions of the Euler angles (ref. 7). When the latter method is used and the rotational order of the Euler angles is ψ, θ, Φ, the direction cosines l_Z, m_Z, and n_Z, which relate the space Z-axis and the interceptor body axes, are given by

$$\left.\begin{aligned} l_3 &= -\sin\theta \\ m_3 &= \cos\theta \sin\Phi \\ n_3 &= \cos\theta \cos\Phi \end{aligned}\right\} \qquad (2)$$

Thus, the direction cosine l_3 is always indicative of the pitch angle and for small values of θ, m_3 and n_3 are indicative of the bank angle. However, n_3 is considered more useful than m_3 as it is a cosine function and runs from +1 to -1 when the airplane rolls over onto its back.

In addition to the direction cosines, the miss distances (eqs. (A2) to (A5)) or steering errors (eqs. (A6) and (A7)) are useful in analyzing the records. The miss distances are functions of the airplane motions and indicate, as a first approximation, the manner in which the interceptor is maneuvering with respect to the target. Sometimes it is more convenient to use the steering errors, which are the miss distances divided by future range, to get a first approximation of the interceptor motion relative to the target.

The usual airplane parameters u, v, w, p, q, and r and the control surface deflections δ_a, δ_e, and δ_r were also used to analyze the results.

Basic Interceptor Flight Behavior With Linear Aerodynamics

Flight maneuvers for various initial conditions.- Figures 6 and 7 present the data obtained with basic configuration 1 for each initial condition. In these runs the airplane was represented by the complete six-degree-of-freedom equations of motion and linear aerodynamics. The low-gain longitudinal control was used. The direction cosines l_3 and n_3, the normal acceleration n, and the steering errors, ϵ_a and ϵ_e, are shown in figure 6 and the linear and angular velocity time histories of the airplane are presented in figure 7. As the attack run always starts below the target, a climbing turn to the firing point is indicated. Figure 6 shows such a maneuver in which the interceptor had a normal acceleration of 5g. In this case the normal acceleration and rolling commands were applied simultaneously. The major differences were the length of time the normal acceleration is applied, which depends on ϵ_e, and the magnitude of the initial roll angle (see n_3 time history), which depends primarily on the ratio ϵ_a/ϵ_e. As would be expected, the time of flight of the interceptor for each initial condition is different because of the differences in closing rate.

Characteristics of the motion.- In the normal acceleration time histories, the differences in the initial slopes are caused by differences in the magnitude of the initial ϵ_e. The abrupt changes in slope that occur during the first 2 seconds of the normal acceleration records are caused by the g-limiter operation and rate-limiting effects in the longitudinal control system. As would be expected, these effects are clearly defined in the w and q time histories. In the case of q, for initial conditions II, IV, and V, the initial oscillations are particularly violent because of the large initial ϵ_e value.

When the interceptor has settled down to tracking, an oscillation occurs which is primarily evident in the p, v, and r records shown in figure 7 and the n_z record in figure 6. It was realized beforehand that some such oscillation was bound to occur because of the neglect of gravity in the roll command, since the neglect of gravity corresponds to commanding an uncoordinated maneuver. Consequently, when the interceptor banks it tends to drop off, that is, develop a lateral acceleration along the direction of the dipped wing. This lateral acceleration causes the interceptor to have a lateral velocity when ϵ_a approaches zero of such a sign as to cause the interceptor to "swoop" through the $\epsilon_a = 0$ position. The interceptor then tends to reverse its bank to counteract the overshoot in ϵ_a, and some sort of oscillation may be expected to result in the final stages of the motion, involving primarily p, v, and r. Because of the gravity drop-off during the uncoordinated maneuver, the interceptor tends to come at the target from below, so that the final oscillation tends to be about the zero-bank condition. It may perhaps be roughly visualized as comparable to the swinging of a pendulum under the influence of gravity.

A number of things may have a considerable effect on this oscillation, such as: various methods of including gravity in the roll command, any parameters affecting the lateral accelerations while the airplane is rolling, the fact that the roll command tends to become indeterminate when both ϵ_a and ϵ_e approach zero, and the fact that the resolvers used in the simulator may tend to hunt when the roll command becomes indeterminate. In the present investigation there was not sufficient time available to evaluate the parameters affecting this oscillation. However, during the investigation of the effects of the nonlinear dynamic terms in the equations of motion of the airplane, it was found that the $p \Delta w$ term, which has an important effect on the lateral acceleration while rolling, also very strongly affects the final "swooping" oscillation. This phenomenon will be more fully discussed in a later section.

A comparison of the data in figure 6 for each initial condition indicates that a qualitative similarity exists between initial conditions I and III and between initial conditions II, IV, and V. The time

histories of the airplane motion in figure 7 show that this similarity carries over to the airplane motions. Thus, two basic types of motion occurred, one where large changes in roll angles and small changes in flight-path angles were required to reduce the errors to zero (initial conditions I and III), and one where small changes in roll angles and large changes in flight-path angles were required to reduce the errors to zero (initial conditions II, IV, and V). Because of this qualitative similarity, results presented in the following sections will be for two initial conditions, one for each basic type of motion.

Comparison of yaw and sideslip dampers.- In the motions presented in figure 7, basic configuration 1 was used; thus, the yaw damper controlled the rudder. The basic configuration was changed to configuration 2 which replaced the yaw damper with the sideslip damper. Figure 8 compares the v, r, and p motions of the airplane for these two rudder controls. The $\dot{\beta}$ rudder control held the sideslip velocity to zero, except for a small excursion at the beginning of the run. The rolling velocity time history shows that p was not greatly affected by the change in rudder control. The yawing velocity is completely changed. The $\dot{\beta}$ rudder control yaws the airplane into the relative wind and in so doing maintains almost zero sideslip. The adverse yaw at the beginning of the run was eliminated and the peak yawing velocity almost doubled. The shape of yawing velocity time history when the sideslip damper was used resembled the shape of the sideslip time history obtained with the yaw damper.

It is interesting to note that the change in rudder control had no effect on the terminal miss distances.

Effects of Variable Aerodynamics

Variable aerodynamics used.- As indicated in the section entitled "Components Simulated," the airplane stability derivatives were analoged to take into account variations with Mach number and angle of attack. The variation of the stability derivatives with Mach number was linear with the exception of C_{n_p} which was quadratic. Equations (A20) and (A21) describe the variation of the stability derivatives. The variations with α occur in C_X, C_m, C_{l_β}, C_{n_β}, and C_{n_p}. The angle-of-attack variation in C_X is caused by the usual change in induced drag with lift coefficient.

In the case of C_{l_β}, a linear variation with angle of attack was included at all times in the basic C_{l_β}. This variation with angle of attack is a wing contribution. The nonlinear angle-of-attack variation

in C_{l_β} and the other stability derivatives are representative nonlinear variations of the stability parameters obtained from wind-tunnel tests of several configurations. The variations shown are not specifically for the configuration considered herein. Equations (A21) show the form used to include these derivatives in the simulation. Since the nonlinearities do not start at $\alpha = 0$, they were made functions of $\alpha - \alpha_{cr}$ where α_{cr} is the angle of attack at which the nonlinearity starts. Provisions were made so that α_{cr} could be varied. Figures 9(a) to 9(d) show the nonlinear variations employed for C_m, C_{n_β}, C_{l_β}, and C_{n_p} for two different Mach numbers and $\alpha_{cr} = 3^\circ$ and 6°. Two forms of nonlinearity in C_{l_p} were studied, a destabilizing one (fig. 9(e)) and a stabilizing one (fig. 9(f)).

In order to define more clearly the effects of the nonlinear pitching moment, the time histories presented in this section are for basic configuration 4, which uses the high-gain longitudinal control system. As the previously presented time histories are for the airplane with the low-gain longitudinal control system, it is necessary to present data for basic configuration 4 with constant aerodynamics to establish a standard so that the effect of the nonlinear pitching moment may be shown.

Figure 10(a) (solid curves) presents the response of the airplane for basic configuration 4 with constant aerodynamics, initial condition III. This record was cut off when α dropped below 3°, which corresponds to a time of 7 seconds. The addition of the nonlinear C_m, $\alpha_{cr} = 6^\circ$, to the simulation caused the airplane response to become unstable. (See dashed lines in fig. 10(a).) Because of this unstable condition, α_{cr} is meaningless for this run and the time testing was cut off at 7 seconds. The saw-tooth character of the δ_e motion indicates that the instability is caused by a rate-limiting oscillation of the control surface.

This same type of oscillation was encountered in the development of the roll control system and is discussed in reference 5. Two methods by which the rate-limiting oscillation may be alleviated are to reduce the control surface deflection limit or add a $\dot{q}$ feedback to the control system. Of these two, the $\dot{q}$ feedback is more effective and is preferred; however, it was somewhat more difficult to incorporate in the analog than a change of control-surface-deflection limit. Therefore, the latter was used in this study.

Figure 10(b) compares n, q, and δ_e for the 10° δ_e limit with and without the nonlinear C_m, $\alpha_{cr} = 6^\circ$. An examination of the case

of linear C_m shows that, when the δ_e limit is reduced, the ability of the airplane to develop normal acceleration is restricted and the average normal acceleration is now about 4g with an overshoot to about $5\frac{1}{2}$g on the initial transient. The control surface is now against the limit stops for about 8 seconds with a break at 1 second when the g-limiter kicked δ_e off the stop to limit normal acceleration. Because δ_e is now on the stop, the elevator is no longer available for damping. Thus, during the first 8 seconds an oscillation at the frequency of the airplane short-period longitudinal oscillation develops. The addition of the nonlinear C_m, which causes the airplane to become less stable as the angle of attack increases and corresponds to decreasing the static margin or increasing n/δ_e, introduces changes in the longitudinal response. The nonlinear C_m introduces a pitch-up, the effects of which are sensed by the autopilot, and less control motion is required to obtain the desired normal acceleration. The elevator is now off the stop after the first three-fourths of a second and is able to damp the airplane short-period longitudinal oscillations. An examination of the normal acceleration presented in figure 10(b) shows that, with the nonlinear C_m, a higher average value of normal acceleration is attained. This causes the duration of the airplane normal acceleration to decrease. This higher normal acceleration was caused by the fact that the g-limiter operation depends on the n/δ_e response of the airplane for the high-gain control system and was not changed to account for the increasing n/δ_e introduced by the nonlinear C_m.

Results similar to the foregoing were obtained for all initial conditions with $\alpha_{cr} = 3^\circ$ or 6°. Figure 11 compares the longitudinal airplane response for the nonlinear pitching moment with $\alpha_{cr} = 3^\circ$ and 6°. When the nonlinearity was strong $(\alpha_{cr} = 3^\circ)$, the normal acceleration rose to higher values and the control surface displacement actually went to zero while the airplane was pulling maximum normal acceleration, because of the strong pitch-up characteristic. These same characteristics appear in the motions for $\alpha_{cr} = 6^\circ$ but the control-surface deflection never reaches zero when the nonlinear C_m is effective. When the low-gain longitudinal control system was used, both values of α_{cr} gave results that paralleled those for the high-gain longitudinal control system. However, the effects were much less pronounced and initial conditions I and III were stable for $\delta_{e_l} = 20^\circ$. This occurred because the rate-limiting oscillation was more stable for the low-gain control system.

As pointed out in the foregoing discussion, the principal effect of the nonlinear pitching moment was to change the elevator motion in a manner that gives the desired command response. Because of the low time lags associated with the sensing instruments in the automatic control system, changes in the airplane motion, primarily the normal acceleration, are rapidly sensed and corrective signals generated. The high performance servomotors are able to move the control surface rapidly enough to compensate for these changes and maintain the desired response.

Effect of nonlinear variations in the lateral stability derivatives.- The lateral stability derivatives, C_{l_β}, C_{n_β}, C_{l_p}, and C_{n_p}, which contained nonlinearities that were functions of the angle of attack, failed to change the lateral response of the airplanes except when the addition included the C_{n_β} nonlinearity with $\alpha_{cr} = 3^\circ$. The C_{n_β} nonlinearity, like the other lateral nonlinearities, did not change the rolling velocity response; however, the loss in directional stability caused the changes in the yawing and sideslip velocities shown in figure 12(a). The lack of change in the rolling velocity response is not surprising, as the guidance commands are calling for a specific rolling velocity and the changes introduced in the airplane response by the nonlinearities are picked up by the sensing instruments and a different control motion is ordered, taking into account these changes, that gives the commanded response. The changes introduced in the aileron response for nonlinear C_{n_β}, C_{l_β}, and destabilizing C_{l_p} are shown in figures 12(b) to 12(d). The other lateral nonlinearities produced no significant change in the aileron motion. The control motions for group additions of these various derivatives followed the trends indicated by the individual derivatives.

Increasing α_{cr} to 6° or a change to the low-gain flight-path control system greatly minimized the effect of the nonlinearities in the lateral stability derivatives on the airplane and aileron motions.

Effects of combined lateral and longitudinal nonlinear aerodynamics.- Figure 13 presents the response of the airplane with all nonlinear aerodynamics included in the simulation for $\alpha_{cr} = 3^\circ$ and 6°. The attack run is defined by initial condition III and the simulation set up by basic configuration 4. Changing α_{cr} from 3° to 6° largely eliminates the effect of the nonlinear lateral stability derivatives. However, the nonlinear C_m still produces a considerable effect. A comparison of the normal-acceleration curves presented in figures 11 and 13 for $\alpha_{cr} = 3^\circ$ shows that the combined lateral and longitudinal nonlinear stability derivatives, principally C_{n_β} and C_m, affect the airplane longitudinal motions to a greater extent than the nonlinear C_m alone.

The most significant differences are the negative normal acceleration developed in the combined case at approximately 6 seconds and the more oscillatory characteristics of the normal acceleration from 6 seconds to the end of the run. When $\alpha_{cr} = 6^{\circ}$ the nonlinearity is less extreme and the coupling of C_m and C_{n_β} nonlinearities is not as evident.

A comparison of the sideslip velocities shown in figures 13(b), all nonlinearities, and 12(a), lateral nonlinearities, for $\alpha_{cr} = 3^{\circ}$ shows that the nonlinearity in C_m affects the lateral response. The difference between the solid and dashed curves of figure 12(a) is caused by the nonlinearity in C_{n_β}. A comparison of the dashed curve of figure 11(a) with the solid curve in figure 12(b) shows that, when the nonlinear C_m is present, large values of v are maintained longer. For example, at 3.75 seconds, $v = 190$ feet per second for the nonlinear C_{n_β} alone, whereas it is 300 feet per second where the nonlinear C_m is present in combination with the nonlinear C_{n_β}. Similar effects are produced in the yawing velocity. (Compare figs. 11(a) and 12(c) for $\alpha_{cr} = 3^{\circ}$.)

These changes in v and r are caused by the fact that the nonlinear C_m produces larger values of normal acceleration (about 8g compared with 5g when C_m is linear) and the larger values of α make the C_{n_β} nonlinearity more pronounced.

Had the command g-limiter taken into account the changes in n/δ_e of the airplane with the changing C_m, no changes in v and r would have been noted as the normal acceleration and, consequently, the angle of attack would have been the same for the linear and nonlinear pitching moments. These data are discussed as they show some of the problems associated with a command g-limiter when the form of the nonlinearity in C_m is not precisely known.

Significance of nonlinear aerodynamic effects.- The primary result was that the guidance and control system was able to adjust itself to extreme variations in the aerodynamic characteristics of the interceptor and still cause it to perform the desired maneuvers and correct the lock-on guidance errors. The effects of loss of static longitudinal and directional stability (represented by the C_m and C_{n_β} nonlinearities) might have been more troublesome, however, had random external disturbances such as noise and gusts been considered. Unfortunately, lack of time available on the analog computer made it necessary to eliminate the investigation of random disturbance effects.

Moreover, even for the command response of the system there were significant secondary effects of the nonlinear aerodynamics on the control-system dynamics. For example, the nonlinearities had a considerable effect on the occurrence of rate-limiting oscillations in the control systems and on the operation of the command-type g-limiter assumed. Therefore, it is necessary to include nonlinear aerodynamic effects in simulating the command response of the automatic interceptor.

The Dynamic Representation of the Interceptor

Comparison of the complete and linear representations of the airplane.- The six-degree-of-freedom rigid body equations of motion, which will be referred to as complete equations, are:

$$\left.\begin{aligned}
&m(\dot{u} + qw_o) + \left\{m\left[q(\Delta w) - rv\right]\right\} = Wl_3 + F_X \\
&m(\dot{v} + ru_o - pw_o) + \left\{m\left[r(\Delta u) - p(\Delta w)\right]\right\} = Wm_3 + F_Y \\
&m(\dot{w} - qu_o) + \left\{m\left[pv - q(\Delta u)\right]\right\} = Wn_3 + F_Z \\
&I_X\dot{p} + \left[\left(I_Z - I_Y\right)qr\right] = L \\
&I_Y\dot{q} + \left[\left(I_X - I_Z\right)pr\right] = M \\
&I_Z\dot{r} + \left[\left(I_Y - I_X\right)pq\right] = N
\end{aligned}\right\} \qquad (3)$$

The linear equations used in this study were obtained by deleting the terms in brackets from the complete equations.

As the complete equations accurately define rigid airplane motions and during its flight the rigid airplane actually solves the complete equations, differences between the interceptor motions for the complete and linear equations must be regarded as errors introduced by the use of a linear representation of the airplane.

Figure 14 shows the motion of the center of gravity of the interceptor and the bank angle for basic configurations 1 (complete equations) and 6 (linear equations). The first 3.5 seconds of an attack run defined by initial condition I are presented. In both cases the interceptor starts to bank toward the target, which is above and to the left of the $t = 0$ position of the interceptor. When complete equations are used to represent the airplane, the initial center-of-gravity motion is just what would be expected. It starts with a fall-off to the left due to gravity, but as normal acceleration develops the interceptor pulls upward to the left at the target. However, when linear equations are used to represent the airplane, the center of gravity moves to the right and swoops violently upward as the airplane banks, before it starts to move left toward

the target. Thus, the use of a linear representation of the airplane introduces large errors in the center-of-gravity motion during the initial bank and considerable errors in the bank angle.

These differences in the motion indicate that large forces exist in the linear case that do not exist when the complete equations are used. These forces can be considered as spurious forces which are introduced because of the neglect of the nonlinear inertial terms enclosed in brackets in equations (3). Moreover, the initial upward swoop of the center of gravity caused by these apparent forces can be expected to greatly aggravate the previously discussed swooping oscillations, which occur in the later part of the attack run. An analysis of the cross-product terms which are neglected in the linear equations indicates that $p(\Delta w)$, pv, $q(\Delta w)$ are the important terms in the force equations, whereas pq and pr appear to be the important terms in the moment equations. Of these terms the lateral acceleration term $p(\Delta w)$ and the normal acceleration term pv would have a direct effect on the initial center-of-gravity motion shown in figure 14. The significance of these apparent or spurious forces can most easily be seen in the following manner.

Consider the side-force equation, from equations (3), which is

$$m(\dot{v} + ru_o - pw_o) + m\left[r(\Delta u) - p(\Delta w)\right] = Wm_3 + F_Y$$

and correctly states the side or Y-forces acting on a rigid body. When this equation is linearized under the assumption of small velocities and displacements the following equation results:

$$m(\dot{v} + ru_o - pw_o) = Wm_3 + F_Y$$

and correctly states the Y-forces acting on the rigid body when the assumptions of linearization are not violated. However, if the parameters that are multiplied to give the neglected terms become large, and the magnitude of the neglected terms approaches or exceeds the magnitude of the retained terms, the linear equation is no longer a true statement of the Y-forces acting on the rigid body and the spurious or apparent forces occur. The nature of these spurious forces can be determined by changing the details of the method of linearization. Instead of deleting the cross-product terms, the linearization may also be accomplished by adding a force F_Y' to the right-hand side of the general side-force equation that at all times is exactly equal to $m(r\,\Delta u - p(\Delta w))$. Thus $F_Y' = m(r\,\Delta u - p(\Delta w))$ is the spurious force that occurs in the linear equation.

In order to obtain some insight as to the magnitude of the terms being neglected when the cross products are deleted from the complete

equations $p(\Delta w)$, pv, pq, pr, and $q(\Delta w)$ were computed and are presented in figure 15. As can be seen, very large forces are neglected at the beginning of the attack run. Because of the interaction of these terms, that is, $p(\Delta w)$ affects w through pv which in turn affects v through $p(\Delta w)$, the magnitudes of the cross-product terms under consideration for the complete equations are not the same as when linear equations are used. The cross-product terms which exactly represent the spurious forces in the linear case were computed and are presented in figure 15. The most significant difference with regard to the incorrect initial center-of-gravity motion is that in the actual linearized run the $p(\Delta w)$ term is considerably larger than the pv term. Therefore, the $p(\Delta w)$ term appears to be of primary importance in accounting for the difficulties caused by the linear representation of the airplane.

The interceptor system was next run on the simulator with the linear equations representing the airplane with the cross-product terms $p(\Delta w)$, pv, pq, pr, and $q(\Delta w)$ added in a systematic manner so as to determine their effect on the system and airplane responses. In addition, the effect of the other nonlinear terms was also checked during this part of the investigation. Figure 16 presents the corrections made by various cross-product terms to airplane motions, for initial condition I. A comparison of figure 7(a) with figure 16 shows that the terms $p(\Delta w)$, pv, and pq definitely corrected errors in the airplane motion, and when these three cross-product terms are included the resulting airplane response is almost the same as it is for the complete equations. Inclusion of the $p(\Delta w)$ term alone was sufficient to eliminate the gross errors, thus confirming its relative importance as shown in figure 15. The term $q(\Delta w)$ contributed a small but detectable loss in forward speed that was considered unimportant. All other cross-product terms had little effect on the airplane motion.

Figure 17 is included to show the effect of the nonlinear cross-product terms on the steering errors normal acceleration and direction cosine n_z. There are considerable differences in these parameters during the attack run for the two representations of the airplane. At the firing time, $t_g = 0$, a small azimuth error and large elevation errors exist for the linear representation, whereas both steering errors are almost zero when the complete equations represent the airplane. The steering errors that exist at $t_g = 0$ for the linear airplane correspond to predicted terminal miss distances of 300 feet in azimuth and 500 feet in elevation.

When the linear representation is used, the steering error in the latter part of the run remains relatively constant even though, as shown in figure 17(b), the airplane is pulling considerably more than 1g during this part of the motion. Therefore, the aerodynamic load on the airplane

is apparently working against the spurious forces. In fact, a rough check of the average g-increment in the last 5 seconds showed that it was indeed very close to the average magnitude of the $p(\Delta w)$ and pv values during this time.

So far, the dynamic representation of the interceptor has been discussed for the case of high rolling velocities, which corresponds to initial conditions I and III. In initial conditions II, IV, and V, the rolling velocity is much lower and since the important cross-coupling effects are functions of the rolling velocity one would expect different results for these initial conditions. An attack run for initial condition IV, which is a beam attack, will be used to illustrate the effect of reduced roll velocity on the dynamic representation of the interceptor. In this initial condition the maximum roll rate is 1.4 radians per second, compared with 3.5 radians per second for initial condition I. Figures 18(a) and 18(b) present the normal acceleration n, the direction cosine n_3, and the steering errors ϵ_a and ϵ_e, and figures 18(c) and 18(d) compare the linear and angular motions for the complete and linear representations of the airplane when the attack run is defined by initial condition IV. Basic configuration 1 defines the simulator setup for the complete equations and configuration 6 does the same for the linear equations. These time histories show that the roll cross-coupling effects are still present but the scale of the effect is greatly reduced. This is because the low rolling velocity causes the accelerations $p(\Delta w)$, pv, and pq to have much smaller magnitudes and consequently the errors introduced by the omission of these terms is much smaller. In this attack run the increased loss in forward speed and increased Δw, compared with initial condition I (see figs. 7(a) and 7(d)), cause an increase in the importance of two cross-product terms in the airplane motions. These terms are $q(\Delta w)$ in the X-force equation and $q(\Delta u)$ in the Z-force equation. The $q(\Delta w)$ term causes the velocity to fall off more rapidly and changes the shape of the Δu curve (fig. 18(c)). The effect of $q(\Delta u)$ is to change the normal acceleration and w velocity over the midportion of the attack run. Figure 19 shows the effect of this term. These same effects were noted in initial conditions IV and V; however, in initial conditions I and III, the $q(\Delta u)$ term has negligible effect.

The effects of the cross-product terms on the airplane motion apply to all initial conditions. However, in initial condition V, the beam attack that degenerates into a tail chase, the final miss distances were small for both the linear and nonlinear representations of the airplane dynamics. It is felt that the combination of low rolling velocity, which reduces the coupling, and the long time of flight from lock-on to the firing point may be important factors in the difference in system effectiveness between initial condition V and the other initial conditions.

Effect of dynamic representation on control systems.- An important interaction between the airplane and control system was found during this study. When the rate limit on control-surface deflection was reduced from 100° per second to 50° per second with basic configuration 6 (linear equations) a rate-limiting oscillation occurred which caused the airplane to become unstable. For a similar reduction in the rate limit for basic configuration 1 (complete equations) the oscillation was greatly reduced and consequently the instability did not occur. The elevator and pitching velocities time histories for these two basic configurations are shown in figure 20. The important cross-product terms in this case were, as before, $p(\Delta w)$, pv, and pq. However, the pv and pq terms are now of almost the same importance as the $p(\Delta w)$ term.

The use of the $\dot{\beta}$ rudder control and/or the use of variable aerodynamics did not change the results for the dynamic representation of the airplane. When nonlinear aerodynamics were included in the simulation, there was a definite tendency for rate-limiting oscillations to develop at $\delta_{e_l} = 100°$ per second. Thus, as previously pointed out in the rate-limiting study, the pv and pq terms assume greater importance than in the case of linear aerodynamics.

Effects of Target Maneuvers

A series of runs were made with a maneuvering target to determine the effect of target maneuver on the results pertaining to nonlinear aerodynamics and the dynamic representation of the airplane. In this study the target performed a ±2g vertical-plane maneuver. The target maneuver did not qualitatively change the results obtained for variable aerodynamics and the dynamic representation of the airplane with a straight-line target.

CONCLUDING REMARKS

The basic flight maneuver of the interceptor was a 5g climbing turn towards the target. In this maneuver, the pitch and roll commands were applied simultaneously. These attack-run results indicate that an automatic interceptor system that omits gravity corrections from the roll command can be made practical from a stability and control point of view, particularly if there is no overshoot in the longitudinal response, as was the case in the low-gain longitudinal control system. However, the large rolling motions in the final portion of the attack runs might present serious difficulties in connection with pilot comfort and radar tracking. More study is needed of the relationships between the command computer, automatic pilot, and guidance system.

When considered separately, the nonlinearities in the stability derivatives, except in the case of the nonlinear yawing moment due to sideslip C_{n_β} produced no gross changes in the airplane motions. However, the control-surface motion required to produce the commanded response was considerably altered by pitching-moment coefficient C_m, C_{n_β}, rolling moment due to sideslip C_{l_β}, and damping-in-roll parameter C_{l_p} to a lesser extent. In the case of nonlinear C_{n_β} large changes occurred in the yawing and sideslip velocities, in addition to the changes introduced in the aileron motion. The combined nonlinearities in C_m and C_{n_β} showed definite coupling characteristics. Radar noise and atmospheric turbulence could have considerable effect on the airplane response when nonlinear aerodynamics are present. There is need for more research on this problem.

The sideslip-angle rate rudder control proved effective in controlling the sideslip velocities encountered when linear aerodynamics was used in the simulation. The higher sideslip velocities introduced by the nonlinear C_{n_β} were also reduced by the sideslip damper.

The study of the dynamic representation of the airplane showed that errors in airplane motion are introduced when a linear representation of the airplane is assumed. The addition of the cross-product terms $p(\Delta w)$, pv, pq, and pr to the linear equations corrected these errors. Of these, the $p(\Delta w)$ term was most important. When the magnitude and time of application of normal acceleration increased, the cross-product terms $q(\Delta u)$ and $q(\Delta w)$ became more important, indicating that for a maneuvering target these terms may become important.

A vertical-plane target maneuver of $\pm 2g$ did not change the results for variable aerodynamics and the dynamic representation of the airplane obtained with a straight-line target.

The results presented in this report are for one type of automatic interceptor system and are limited in Mach number and initial condition. Thus, these results are of limited generality, and extensions to airplanes in other interceptor systems should be made with caution.

Langley Aeronautical Laboratory,
National Advisory Committee for Aeronautics,
Langley Field, Va., September 25, 1956.

APPENDIX A

DISCUSSION OF THE ATTACK PHASE OF THE AUTOMATIC INTERCEPTOR SYSTEM SIMULATED ON THE TYPHOON COMPUTER

Reference 8 is a comprehensive review of the airborne fire-control problem. The general theories of airborne fire control are developed in this reference. This appendix is limited to a discussion of the specific interceptor system set up for the Typhoon computer.

Figure 21 is a detailed block diagram for the simulation of this interceptor system. Information and information flow routes and the relationship of the equations to each other and as part of the interceptor system are indicated by this diagram. The numbers within the blocks refer to equations in this appendix.

The target (figs. 1 and 2) was programmed to fly a straight-line course at an altitude of 50,000 feet or perform a ±2g vertical-plane maneuver that starts at the same altitude. When the maneuver was used, it was started at radar lock-on. The target flight was along the earth Y-axis in a positive direction or confined to the YZ-earth plane during the maneuver. The following equations were used to simulate the target:

$$\left(\overrightarrow{V_T}\right)_{PA} = \left[\left(\overrightarrow{V_T}\right)_{EA}\right]\left[T - l\right] \tag{A1}$$

where

$$T - l = \begin{bmatrix} l_1 & l_2 & l_3 \\ m_1 & m_2 & m_3 \\ n_1 & n_2 & n_3 \end{bmatrix}$$

$$V_T = \overrightarrow{i}\,(0) + \overrightarrow{j}\,V_T \cos \dot{\gamma}_T t - \overrightarrow{k}\,V_T \sin \dot{\gamma}_T t$$

and

$$\dot{\gamma}_T = \frac{n_T \overrightarrow{g}}{V_T}$$

where

$n_T = 0$ for a nonmaneuvering target

$n_T = +1$ or $+2$ for an upward-maneuvering target

$n_T = -1$ or -2 for a downward-maneuvering target

The coordinate transformation T - 1 as indicated consists of the direction cosine matrix, the direction cosines being obtained from equation (A14). Equation (A1) converts the target velocities from earth axes to the interceptor principal body axes. In this problem V_T was a constant.

The radar was assumed to be dynamically perfect and therefore could be simulated by using the geometry and kinematic relations between the interceptor and target. The range rate is given by

$$\left.\begin{aligned} \dot{R}_X &= V_{T_1} - u \\ \dot{R}_Y &= V_{T_2} - v \\ \dot{R}_Z &= V_{T_3} - w \end{aligned}\right\} \tag{A2}$$

where u, v, and w are the components of the interceptor velocity vector in principal body axes. Then the components of R are given by

$$\left.\begin{aligned} R_X &= R_{X_o} + \int_0^t \left(\dot{R}_X - qR_Z + rR_Y\right)dt \\ R_Y &= R_{Y_o} + \int_0^t \left(\dot{R}_Y - rR_X + pR_Z\right)dt \\ R_Z &= R_{Z_o} + \int_0^t \left(\dot{R}_Z - pR_Y + qR_X\right)dt \end{aligned}\right\} \tag{A3}$$

and the radar gimbal angles θ_a, θ_e, and R are given by

$$\left.\begin{aligned} R_X \sin \theta_a - R_Y \cos \theta_a &= 0 \\ R_X \cos \theta_a + R_Y \sin \theta_a &= \sqrt{R_X^2 + R_Y^2} \\ \sqrt{R_X^2 + R_Y^2} \sin \theta_e + R_Z \cos \theta_e &= 0 \\ \sqrt{R_X^2 + R_Y^2} \cos \theta_e - R_Z \sin \theta_e &= R \end{aligned}\right\} \tag{A4}$$

The fire-control computer was assumed a director-type computer, which uses the range and rate information to solve the equations of a lead collision rocket-firing course. In setting up the solution of these equations, it was assumed that no miss existed along the radar line sight, which is equivalent to assuming a two-component miss-distance vector in radar axes. The equations solved by the fire-control computer are

$$\left.\begin{aligned} &\frac{R}{t_g + \tau} + \left[\dot{R}_X - \frac{V_m \tau}{t_g + \tau}\right] \cos \theta_a \cos \theta_e + \\ &\left[\dot{R}_Y - \frac{\beta V_m \tau}{t_g + \tau}\right] \sin \theta_a \cos \theta_e - \left[\dot{R}_Z - \frac{\alpha V_m \tau}{t_g + \tau}\right] \sin \theta_e = 0 \\ &\frac{M_a}{t_g + \tau} = \frac{R_Y}{t_g + \tau} + \left[\dot{R}_Y - \frac{\beta V_m \tau}{t_g + \tau}\right] \\ &\frac{M_e}{t_g + \tau} = \frac{R_Z}{t_g + \tau} + \left[\dot{R}_Z - \frac{\alpha V_m \tau}{t_g + \tau}\right] \end{aligned}\right\} \tag{A5}$$

These equations are written in a mixed axes system. The first equation is written in radar axes and the last two in interceptor axes. This was done so that the output of the guidance computer, $\frac{M_a}{t_g + \tau}$ and $\frac{M_e}{t_g + \tau}$, could be used to compute automatic pilot commands without making a transformation from radar axes to interceptor axes. It should also be noted that these equations were divided by $t_g + \tau$. This was done to improve scale factors and voltages in the computer simulation.

The fire-control-computer output was converted to unfiltered steering errors by the following equations:

$$\left.\begin{aligned} E_a &= \frac{M_a/(t_g + \tau)}{V_f + \frac{V_m\tau}{t_g + \tau}} \\ E_e &= \frac{M_e/(t_g + \tau)}{V_f + \frac{V_m\tau}{t_g + \tau}} \end{aligned}\right\} \tag{A6}$$

These unfiltered steering errors were then passed through the filter and corrected for cross roll. These modified steering errors are given by

$$\left.\begin{aligned} \epsilon_a &= \frac{1}{1 + \tau_{fl}D}(E_a - \tau_{fl}p\epsilon_e) \\ \epsilon_e &= \frac{1}{1 + \tau_{fl}D}(E_e + \tau_{fl}p\epsilon_a) \end{aligned}\right\} \tag{A7}$$

The ϵ_e that comes from equation (A7) is the unlimited vertical flight-path change command. The ϵ_e is passed through a g-limiter that restricts the command to a predetermined level. The equation of the g-limiter is

$$-\epsilon_{e_{min}} < \epsilon_e < \epsilon_{e_{max}} \tag{A8}$$

and the output is identified as $\hat{\epsilon}_e$ which is the limited value of ϵ_e. The minus sign is attached to $\epsilon_{e_{min}}$ because it was computed as a positive number.

The limits used in equation (A8) are independent of the airplane and automatic pilot characteristics when the low-gain flight-path control system is used, whereas the limit is dependent on the airplane and autopilot parameters when the high-gain flight-path control system is used. These normal acceleration limits were computed by the following formulas for the flight-path control system:

For the low-gain system

$$\epsilon_{e_{max}} = \frac{n_L^+ g}{V_F K_4} \qquad \epsilon_{e_{min}} = \frac{n_L^- g}{V_F K_4} \tag{A9a}$$

For the high-gain system

$$\epsilon_{e_{max}} = \frac{n_L^+ g(K_6 + K_{12} + 3.96)}{V_F K_4 K_6} \qquad \epsilon_{e_{min}} = \frac{n_L^- g(K_6 + K_{12} + 3.96)}{V_F K_4 K_6} \tag{A9b}$$

The output of the g-limiter $\hat{\epsilon}_e$ (see eq. (A8)) is the command to the flight-path control system.

The roll command was computed as

$$\phi_c = \tan^{-1} \frac{\epsilon_a}{\epsilon_e} \tag{A10}$$

As the outer feedback loop for this control system is through the radar and computer, the inputs to the automatic pilot, ϵ_e and ϕ_D, are used to command a flight-path angular velocity and rolling velocity.

Gravity was neglected in computing the roll and flight-path commands in this study. This was done because it was one of the objectives of this study to determine if a successful system could be set up neglecting these gravity corrections.

The automatic pilot used in this study is represented by the following equations:

$$\left.\begin{aligned} (1 + \tau_{SE}D)\delta_e &= -\left(K_6 + \frac{K_8}{D}\right)\left(K_4\hat{\epsilon}_e - \dot{\gamma}\right) + K_{12}q + K_{20}\frac{M}{I_2} \\ (1 + \tau_{SA}D)\delta_a &= -K_3\phi_c + K_9 p + K_{10}\frac{L}{I_1} \end{aligned}\right\} \tag{A11}$$

The rudder commands, which were regulatory in nature, were given by

$$\left.\begin{aligned} (1 + \tau_{SR}D)\delta_r &= K_{11}r \\ \text{or} \qquad (1 + \tau_{SR}D)\delta_r &= -K_{11}\dot{\beta} \end{aligned}\right\} \tag{A12}$$

The block diagrams of these control systems are presented in figures 3 and 4.

As indicated in the equations and system constants given at the end of this appendix, the roll control system is characterized by a high forward loop gain, a first-order servo, and a rolling velocity and rolling acceleration feedback. The rolling velocity feedback is for damping and to close the inner loop of the control system. The rolling acceleration feedback is included to relieve rate-limiting oscillations (ref. 3). The flight-path control system has a first-order servo and a $\dot{\gamma}$, flight-path rate, feedback to close the inner control loop and a $\dot{\theta}$, pitching velocity, feedback is included to supply damping. A low-gain system that gives $\frac{\dot{\gamma}}{\epsilon_e} = 0.4$ was used for nonmaneuvering target and a high-gain system with $\frac{\dot{\gamma}}{\epsilon_e} = 1.4$ for the maneuvering target as well as for the case of the nonmaneuvering target. The rudder is controlled by either an r, yaw-rate, or $\dot{\beta}$, sideslip-angle rate, feedback. The yaw-rate feedback is used to damp the Dutch roll mode and is not effective in controlling the sideslip. Therefore, the airplane turn is poorly coordinated when the r feedback is used. The $\dot{\beta}$ feedback provides Dutch roll damping and, in addition, improves the turn coordination.

The servomotors were simulated as first order with a time lag of 0.03 second. Provisions were incorporated in the servomotor analog so that the maximum rate and displacement of the control surface could be limited.

With the high gains used in these control loops, there is a possibility that second-order servomotors might produce an unstable control system for the same conditions that a control system with first-order servomotors would indicate stable conditions. Accordingly, an analysis was made using a second-order servomotor which would have an equivalent time lag of 0.03 second to first order. The damping ratio assumed was 0.35, and the natural frequency was 3.72 cycles per second. The results of this analysis indicated that the rolling velocity and flight-path rate-control systems as used in this interceptor study would be stable with second-order servos.

The use of a flight-path control system is inconsistent with the omission of gravity corrections as the most practical way to measure $\dot{\gamma}$ is $\dot{\gamma} = \frac{1}{V_f}(a_Z - gn_3)$. As originally planned, the longitudinal control system was a $\dot{\theta}$, pitching-velocity, control system. The $\dot{\gamma}$ control system was substituted for the $\dot{\theta}$ control system when the vertical-plane studies of the attack problem indicated that a $\dot{\gamma}$ control system would be more satisfactory and easier to develop than the $\dot{\theta}$ control system. Unpublished results from vertical-plane studies, made during and since the Typhoon work, have indicated that a $\dot{\theta}$ control system as satisfactory as the $\dot{\gamma}$ control system should be obtainable.

Since $\dot{\gamma}$ could be obtained on the simulator without a vertical reference and because it was one of the objectives of this study to find out if a system without a vertical reference was possible, such a device was not included as part of the simulation.

For the Typhoon study the interceptor was represented by the six-degree-of-freedom rigid body equations of motion. Engine momentum terms were neglected as ramjet power was assumed for the attack run. The equations of motion were referenced to principal body axes, thereby making the product of inertias zero. Thus, the equations of motion become

$$\left.\begin{aligned}
&m(\dot{u} + qw_o) + \left\{m\left[q(\Delta w) - rv\right]\right\} = F_X + l_3W \\
&m(\dot{v} + ru_o - pw_o) + \left\{m\left[r(\Delta u) - p(\Delta w)\right]\right\} = F_Y + m_3W \\
&m(\dot{w} - qu_o) + \left\{m\left[pv - q(\Delta u)\right]\right\} = F_Z + n_3W \\
&I_X\dot{p} + \left[(I_Z - I_Y)qr\right] = L \\
&I_Y\dot{q} + \left[(I_X - I_Z)pr\right] = M \\
&I_Z\dot{r} + \left[(I_Y - I_X)pq\right] = N
\end{aligned}\right\} \qquad (A13)$$

where the terms in the brackets are the nonlinear cross-product terms that are deleted to obtain the linear equations. These equations were analoged so that all or any one or combination of the nonlinear could be deleted from the simulation. The linear equations used in this study differ slightly from the classical linear equations in that the direction cosine computation was not linearized and, therefore, the gravity terms in the force equations contain no linearizing assumptions as they do in the classical linear stability equations.

The direction cosines were computed by the following equations:

$$\left.\begin{aligned} l_i &= l_{i_o} + \int_0^t (m_i r - n_i q)dt \\ m_i &= m_{i_o} + \int_0^t (n_i p - l_i r)dt \\ n_i &= n_{i_o} + \int_0^t (l_i q - m_i p)dt \end{aligned}\right\} \quad (i = 1, 2, 3) \quad \text{(A14)}$$

The aerodynamic forces and moments are F_X, F_Y, and F_Z and L, M, and N of equations (A13) and consist of the control-surface forces and moments, the damping forces and moments, and the static forces and moments.

The control-surface forces and moments were computed by

$$\left.\begin{aligned} \left(\frac{X}{m}\right)_{\delta_e} &= C_{X_{\delta_e}} \delta_e \frac{q_s M^2 S}{m} \\ \left(\frac{Y}{m}\right)_{\delta_r} &= C_{Y_{\delta_r}} \delta_r \frac{q_s M^2 S}{m} \\ \left(\frac{Z}{m}\right)_{\delta_e} &= C_{Z_{\delta_e}} \delta_e \frac{q_s M^2 S}{m} \end{aligned}\right\} \quad \text{(A15)}$$

$$\left.\begin{aligned} \left(\frac{L}{I_X}\right)_{\delta_a, \delta_r} &= \left(C_{l_{\delta_a}} \delta_a + C_{l_{\delta_r}} \delta_r\right) \frac{q_s M^2 s b}{I_X} \\ \left(\frac{M}{I_Y}\right)_{\delta_e} &= C_{m_{\delta_e}} \delta_e \frac{q_s M^2 S \bar{c}}{I_Y} \\ \left(\frac{N}{I_Z}\right)_{\delta_r} &= C_{n_{\delta_r}} \delta_r \frac{q_s M^2 S \bar{c}}{I_Z} \end{aligned}\right\} \quad \text{(A16)}$$

The remaining forces and moments which are caused by the airplane motions are computed by

$$\left.\begin{aligned} \frac{X}{m} &= \frac{X_o}{m} + \frac{C_X q_s M^2 S}{m} \\ \frac{Y}{m} &= \frac{C_{Y_\beta} \beta q_s M^2 S}{m} \\ \frac{Z}{m} &= C_Z \frac{q_s M^2 S}{m} \end{aligned}\right\} \tag{A17}$$

$$\left.\begin{aligned} \frac{L}{I_X} &= \left[\frac{bC_{l_p}}{2V_s} p + \frac{bC_{l_r}}{2V_s} r + MC_{l_\beta}\beta\right] q_s \frac{MSb}{I_X} \\ \frac{M}{I_Y} &= \frac{M_o}{I_Y} + \left[\frac{\bar{c}C_{m_q}}{2V_s} q + MC_m\right] q_s \frac{MS\bar{c}}{I_Y} \\ \frac{N}{I_Z} &= \left[\frac{bC_{n_p}}{2V_s} p + \frac{bC_{n_r}}{2V_s} + MC_{n_\beta}\beta\right] q_s \frac{MSb}{I_Z} \end{aligned}\right\} \tag{A18}$$

and for equations (A13)

$$\begin{Bmatrix} \frac{F_X}{m} \\ \frac{F_Y}{m} \\ \frac{F_Z}{m} \end{Bmatrix} = (A15) + (A17)$$

and

$$\begin{Bmatrix} \frac{L}{I_X} \\ \frac{M}{I_Y} \\ \frac{N}{I_Z} \end{Bmatrix} = (A16) + (A18)$$

The problem required that the angle of attack α, the sideslip angle β, and Mach number be supplied, as well as values for the stability derivatives. The following equations were used to compute α, β, and Mach number, as well as V, $\dot{\beta}$, and $\dot{\gamma}$ which were used in the guidance and automatic pilot:

[redacted]

$$\left.\begin{aligned} \alpha &\approx \frac{w}{V} \\ \beta &\approx \frac{v}{V} \\ V_f &= \frac{2u}{2 - \alpha^2} \\ M^* &= \frac{V}{V_s} \\ \dot{\beta} &\approx \frac{\dot{v}}{V} \\ \dot{\gamma} &= - \frac{F_Z + gn_Z}{mV} \end{aligned}\right\} \qquad \text{(A19)}$$

The aerodynamic stability derivatives, except C_X, and the control surface effectiveness were determined by analytical investigation and the results were published in reference 9. These stability derivatives are the linear derivatives and are functions of Mach number. The control surface effectiveness and the drag coefficient C_X were obtained from unpublished wind-tunnel tests. Thus, the drag coefficient is a nonlinear function of angle of attack, as well as a function of Mach number. In addition, the basic C_{l_β} is composed of two parts, a contribution from the wing and a contribution of the fuselage and tail. The contribution to C_{l_β} from the wing is a function of angle of attack. Therefore, the basic C_{l_β} is a function of angle of attack, as well as of Mach number.

The pitching-moment coefficient C_m and the stability derivatives C_{l_β}, C_{n_β}, C_{l_p}, and C_{n_p} were programmed with a nonlinear tail that is a function of the parameter $\alpha - \alpha_{cr}$. Here α is the angle of attack from zero lift and α_{cr} is the angle of attack at which the nonlinear tail starts. Provisions were so that α_{cr} could be varied; two values were used in this study, 3° and 6°.

All stability derivatives used were plotted as functions of the Mach number and angle of attack. These curves were then fitted by least squares, to obtain a polynomial function of Mach number and angle of attack that did not vary more than ±10 percent from the original curve. This procedure led to the following equations, which were used on the Typhoon computer to make a continuous determination of the stability derivatives as the Mach number and angle of attack changed

[redacted]

$$\left.\begin{aligned} M^*C_{X_{\delta_e}} &= (0.4437 - 0.0335M)\alpha \\ M^*C_{Y_{\delta_r}} &= 0.272 \\ M^*C_{l_{\delta_a}} &= -0.1514 \\ M^*C_{l_{\delta_r}} &= 0.0537 \\ M^*C_{m_{\delta_e}} &= -0.8438 \\ M^*C_{n_{\delta_r}} &= -0.2297 \end{aligned}\right\} \quad \text{(A20)}$$

and

$$M^*C_X = -0.2425 - 0.1325M^* + \left(47.105 - 38.364M^* + 7.38M^{*2}\right)\alpha^2 \quad \text{(A21a)}$$

$$M^*C_{Y_\beta} = 0.7644 - 0.284M^* \quad \text{(A21b)}$$

$$M^*C_Z = -5.15\alpha \quad \text{(A21c)}$$

$$M^*C_{Z_{\delta_e}} = -0.4437 + 0.0335M^* \quad \text{(A21d)}$$

$$C_{l_p} = -0.404 + 0.0975M^* \pm 50.7\left(\alpha - \alpha_c\right)^2\mu\left(\alpha - \alpha_{cr}\right) \quad \text{(A21e)}$$

$$C_{l_r} = 0.2689 - 0.0565M^* \quad \text{(A21f)}$$

$$M^*C_{l_\beta} = -0.1957 + 8.10\left(\alpha - \alpha_c\right)^2\mu\left(\alpha - \alpha_{cr}\right) + \phi_4\alpha \quad \text{(A21g)}$$

$$\phi_4 = -6.320 + 3.74M^* \qquad (M^* \leq 1.7988) \quad \text{(A21h)}$$

$$\phi_4 = 0.913 - 0.281M^* \qquad (M^* > 1.7988) \quad \text{(A21i)}$$

$$C_{m_q} = -3.959 + 0.535M^* \quad \text{(A21j)}$$

[redacted]

$$M^*C_m = -1.369\alpha + \left[31.91(\alpha - \alpha_{cr})^2 - 152.4(\alpha - \alpha_{cr})^3\right]\mu(\alpha - \alpha_{cr}) \quad \text{(A21k)}$$

$$C_{n_p} = -0.1864 + 0.1625M - 0.0281M^{*2} - 1.197(\alpha - \alpha_{cr})^2\mu(\alpha - \alpha_{cr}) \quad \text{(A21l)}$$

$$C_{n_r} = -0.955 + 0.18M^* \quad \text{(A21m)}$$

$$M^*C_{n_\beta} = 0.528 - 13.97(\alpha - \alpha_{cr})^2\mu(\alpha - \alpha_{cr}) \quad \text{(A21n)}$$

where

$$\mu(\alpha - \alpha_{cr}) = 0, \alpha < \alpha_{cr}$$

$$\mu(\alpha - \alpha_{cr}) = 1, \alpha > \alpha_{cr}$$

These equations for the aerodynamic forces and moments contain all of the necessary information to obtain continuous aerodynamic information as the interceptor angle of attack and Mach number change. These equations were set up on servo multipliers and arranged so that any of the following combinations could be used:

(a) constant aerodynamics

(b) aerodynamics varying with Mach number

(c) aerodynamics constant with Mach number and varying with $\alpha - \alpha_{cr}$

(d) aerodynamics varying with Mach number and $\alpha - \alpha_{cr}$

The parts of these equations that vary with $\alpha - \alpha_{cr}$ were zero for $\alpha < \alpha_{cr}$ and for $\alpha > \alpha_{cr}$ the computed value was used. The equations were so analoged that the value of α_{cr} could be changed manually. In addition, the α^2 term in C_X and the α term in C_{l_β} could be removed if desired. The stability derivatives $C_{l_{\dot{\beta}}}$, $C_{n_{\dot{\beta}}}$, C_{m_β}, and $C_{m_{\dot{\alpha}}}$ were neglected in this study.

In order to include the nonlinear aerodynamics, variations of air density with altitude had to be neglected. Thus, even though the

interceptor changes its altitude by several thousands of feet, the air density remains constant at the value for 50,000 feet, the initial altitude of the target.

The physical constants used in the problem and airplane characteristics are given in the following tables:

Constants:

g, ft/sec^2	32.17
W, lb	25,000
m, slugs	777
I_1, slugs-ft^2	15,040
I_2, slugs-ft^2	274,800
I_3, slugs-ft^2	287,000
S, sq ft	401
b, ft	35.81
$\bar{c}$, ft	15
V_T, ft/sec	1359.5
V_R, ft/sec	2,000
V_s, ft/sec	971.1
V_{I_o}, ft/sec	2,140
q_s (at H = 50,000), lb/ft^2	170.2
τ, sec	1.5
τ_{fl}, sec	0.6
τ_{SA}, τ_{SE}, τ_{SR}, sec	0.03
α_{cr}, deg	3 or 6
$\frac{X_Q}{m}$ and $\frac{M_Q}{I_Z}$	Values required for $\frac{X}{m} = 0$ and $\frac{m}{I_Z} = 0$ at t = 0

Flight-path autopilot:

	Low gain	High gain
K_4	0.4	2
K_6	14	14
K_8	20	0
K_{12}	2	1
K_{20}	Adjustable constant, 0 to 0.2	

Roll autopilot:

K_3	8
K_9	3
K_{10}	0.1 to 0.2

Rudder autopilot:

	Configuration 1	Configuration 2
K_{11}	1.8	0
K_{11}	0	-1.8

Limiters:

δ_a, δ_e, δ_r, deg . . . . . limited at ±10 or ±20; normal value ±20

$\dot{\delta}_a$, $\dot{\delta}_e$, $\dot{\delta}_r$, °/sec . . . . . limited at ±20, ±50, ±100, ±143; normal value, ±100

g-limiter:

	Low-gain autopilot (*)	High-gain autopilot (*)	
$\epsilon_{e_{max}}$	$\frac{4g}{V_{I_o}K_4}$	$\frac{4g}{V_{I_o}K_4}$	$\frac{K_6 + K_{12} + 3.96}{K_6}$
$\epsilon_{e_{min}}$	$\frac{2g}{V_{I_o}K_4}$	$\frac{4g}{V_{I_o}K_4}$	$\frac{K_6 + K_{12} + 3.96}{K_6}$

*V_{I_o} is initial value of V_I.

APPENDIX B

THE EFFECT OF AUTOMATIC-PILOT FEEDBACKS ON AIRPLANE CHARACTERISTICS

The automatic pilots used in the Typhoon study contain both angular rate and acceleration feedbacks. The use of these feedbacks effectively changes the inertia and aerodynamic damping characteristics of the airplane. The following table shows the effect of the rolling velocity and rolling acceleration, yawing velocity, and pitching velocity on the airplane

	Basic airplane	Change produced by autopilot	Feedback producing change
I_X	15,040	81,400	$\dot{p}$
C_{l_p}	-0.1895	-24.6	p
C_{l_r}	0.1446	5.24	r
C_{n_r}	-0.559	-22.4	r
C_{m_q}	-2.782	-218 (low-gain longitudinal autopilot)	q
		-109 (high-gain longitudinal autopilot)	q

REFERENCES

1. Schy, Albert A., Gates, Ordway B., Jr., Woodling, C. H., Sherman, Windsor L, and Sternfield, Leonard: Simulator Studies of the Attack Phase of an Automatically Controlled Interceptor. I - Preliminary Studies of the Lateral and Longitudinal Control Systems, by Schy, Gates, and Woodling. II - Some Results of a Study Performed on the Typhoon Computer, by Sherman and Sternfield. NACA RM L55E27a, 1955.

2. Serrell, Robert: Project Typhoon - Summary Progress Report No. 2 (Contract No. N6-ori-196, Task Order 1, Project No. NR 720 002, ONR), RCA (Princeton, N. J.), Dec. 31, 1948.

3. Bartberger, C. L.: Post-Solution Analysis Problem Identification Number 3. National Advisory Committee for Aeronautics Interceptor Study - TED Project ADC EL-42003. Rep. No. NADC-AC-5505, U. S. Naval Air Dev. Center (Johnsville, Pa.), Apr. 1955.

4. Ames Research Staff: Equations, Tables, and Charts for Compressible Flow. NACA Rep. 1135, 1953. (Supersedes NACA TN 1428.)

5. Schy, Albert A., and Gates, Ordway B., Jr.: Analysis of the Effects of Airplane Characteristics and Autopilot Parameters on a Roll-Command System With Aileron Rate and Deflection Limiting. NACA RM L55E18, 1955.

6. Woodling, C. H., and Gates, Ordway B., Jr.: Theoretical Analysis of the Longitudinal Behavior of an Automatically Controlled Supersonic Interceptor During the Attack Phase Against Maneuvering and Non-maneuvering Targets. NACA RM L55G18, 1955.

7. Jones, B. Melvill: Dynamics of the Airplane. The Equations of Motion With Solutions for Small Disturbances From Steady Symmetric Flight. Vol. V of Aerodynamic Theory, div. N, ch. V, secs. 1-5, W. F. Durand, ed., The Durand Reprinting Committee (C.I.T.), 1943, pp. 121-124.

8. Nielsen, Kaj L., and Heyda, James F.: The Mathematical Theory of Airborne Fire Control. NAVORD Rep. 1493, Bur. Ord., Dept. Navy, July 20, 1951.

9. Margolis, Kenneth, and Bobbitt, Percy J.: Theoretical Calculations of the Stability Derivatives at Supersonic Speeds for a High-Speed Airplane Configuration. NACA RM L53G17, 1953.

TABLE I

BASIC SYSTEM CONFIGURATIONS FOR DATA GATHERING RUNS

[Target and guidance included in all basic configurations; control surface rate and displacement limits are 20° per second and 100° per second, respectively, unless otherwise noted]

Configuration	Airplane equations	Lateral control	Longitudinal control	Aerodynamics
1	Complete	Roll pilot with yaw damper	Low gain	Constant
2	Complete	Roll pilot with sideslip damper	Low gain	Constant
3	Complete	Roll pilot with yaw damper	Low gain	Varies with Mach number
4	Complete	Roll pilot with yaw damper	High gain	Varies with Mach number
5	Complete	Roll pilot with sideslip damper	High gain	Varies with Mach number
6	Linear	Roll pilot with yaw damper	Low gain	Constant

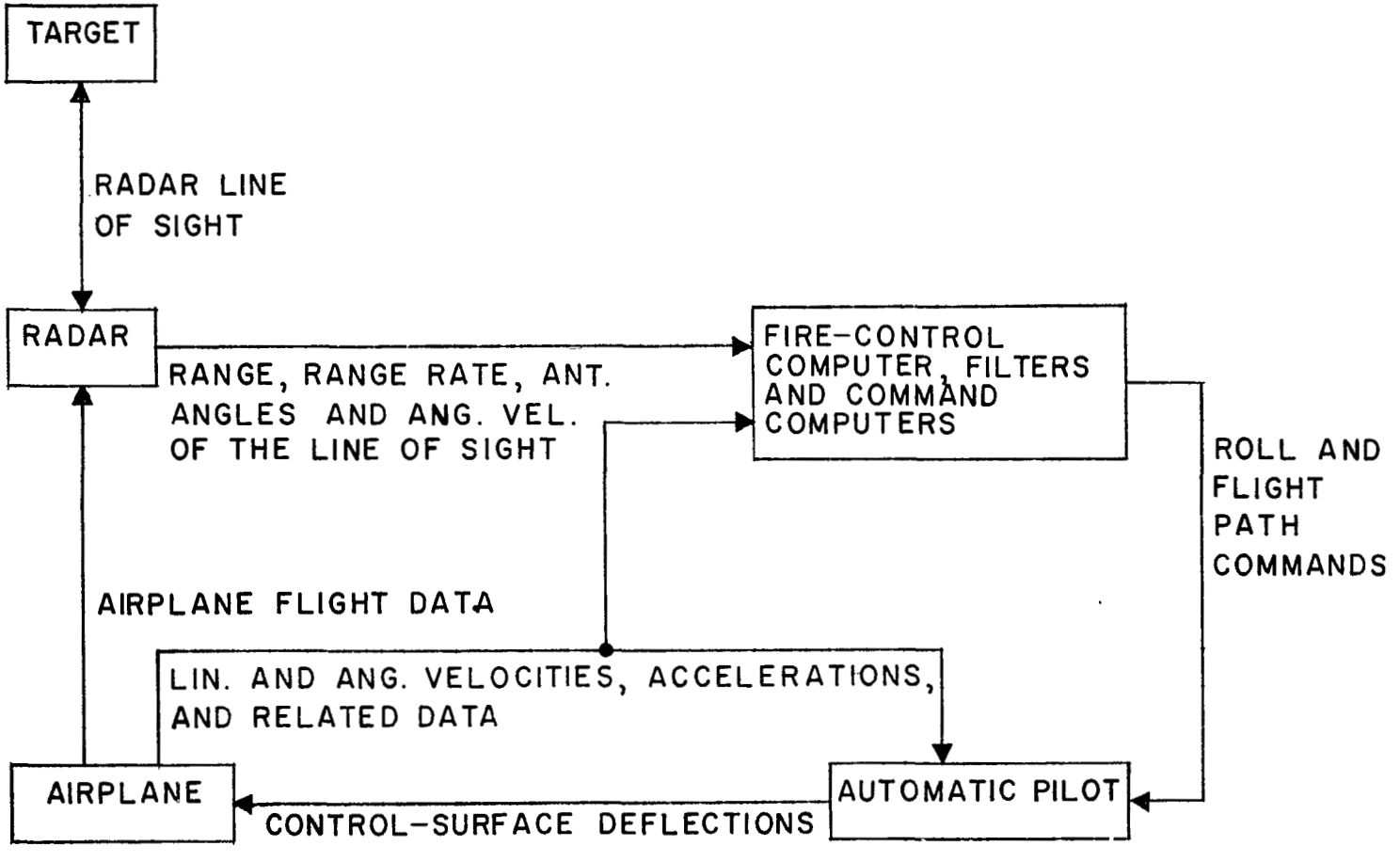

Figure 1.- Information flow diagram for the attack phase of the automatic interceptor.

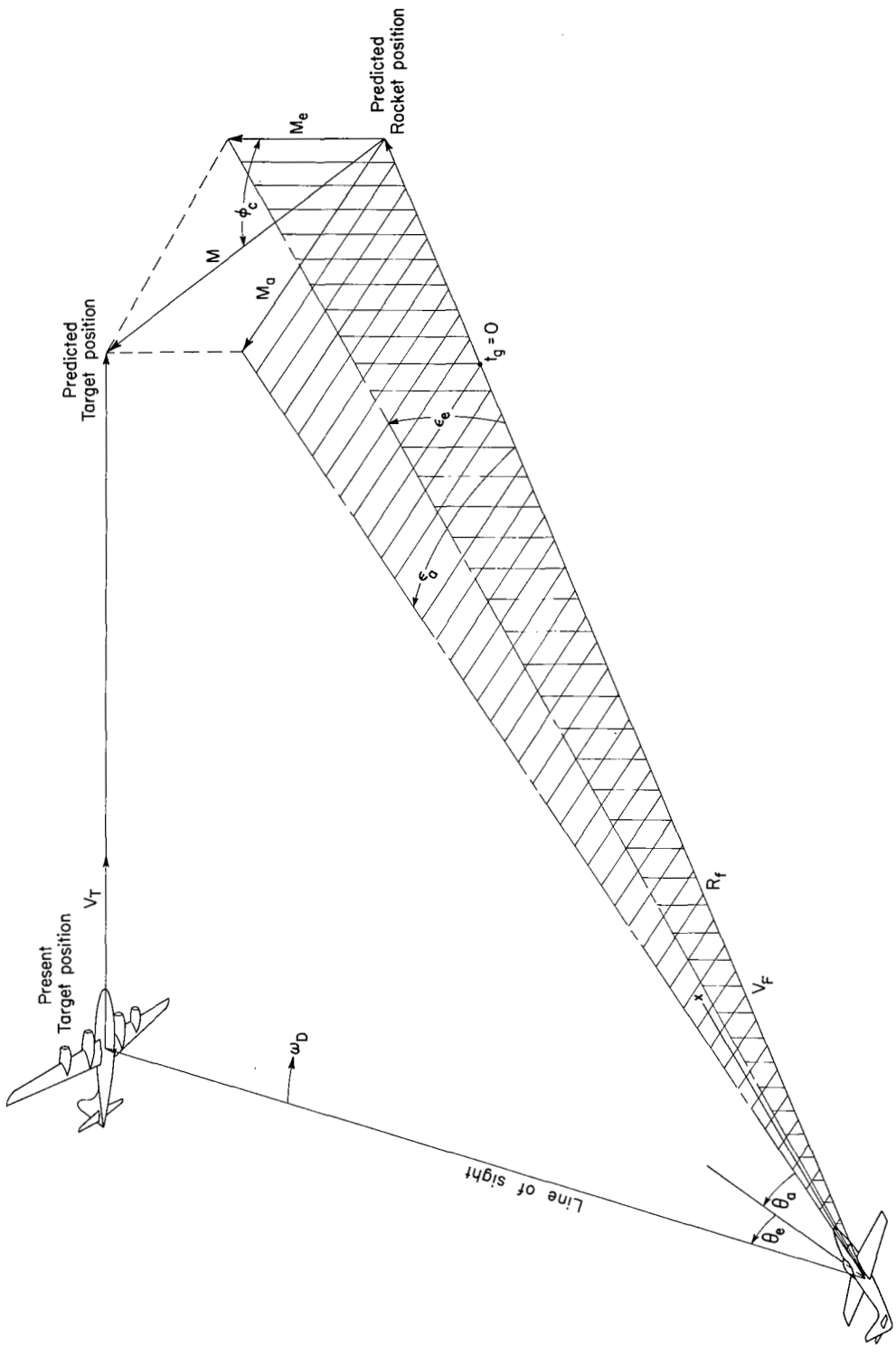

Figure 2.- Geometry of the attack phase of the automatic interceptor problem. For clarity the angles α and β are not shown.

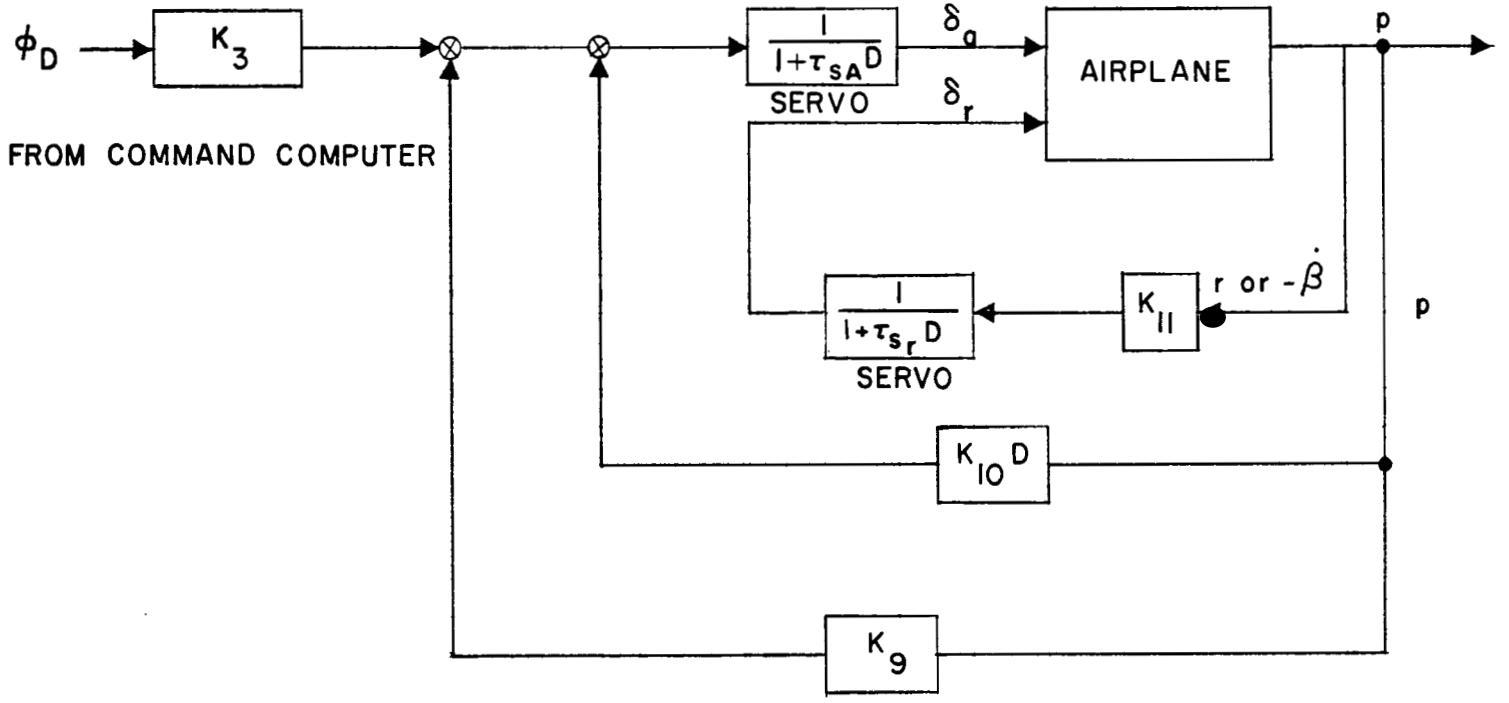

Figure 3.- Block diagram of lateral control system.

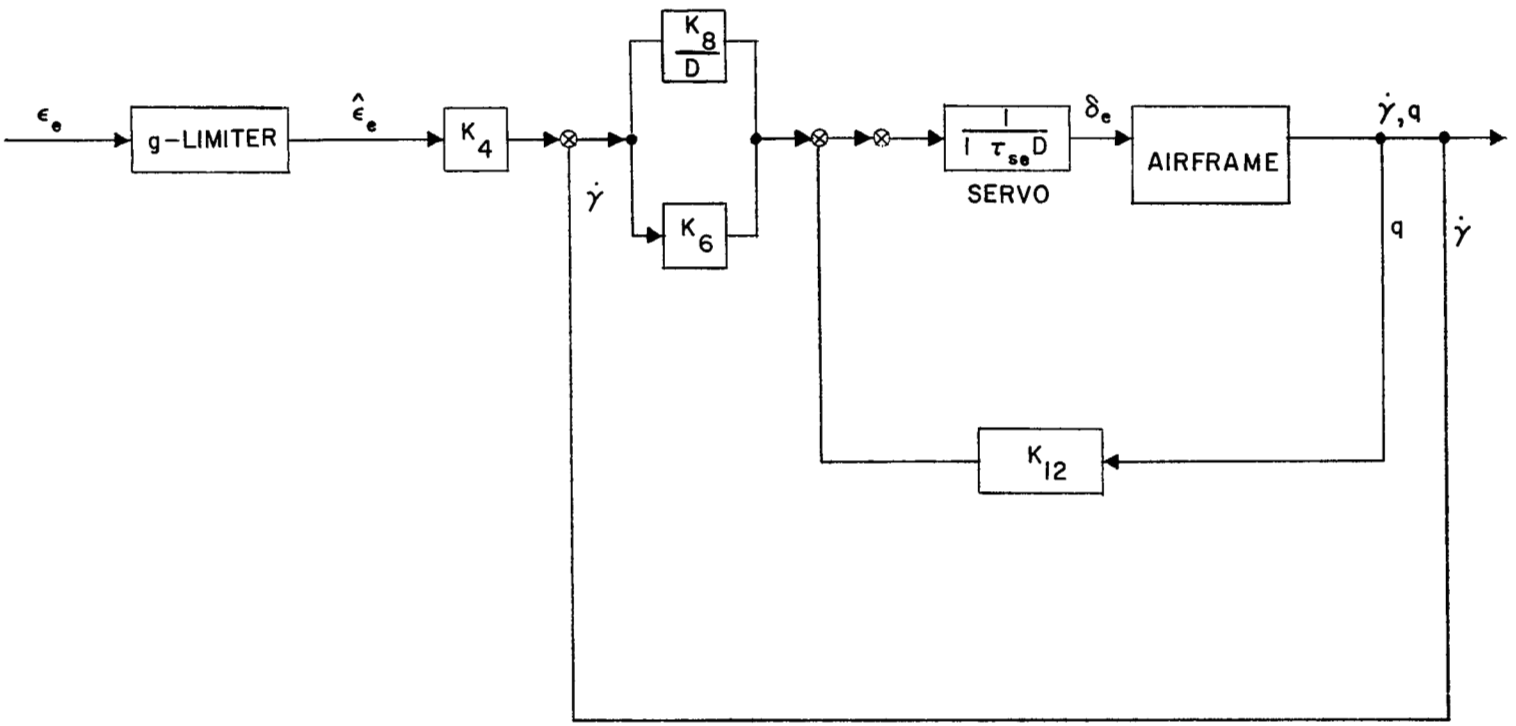

Figure 4.- Block diagram of the flight-path control system.

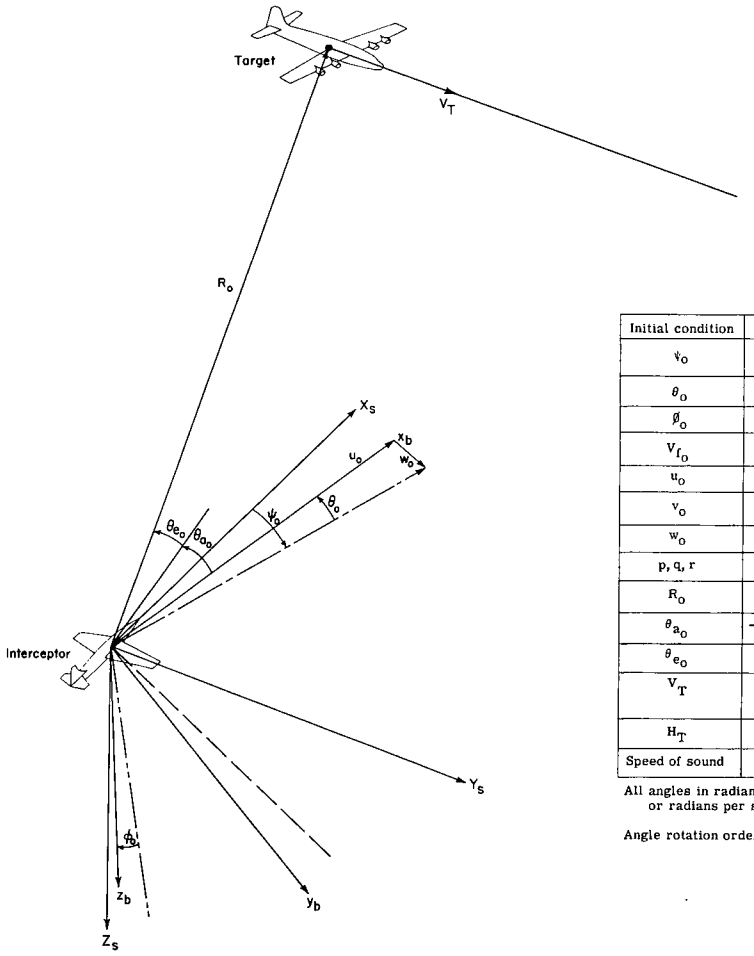

Initial condition	I	II	III	IV	V
ψ_o	$\frac{-\Pi}{2}$	$\frac{-\Pi}{2}$	0	0	0
θ_o	0.0332	0.0332	0.0332	0.0332	0.0332
ϕ_o	0	0	0	0	0
V_{f_o}	2136	2136	2136	2136	2136
u_o	2135	2135	2135	2135	2135
v_o	0	0	0	0	0
w_o	70.52	70.52	70.52	70.52	70.52
p, q, r	All zero initially				
R_o	60,000	60,000	60,000	60,000	60,000
θ_{a_o}	-0.08275	-0.1745	-0.7854	-0.7854	-0.2618
θ_{e_o}	0	0.1745	0	0.2618	0.2618
V_T	1359 for all initial conditions $\vec{V_I} = i(0) + j(1359) + k(0)$ in space				
H_T	50,000 for all initial conditions				
Speed of sound	971 for all initial conditions				

All angles in radians, all distances in feet, all velocities feet per second or radians per second.

Angle rotation order: Euler angles ψ, θ, ϕ reference space
Gimbal angles θ_a, θ_e reference body

(a) Sketch showing the parameters used in defining initial conditions and a table of parameter values for the initial conditions studies.

Figure 5.- Initial conditions for the investigation of the attack phase of the automatically controlled interceptor.

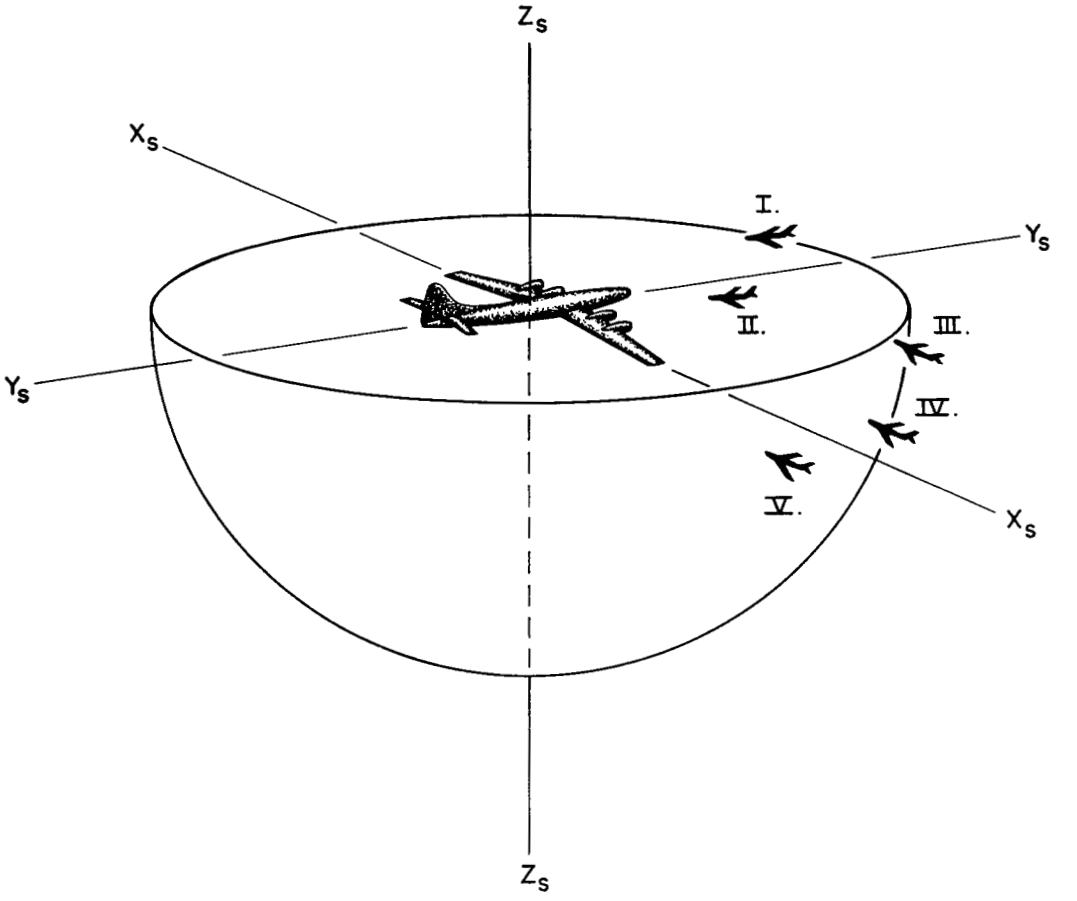

(b) Pictorial presentation of the interceptor target orientation for initial conditions I to V.

Figure 5.- Concluded.

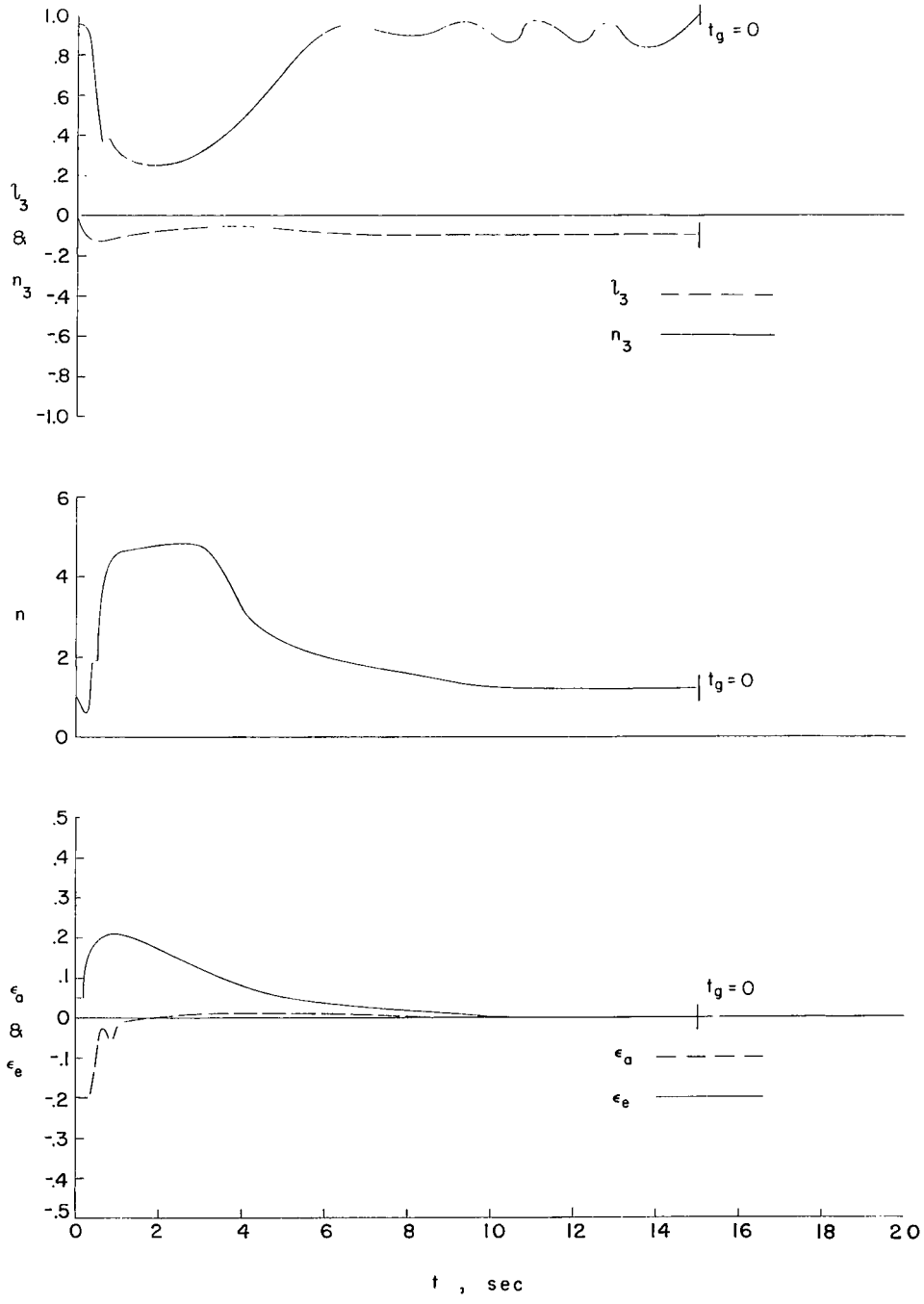

(a) Initial condition I.

Figure 6.- Direction cosines, normal acceleration, and steering errors for the attack run. Interceptor represented by complete equations with constant aerodynamics. Basic configuration 1.

[redacted]

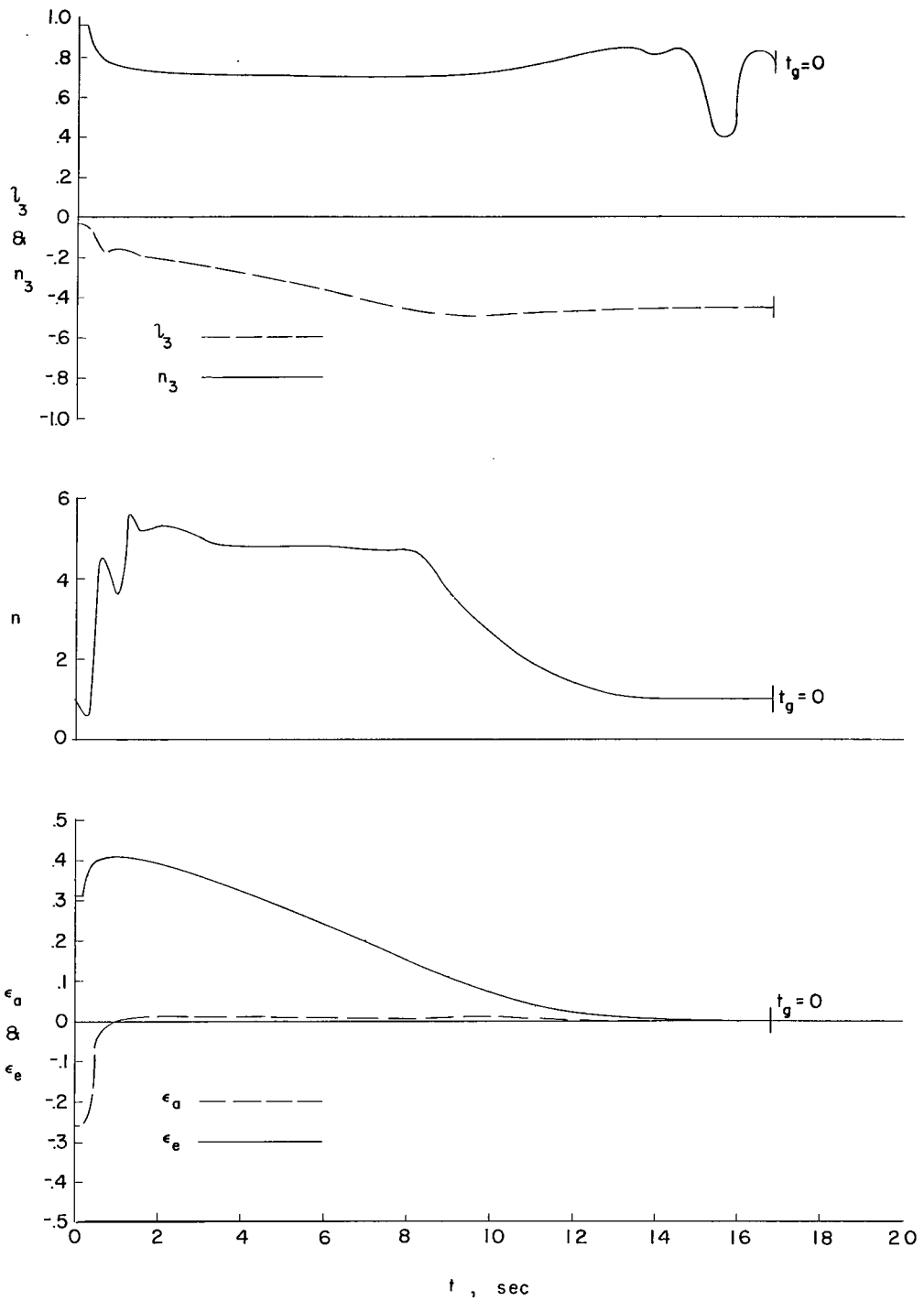

(b) Initial condition II.

Figure 6.- Continued.

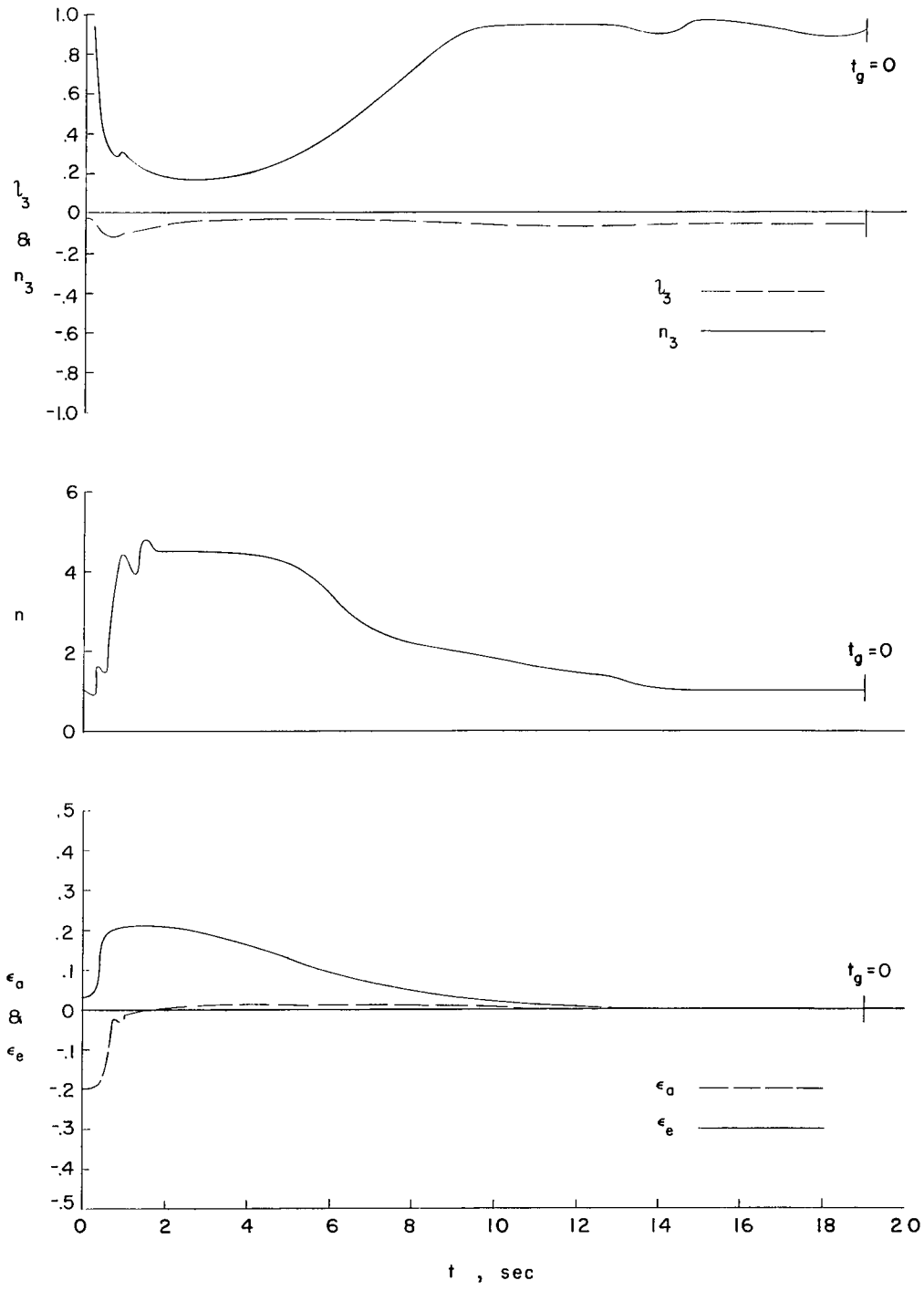

(c) Initial condition III.

Figure 6.- Continued.

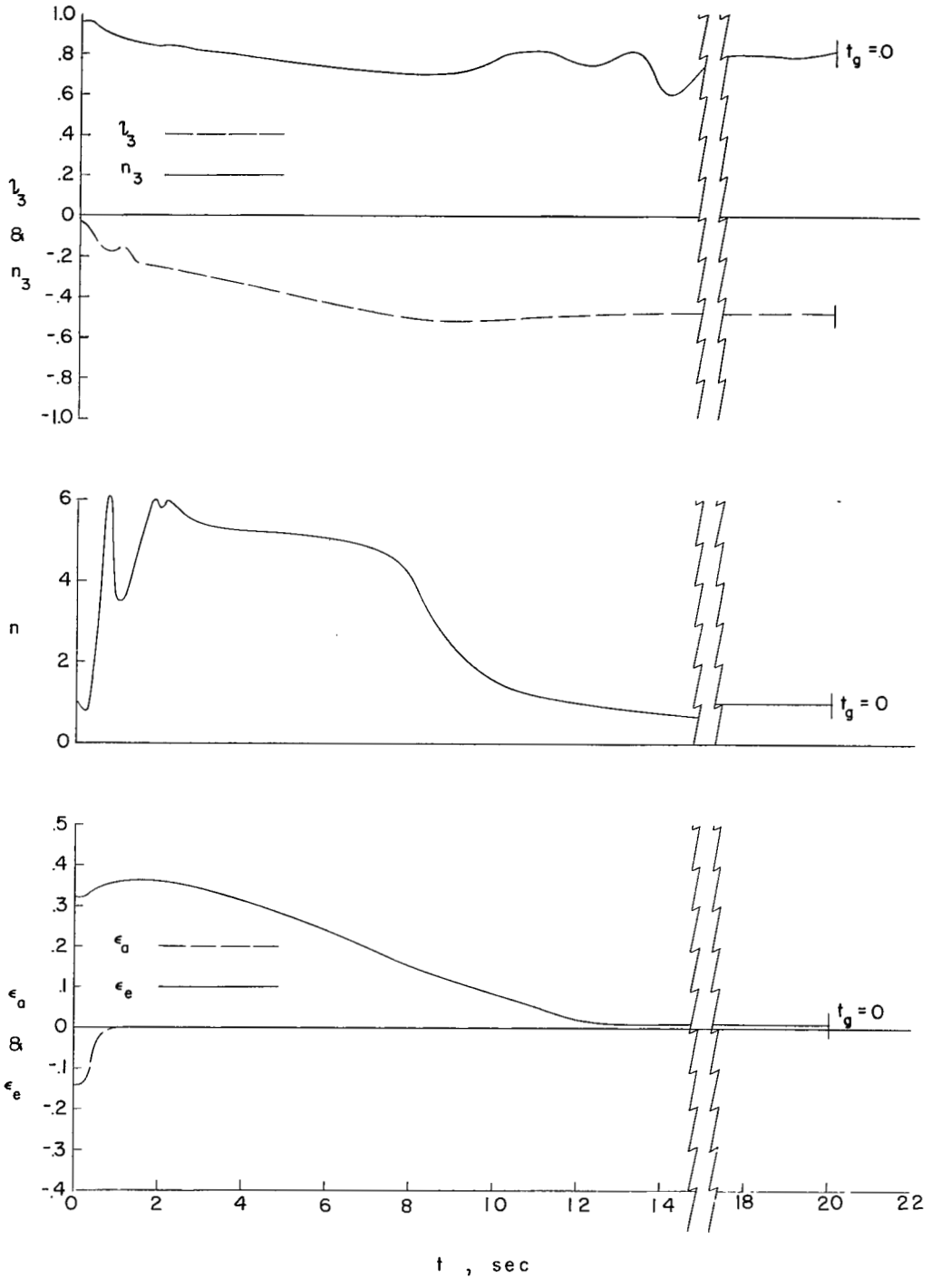

(d) Initial condition IV.

Figure 6.- Continued.

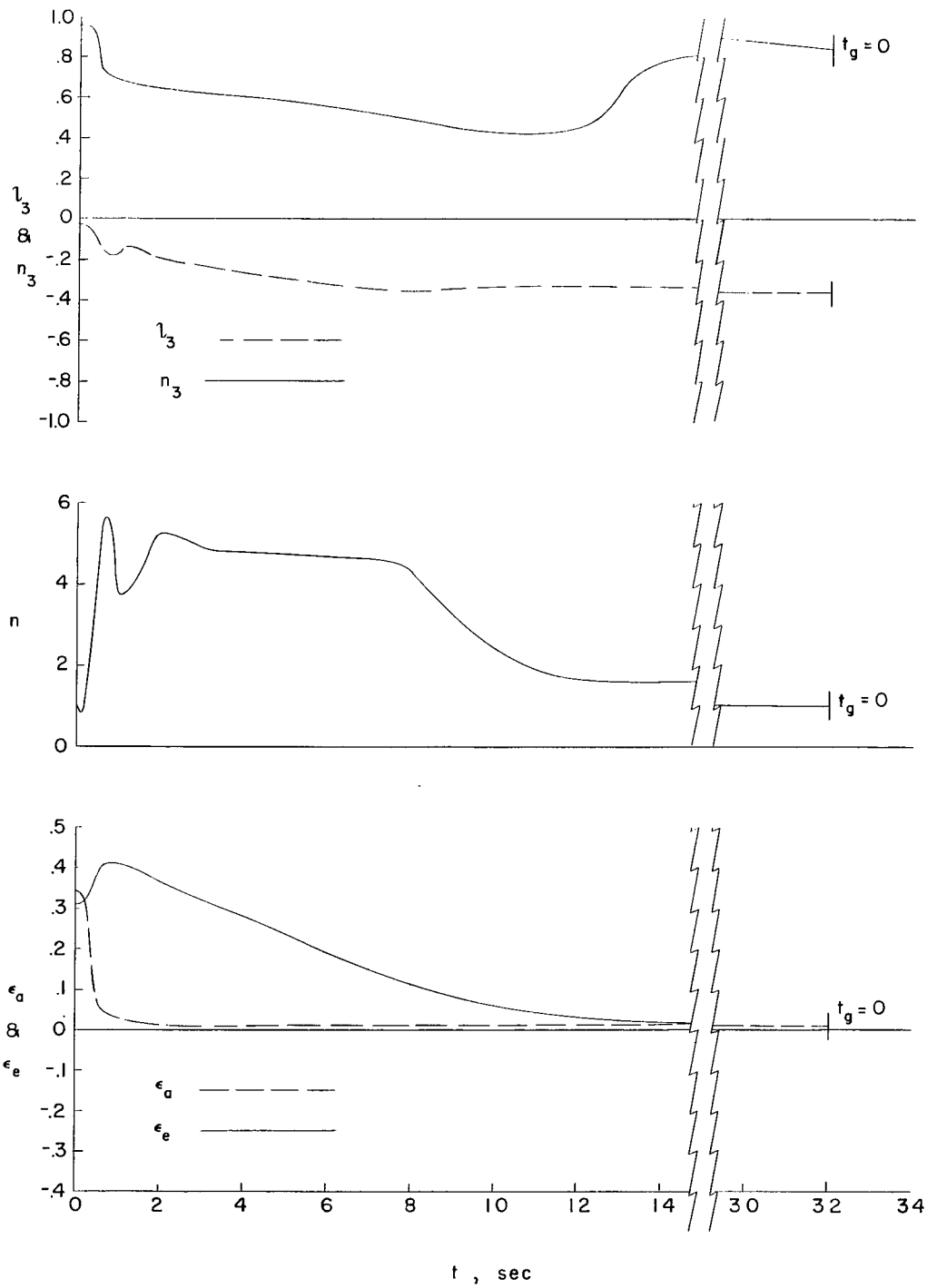

(e) Initial condition V.

Figure 6.- Concluded.

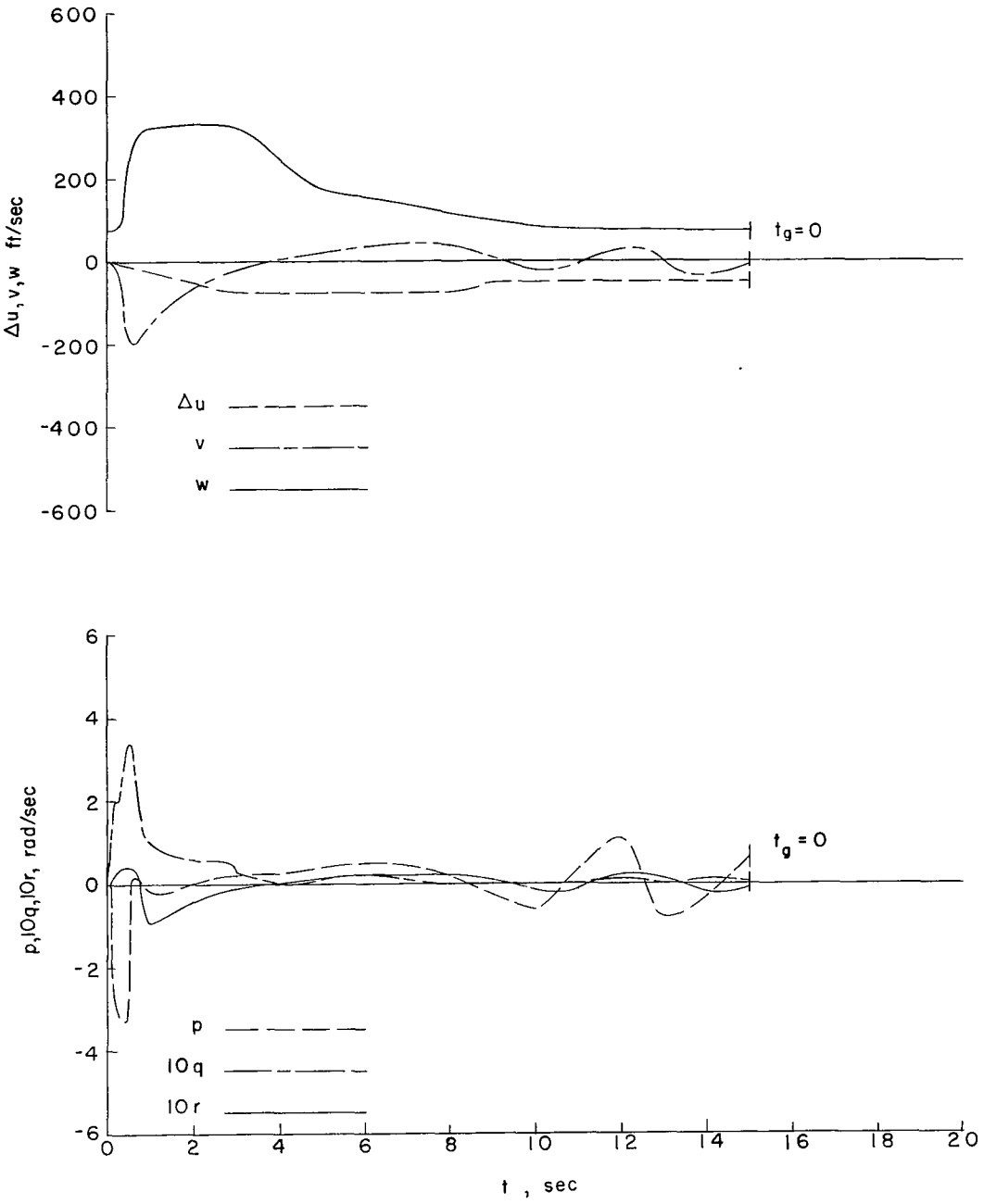

(a) Initial condition I.

Figure 7.- Interceptor response time histories for the attack run. Interceptor represented by complete equations with constant aerodynamics. Basic configuration 1.

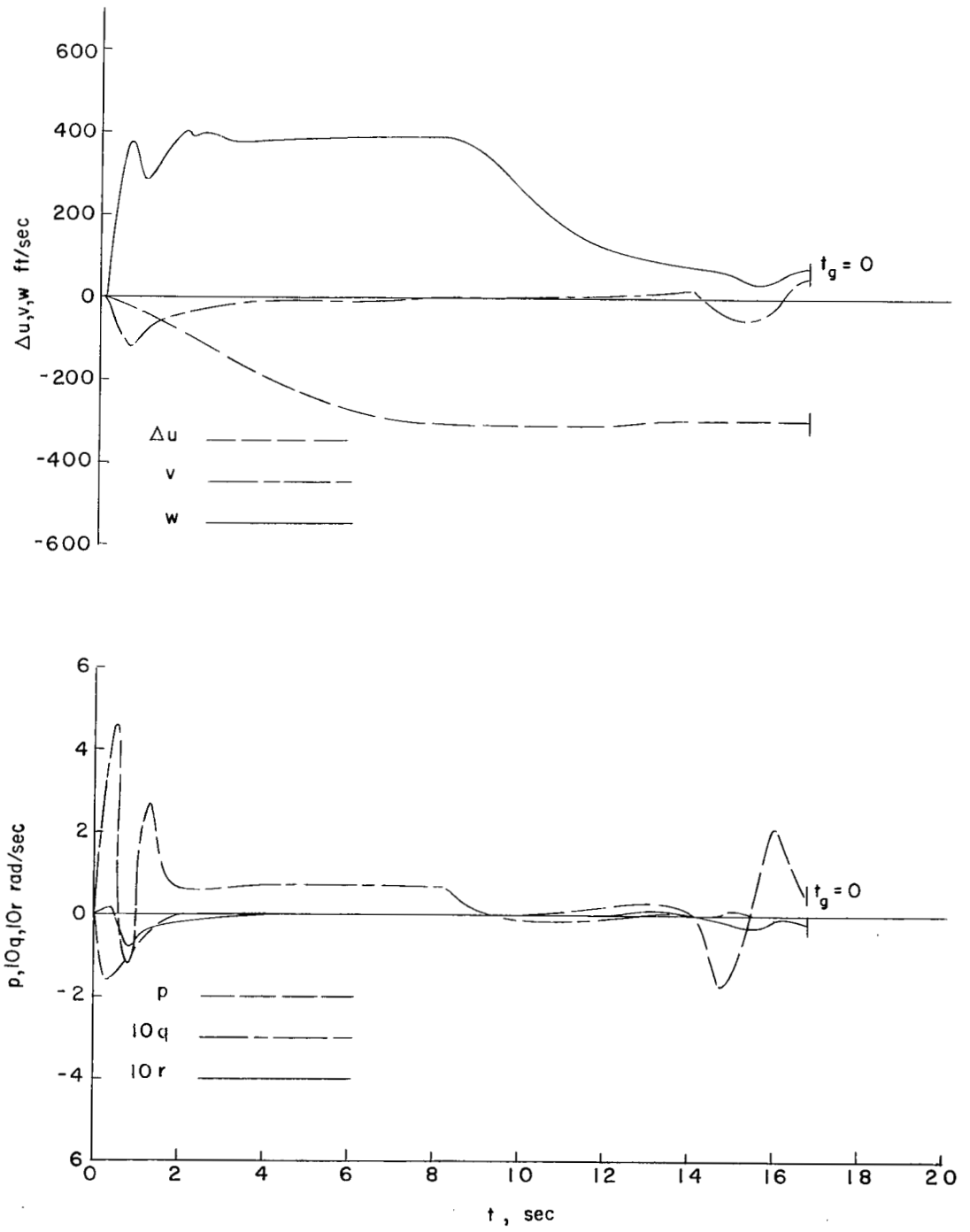

(b) Initial condition II.

Figure 7.- Continued.

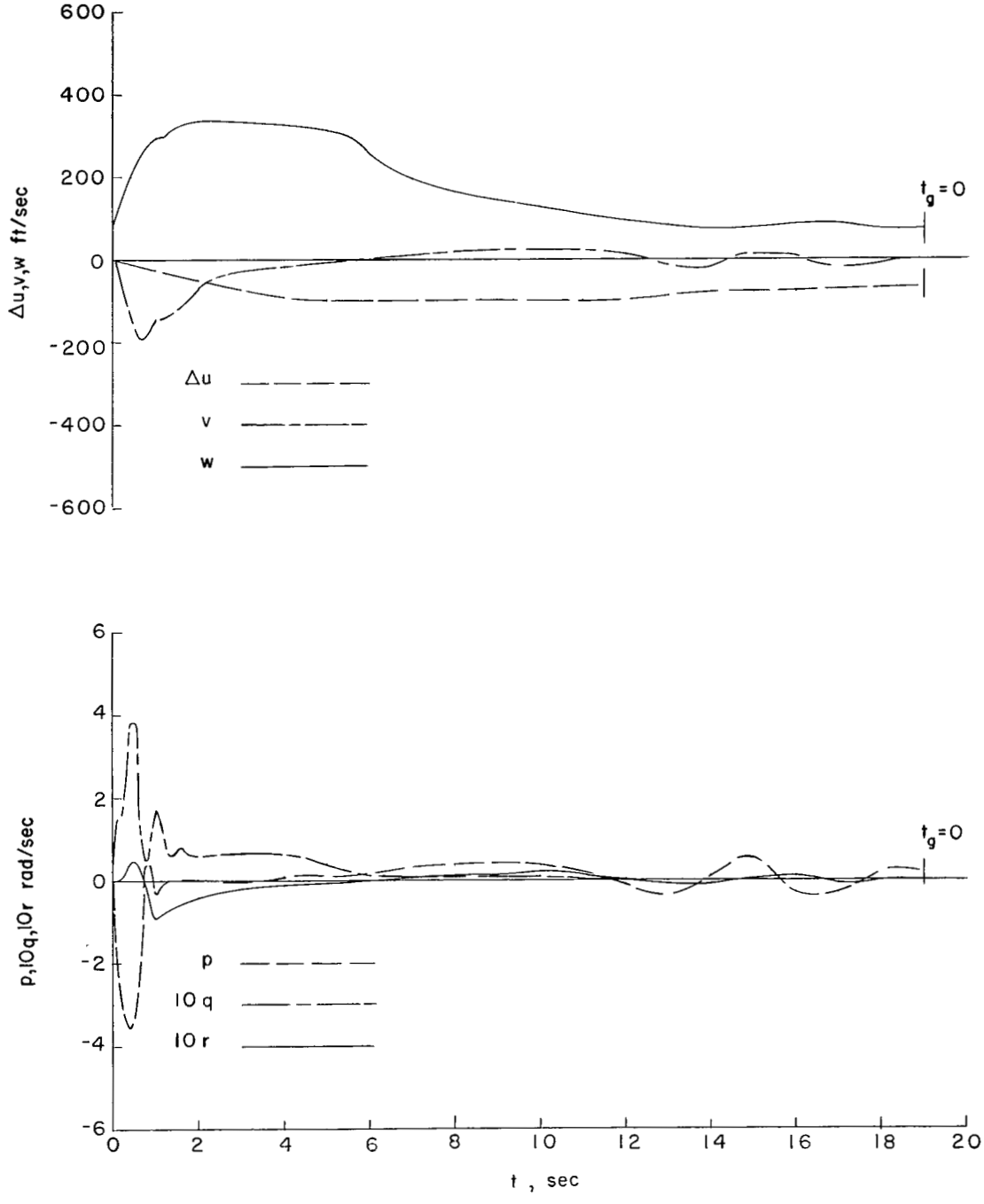

(c) Initial condition III.

Figure 7.- Continued.

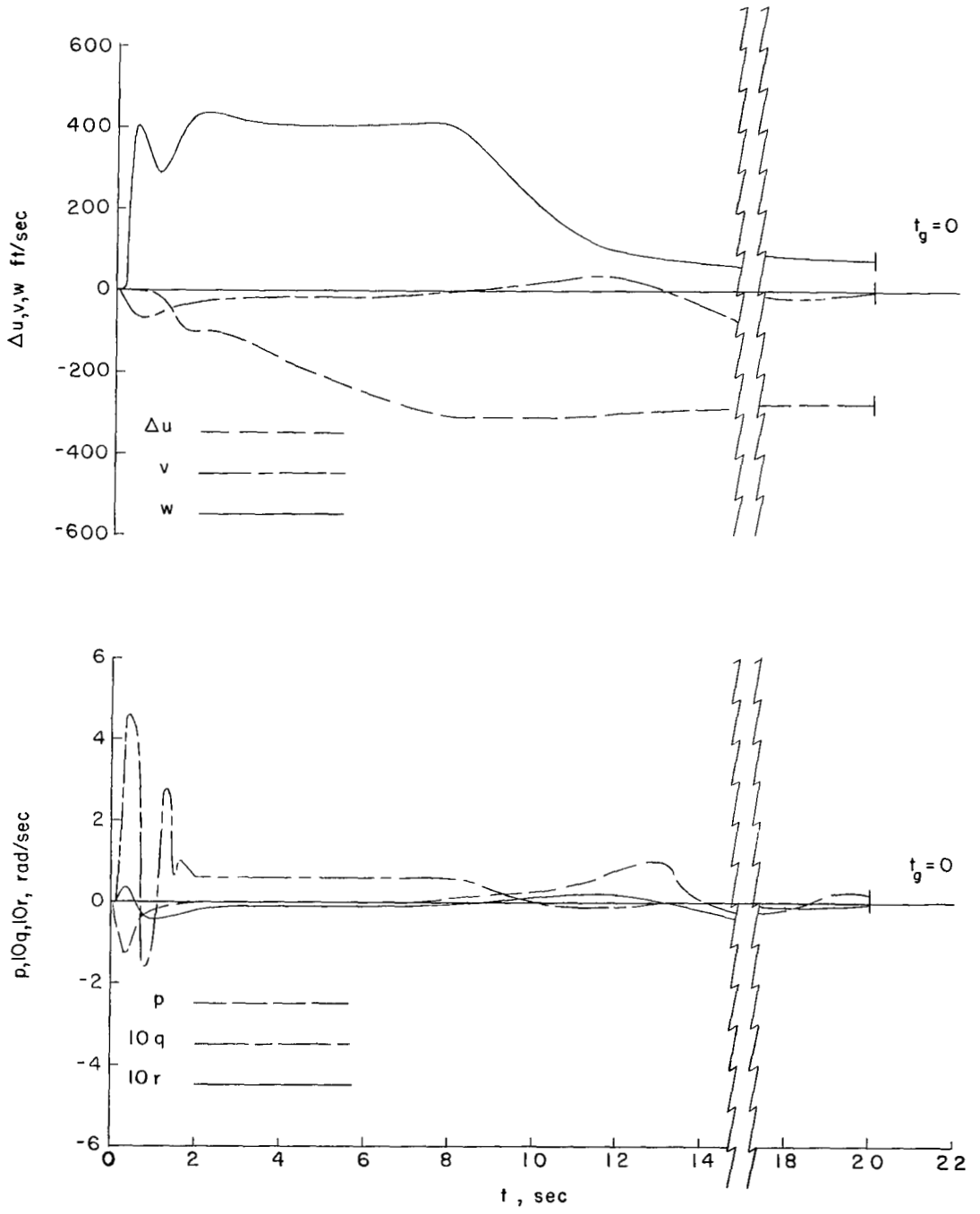

(d) Initial condition IV.

Figure 7.- Continued.

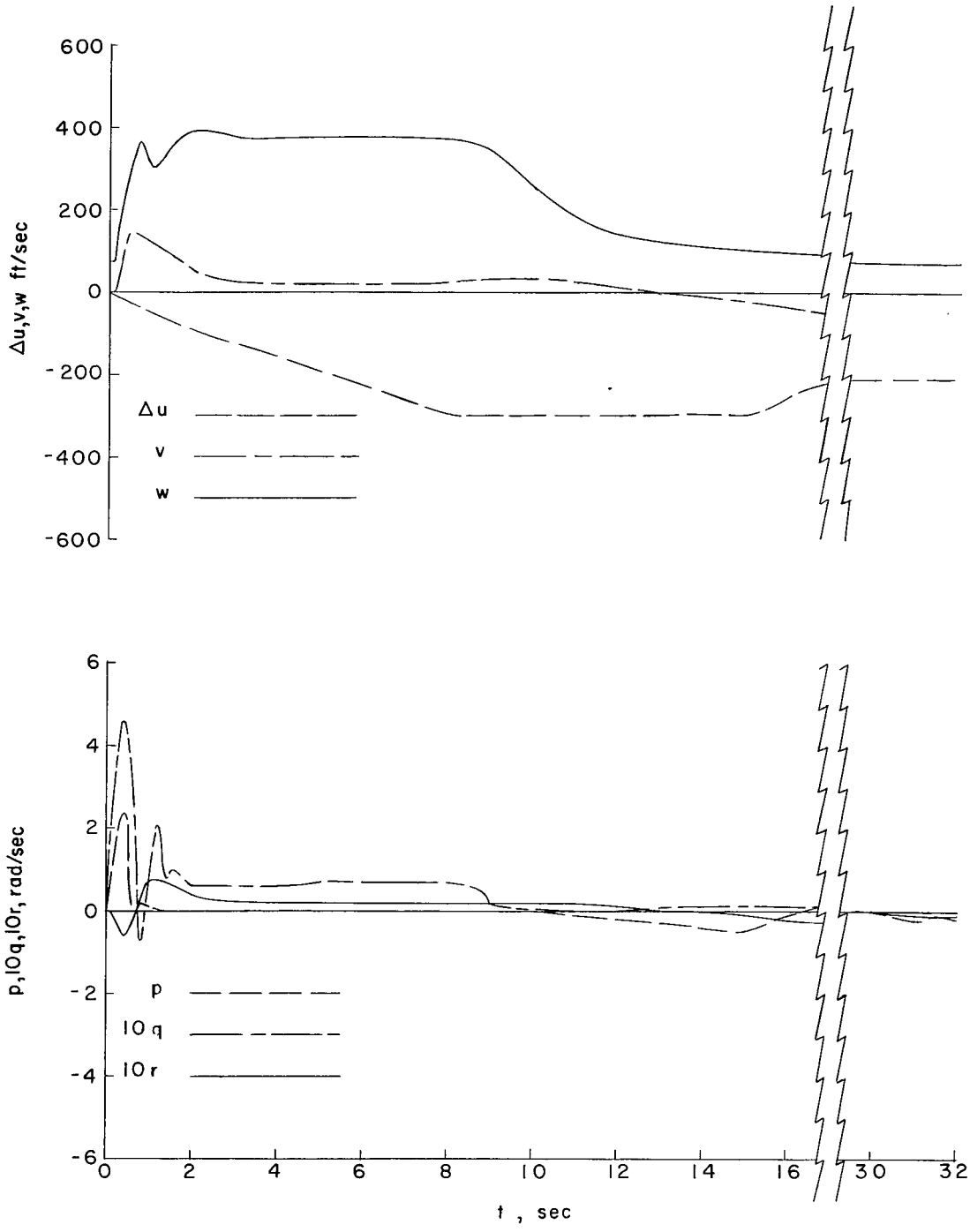

(e) Initial condition V.

Figure 7.- Concluded.

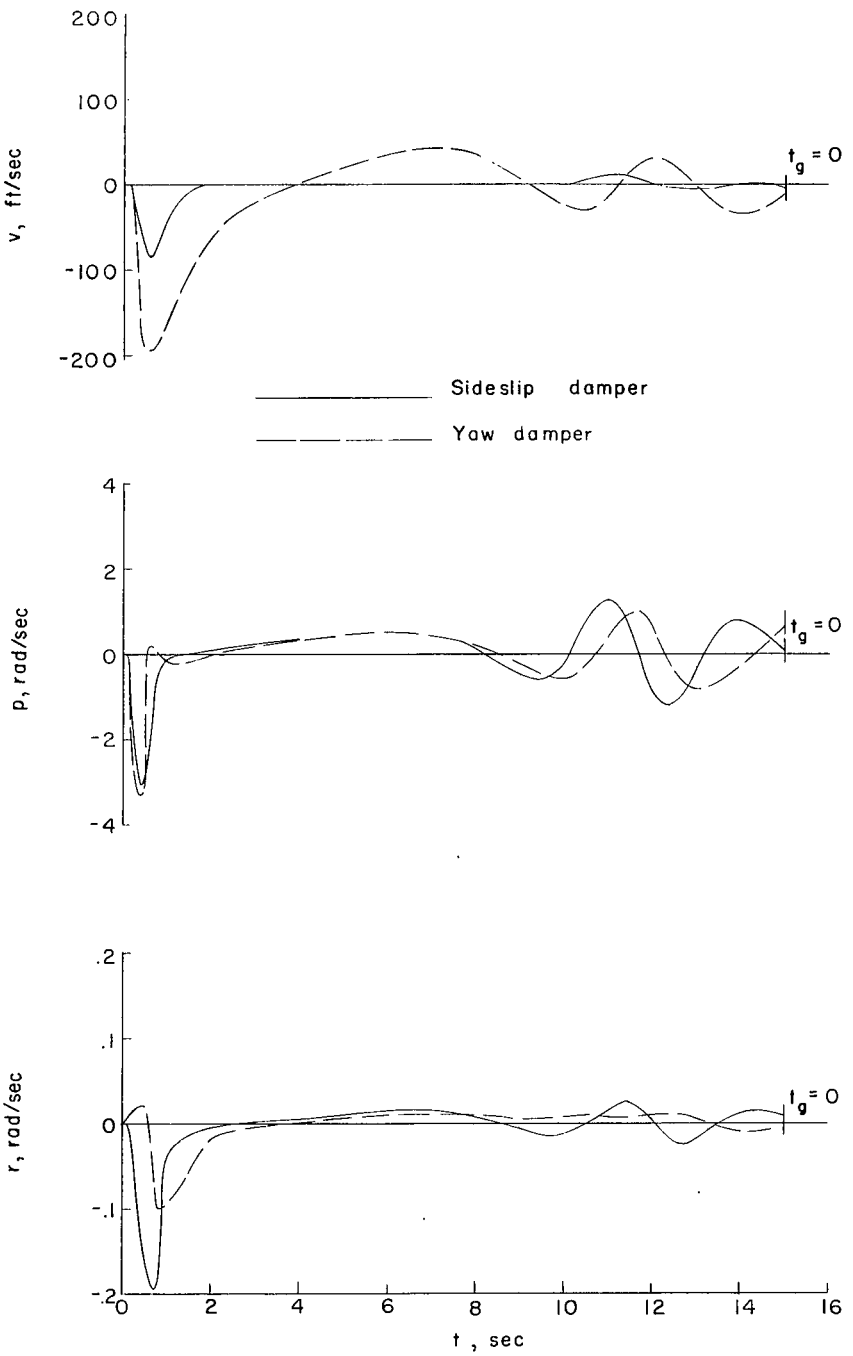

Figure 8.- Comparison of lateral interceptor response for yaw and sideslip dampers. Interceptor represented by complete equations and constant aerodynamics. Initial condition I; basic configurations 1 and 2.

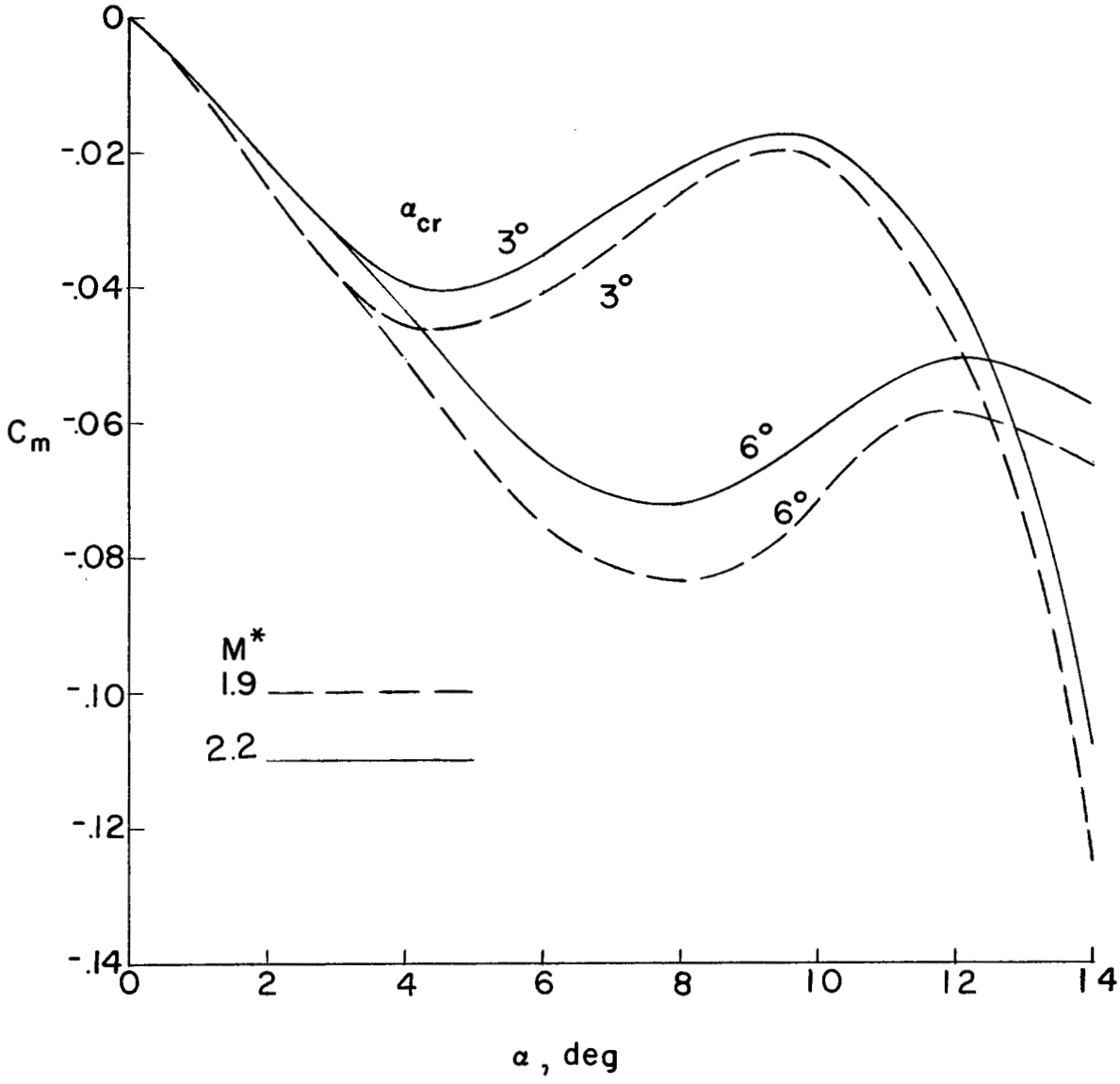

(a) C_m.

Figure 9.- Nonlinear aerodynamic stability derivatives used in the simulation.

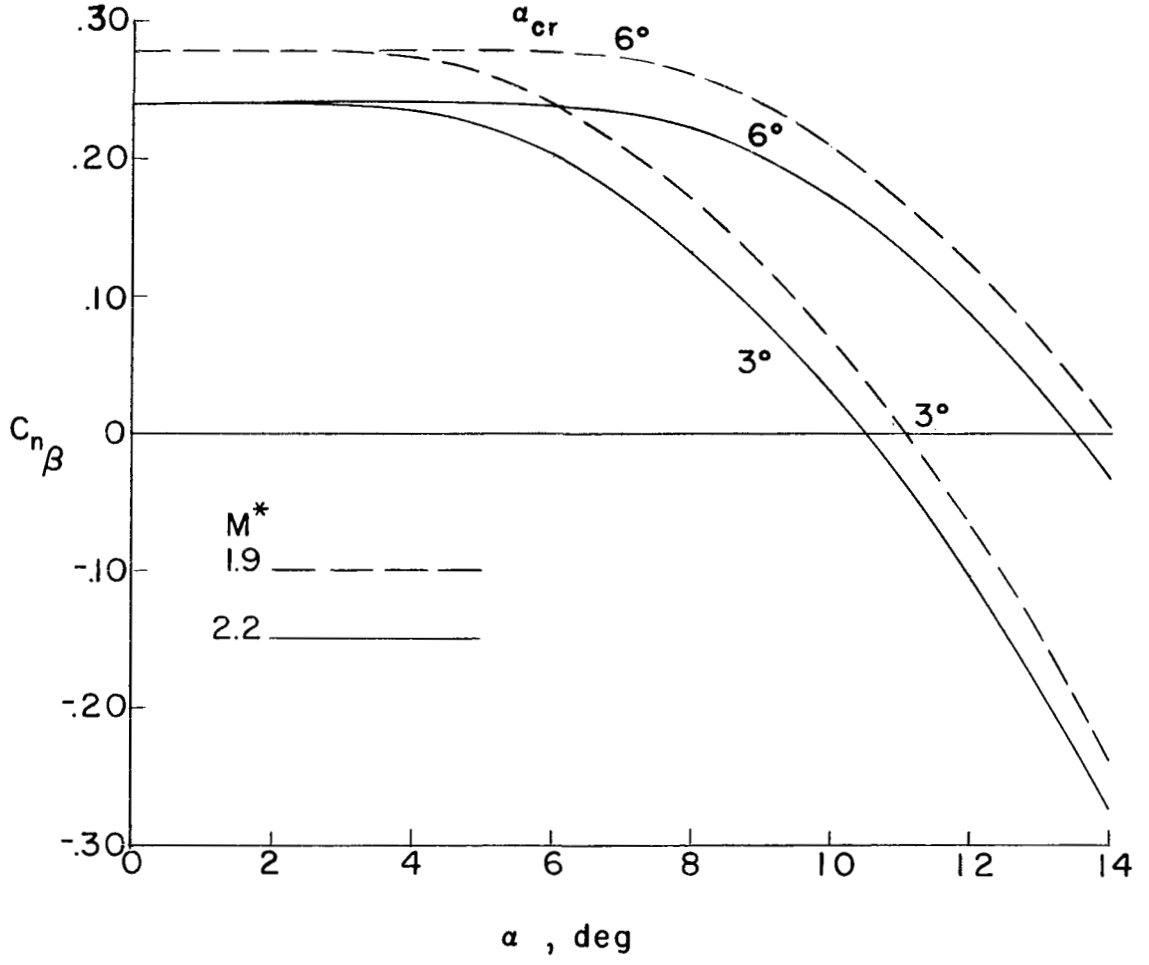

(b) C_{n_β}.

Figure 9.- Continued.

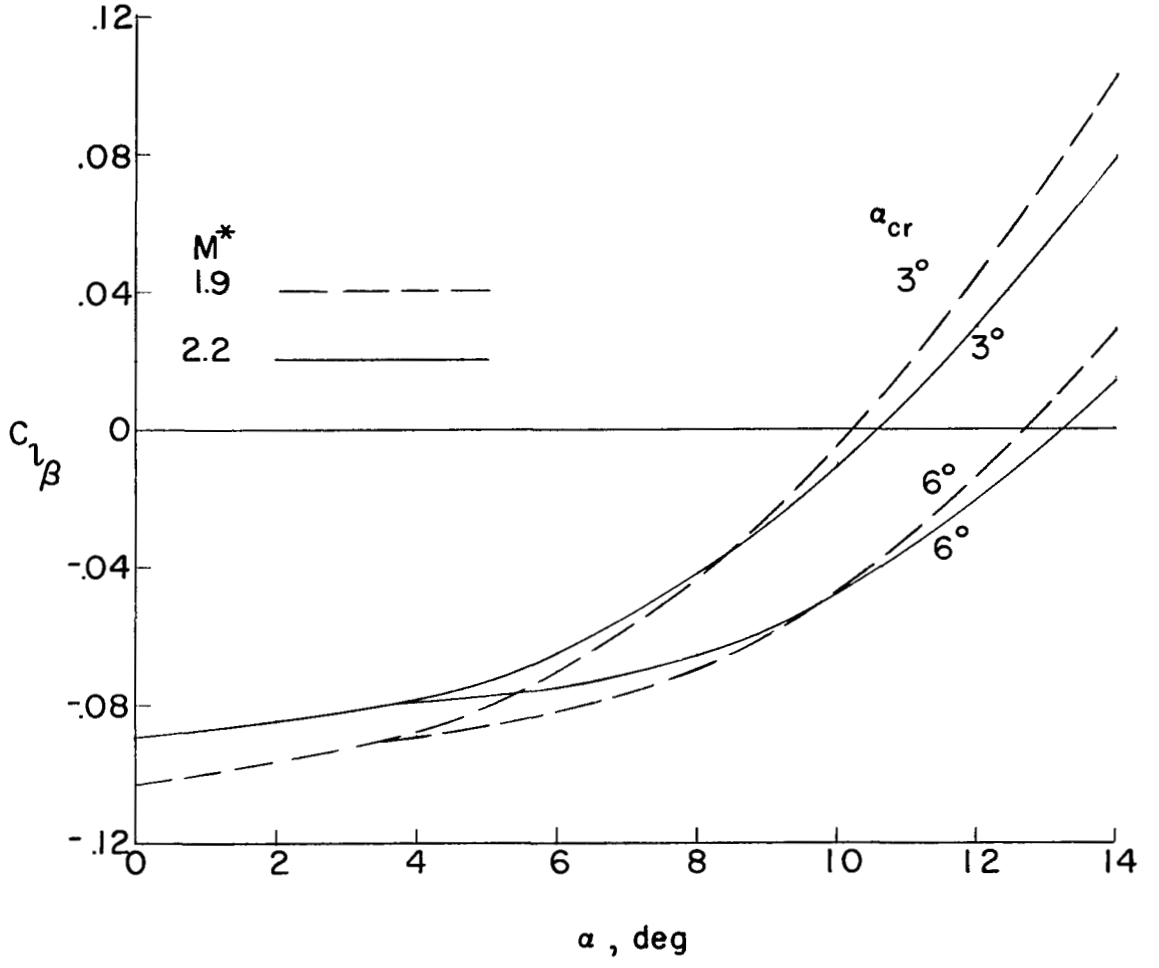

(c) C_{l_β}.

Figure 9.- Continued.

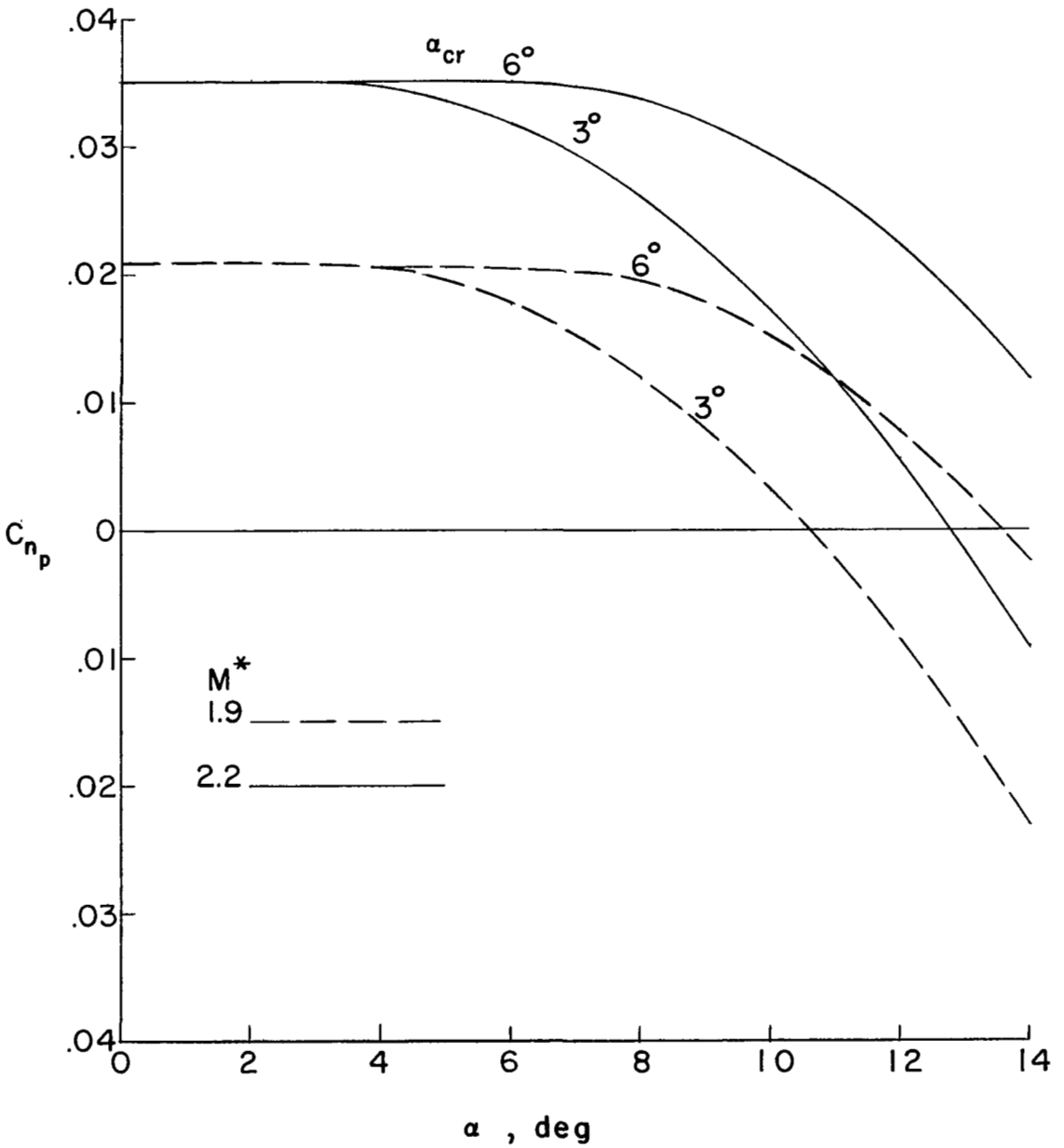

(d) C_{n_p}.

Figure 9.- Continued.

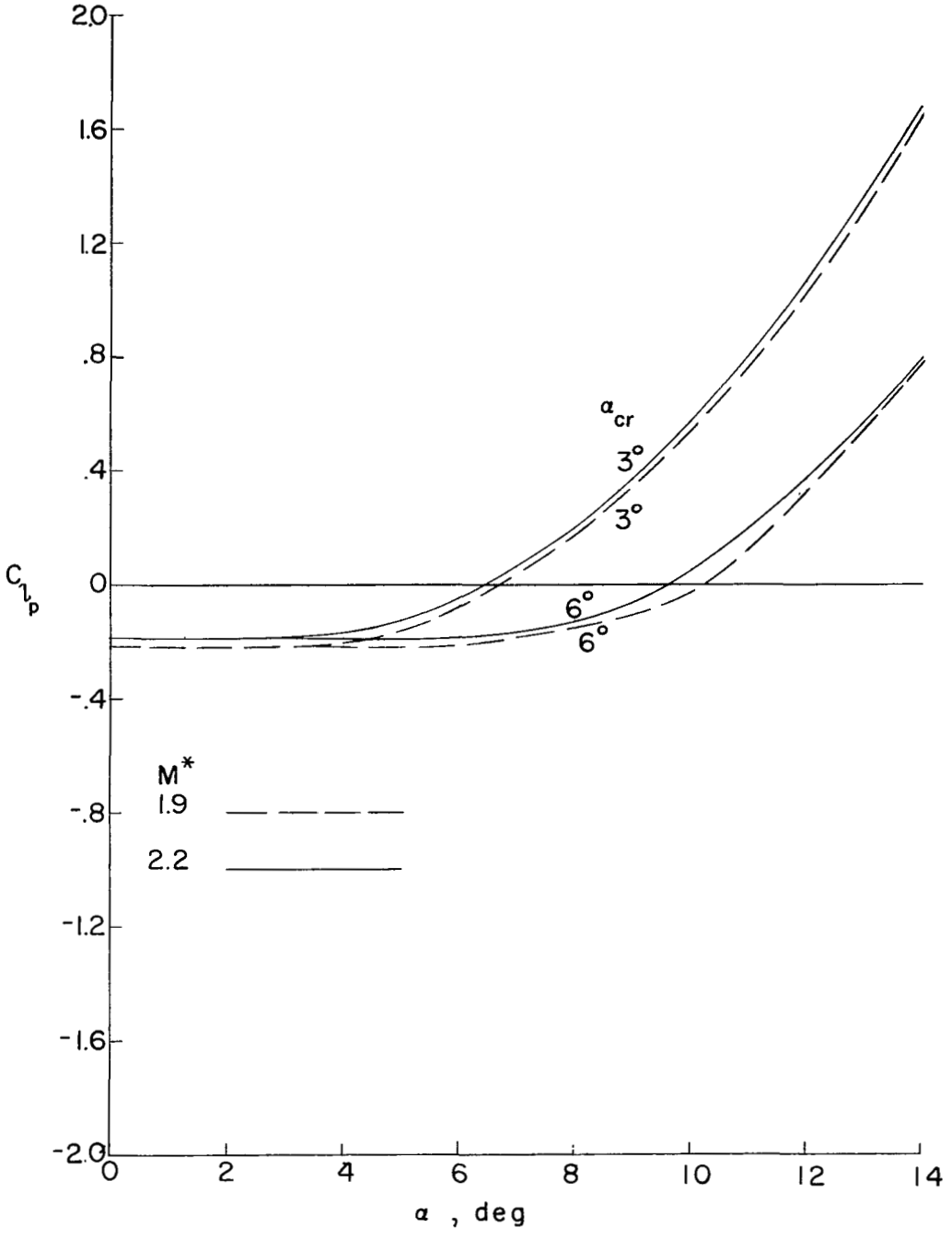

(e) C_{l_p} - destabilizing.

Figure 9.- Continued.

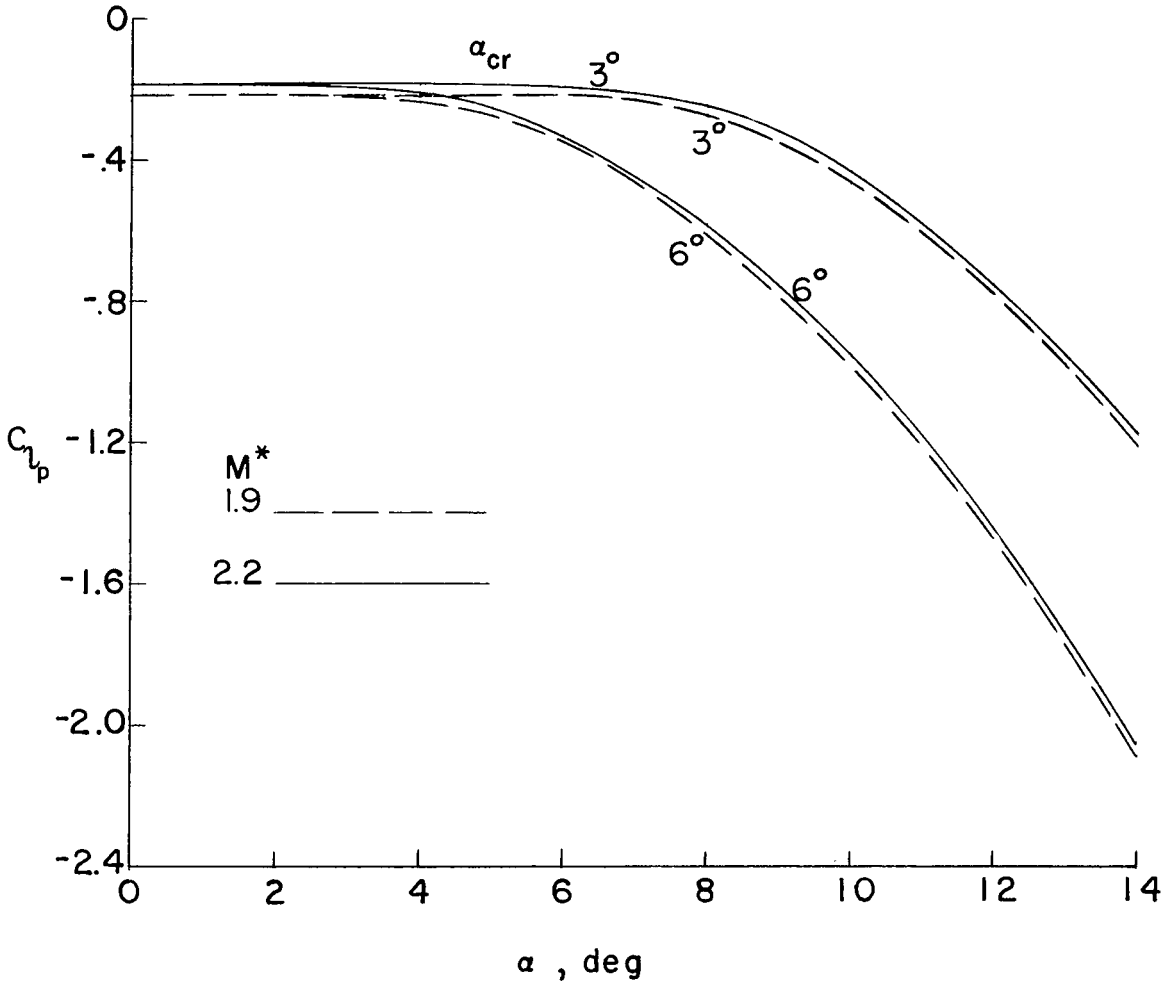

(f) C_{l_p} - stabilizing.

Figure 9.- Concluded.

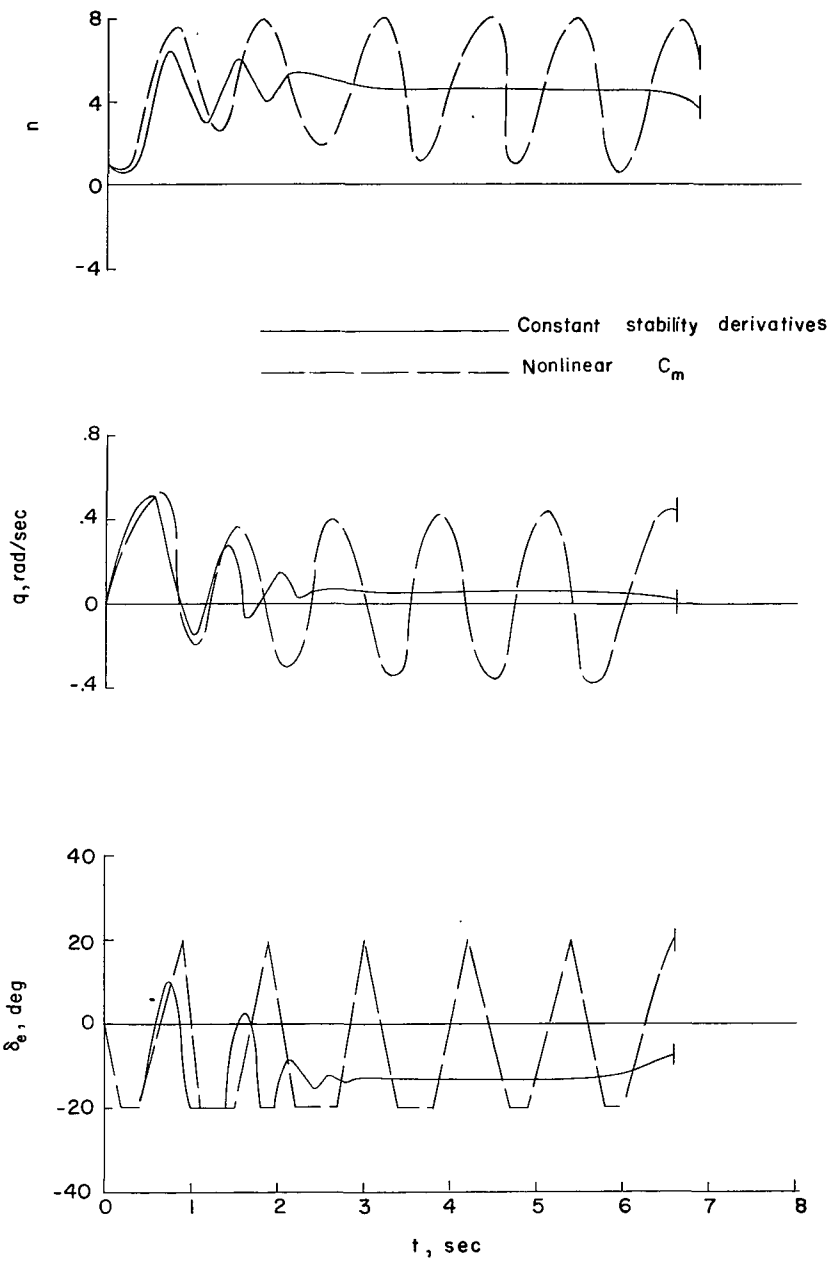

(a) $\delta_{c_e} = 20^\circ$; $\alpha_{cr} = 6^\circ$.

Figure 10.- Effect of nonlinear C_m on the interceptor longitudinal response. Interceptor represented by complete equations, stability derivatives vary with Mach number. Initial condition III; high-gain flight-path control system; basic configuration 4.

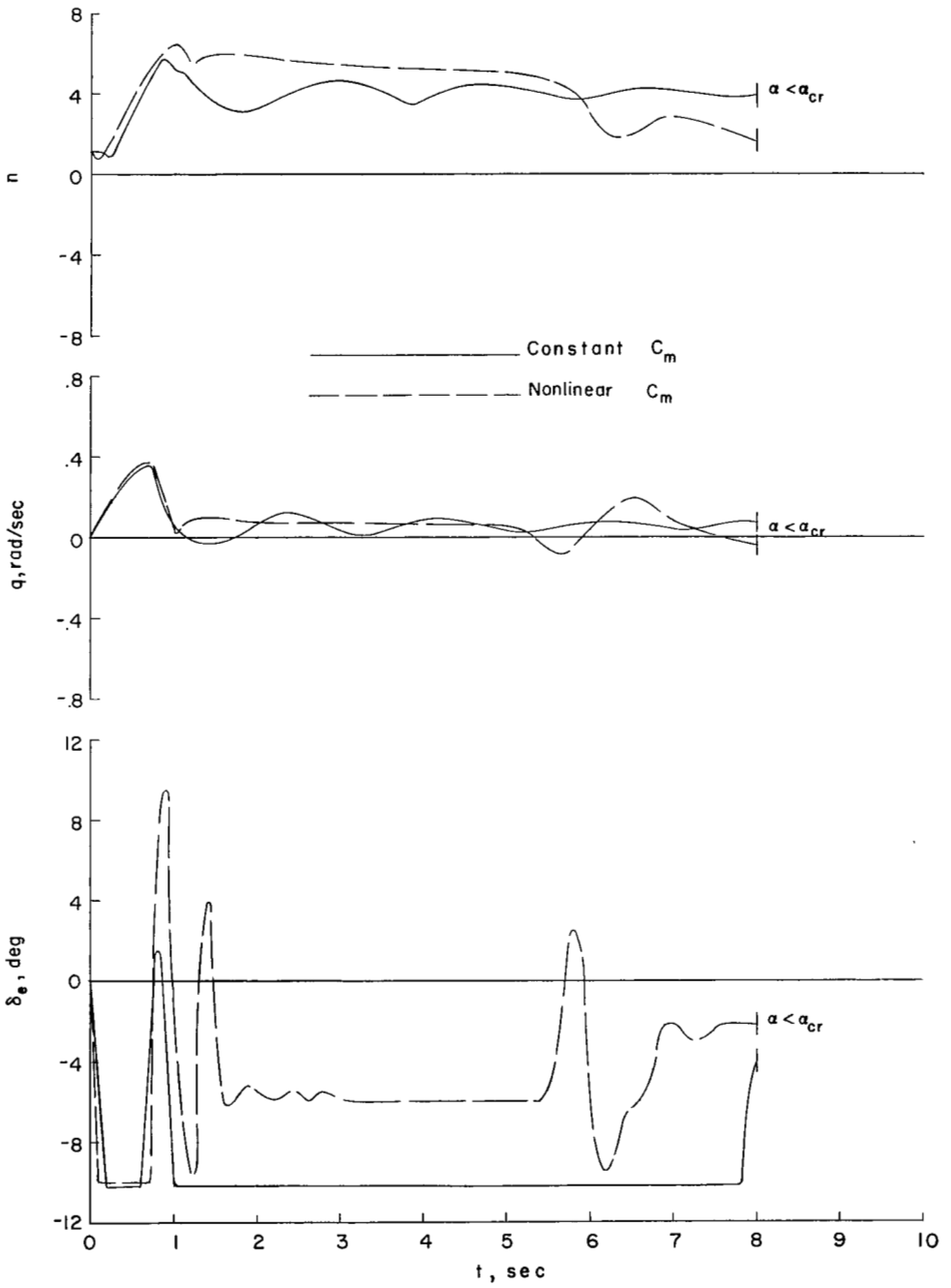

(b) $\delta_{e_l} = 10^\circ$; $\alpha_{cr} = 6^\circ$.

Figure 10.- Concluded.

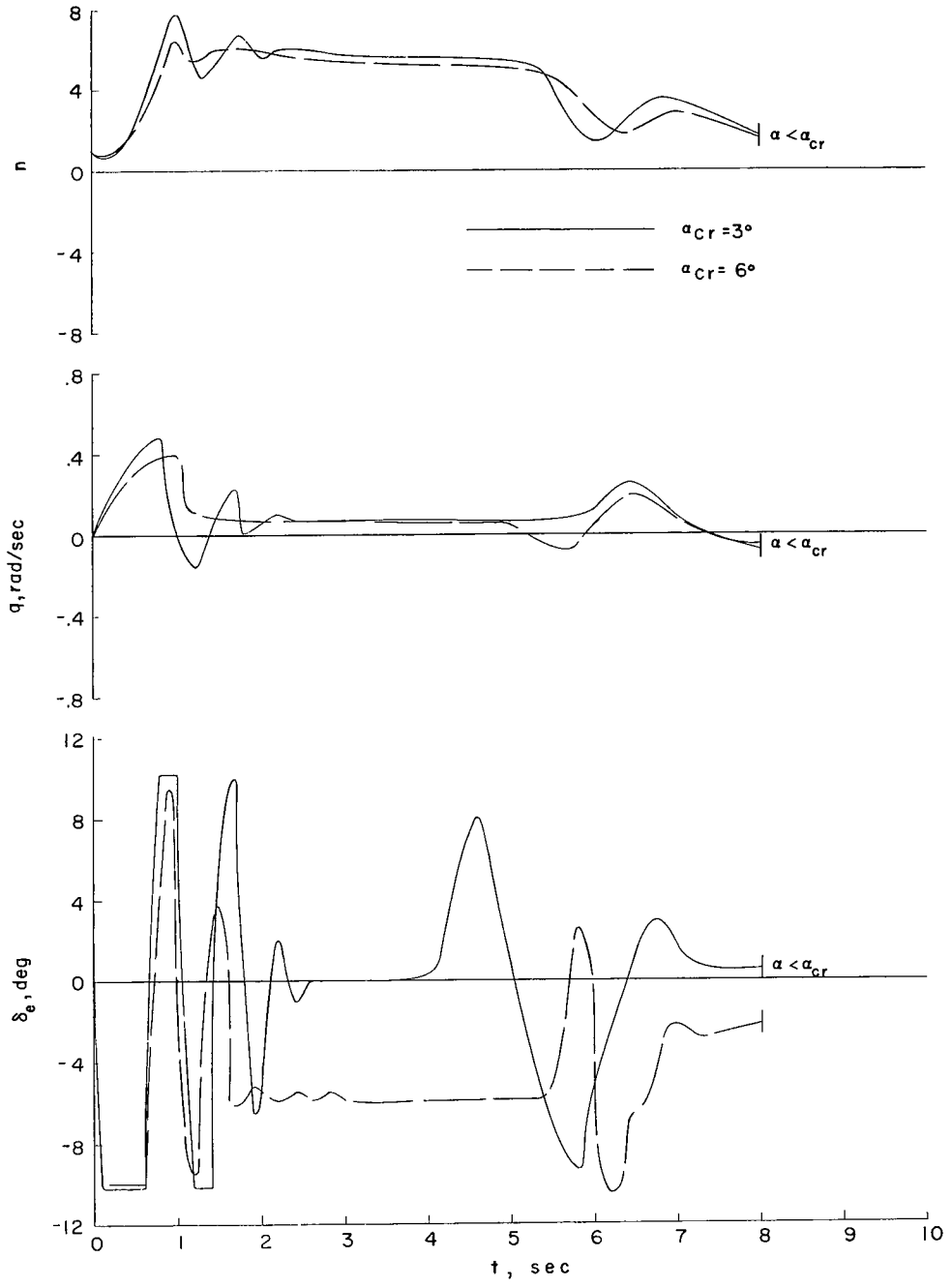

Figure 11.- Effect of changing α_{cr} on the longitudinal airplane response. Initial condition III; basic configuration 4; high-gain longitudinal control system; $\delta_{e_l} = 10^{\circ}$; nonlinear C_m.

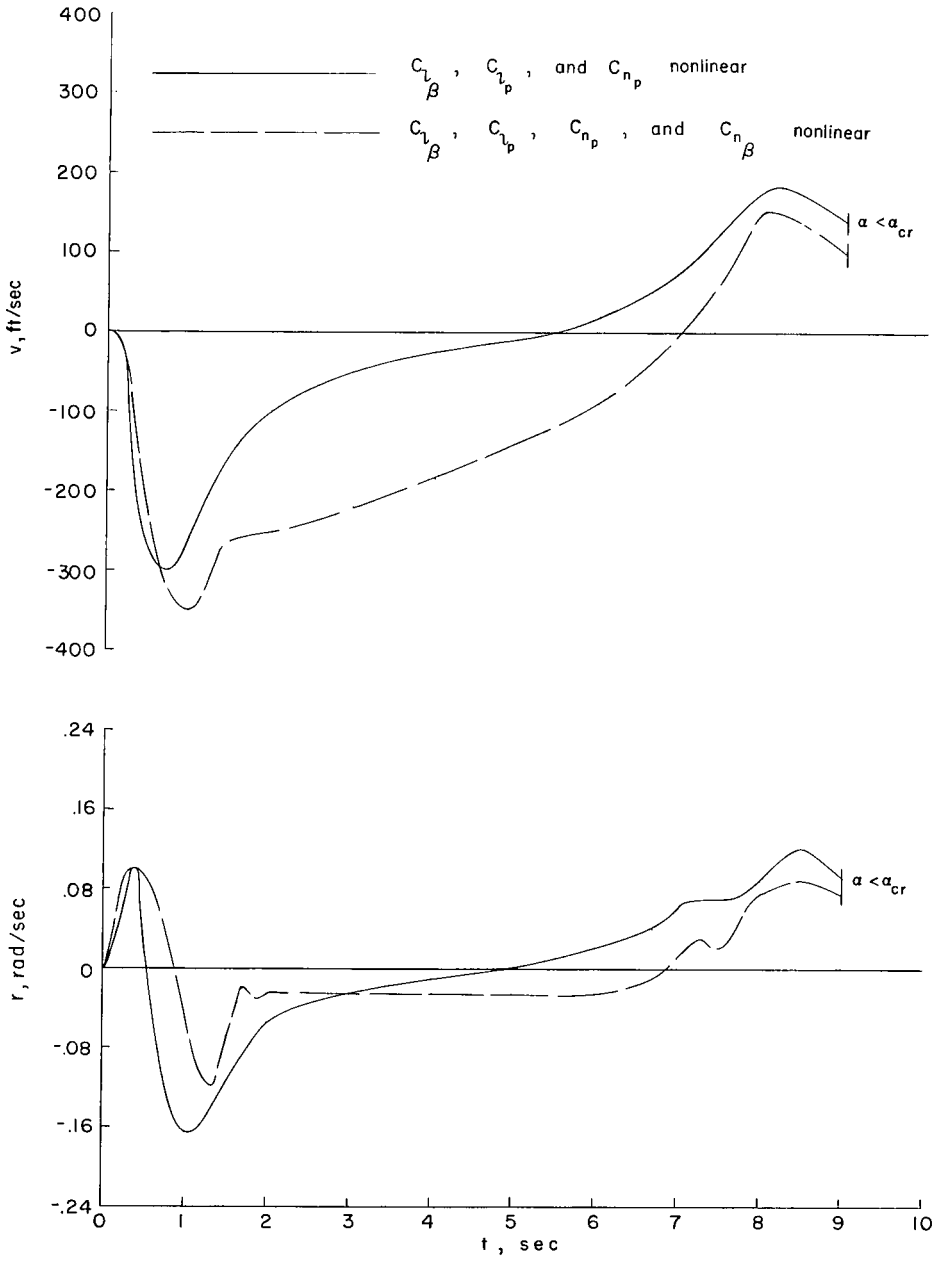

(a) The effect of nonlinear C_{n_β} on the sideslip and yawing velocities.

Figure 12.- The effect of angle-of-attack nonlinearities in the lateral stability derivatives on the airplane response. Initial condition III, basic configuration 4.

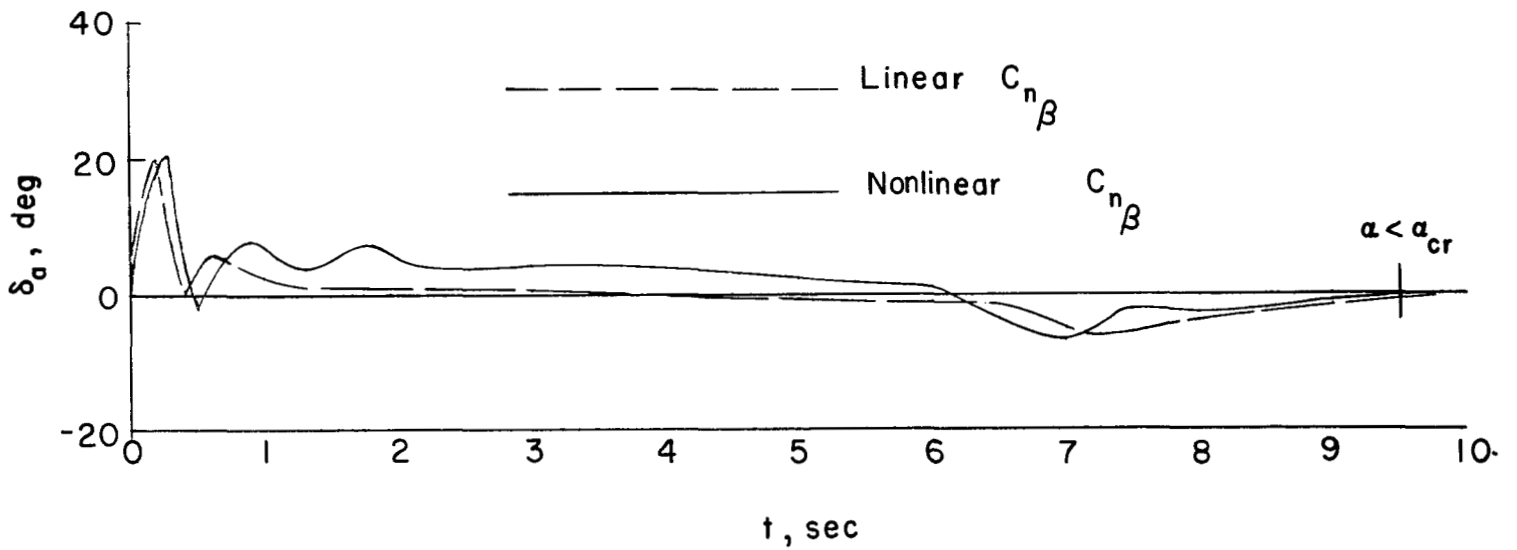

(b) Effect of nonlinear C_{n_β} on the aileron response.

Figure 12.- Continued.

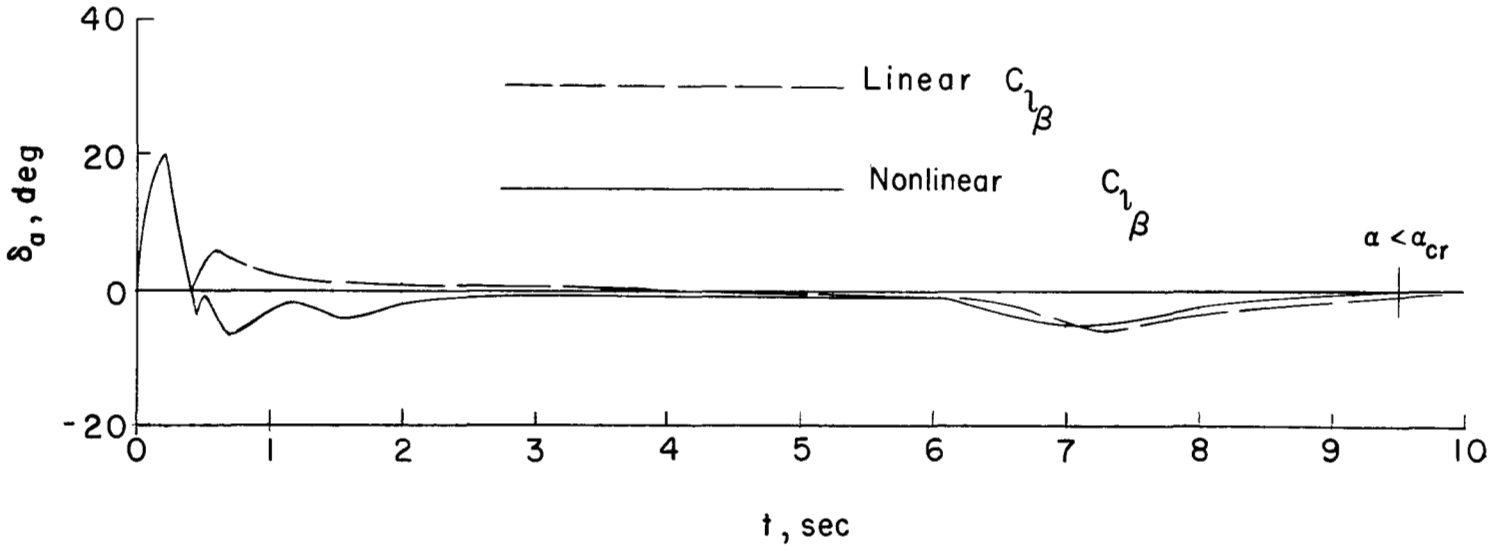

(c) Effect of nonlinear C_{l_β} on the aileron response.

Figure 12.- Continued.

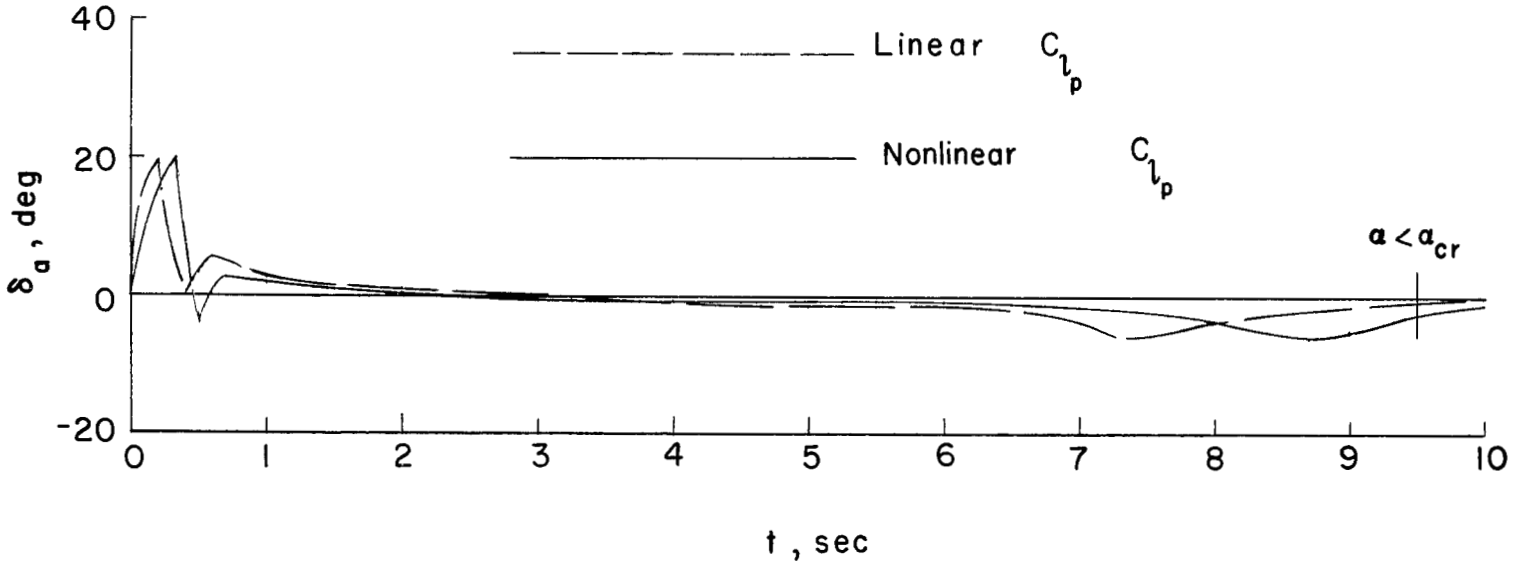

(d) Effect of nonlinear C_{l_p}, destabilizing, on the aileron response.

Figure 12.- Concluded.

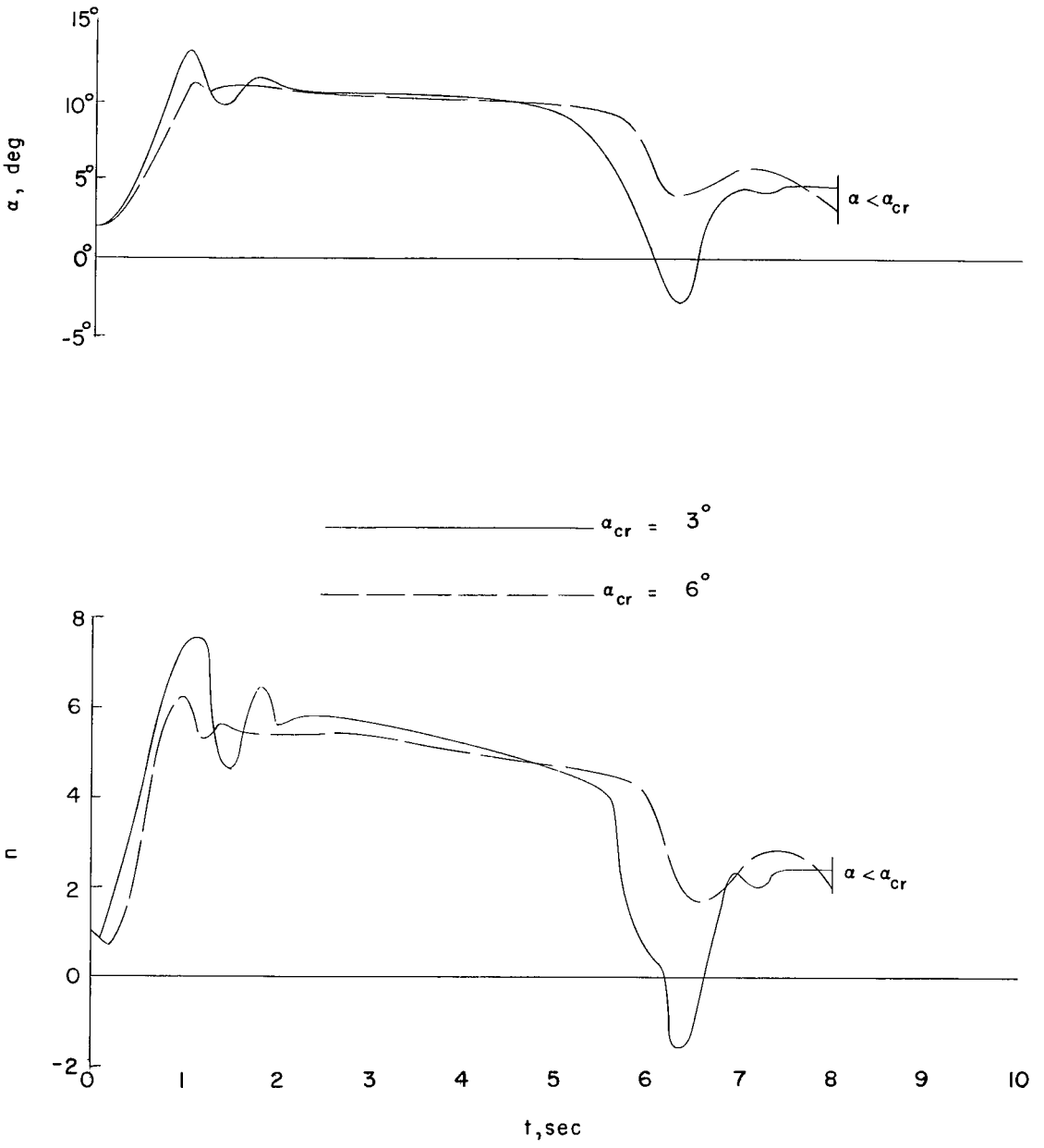

(a) Normal acceleration and angle of attack.

Figure 13.- Effect of all nonlinear stability derivatives at different values of α_{cr} on the interceptor response. Interceptor represented by complete equations and Mach number variation included in stability derivatives. Initial condition III, basic configuration 4.

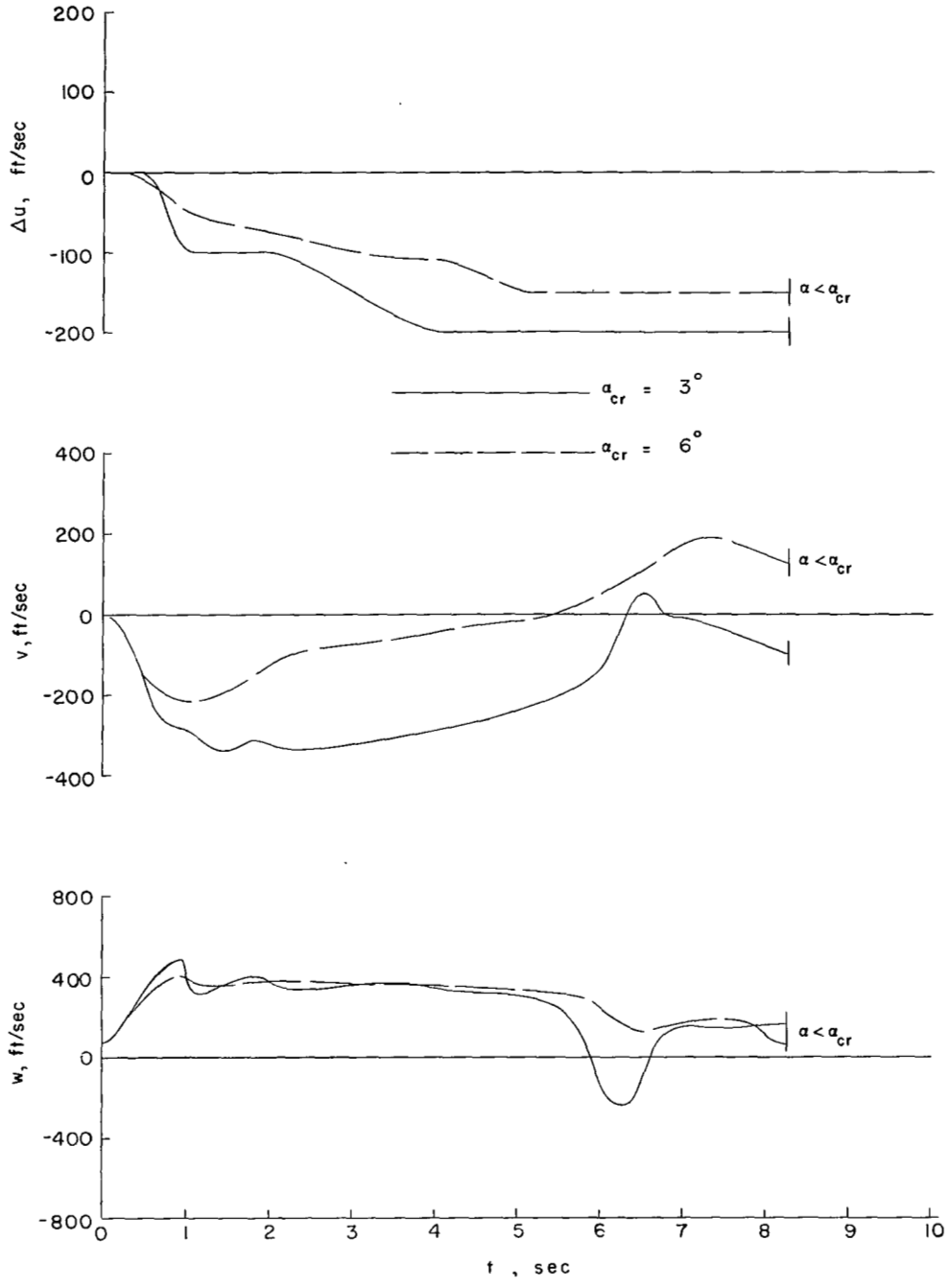

(b) Linear velocities.

Figure 13.- Continued.

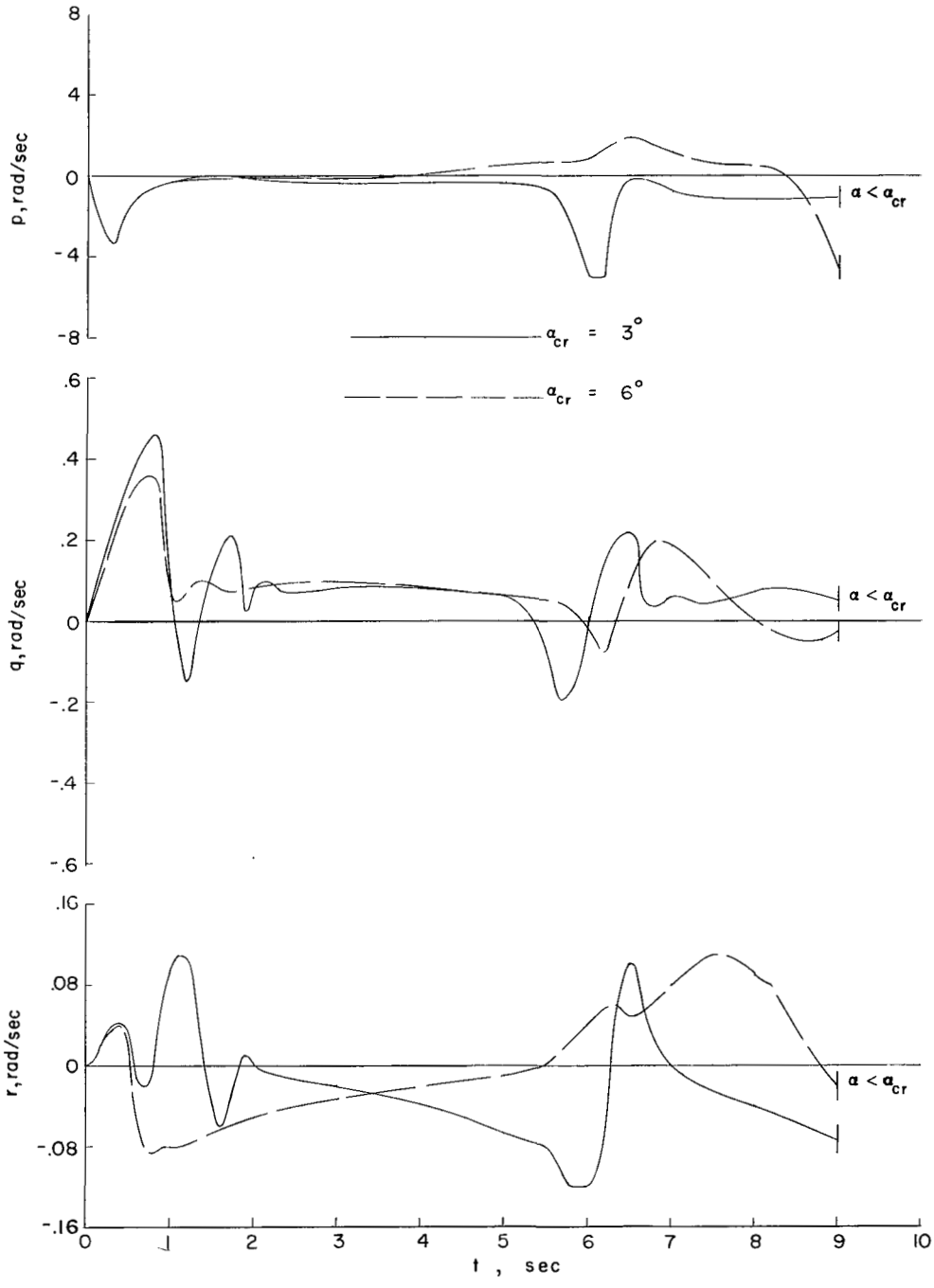

(c) Angular velocities.

Figure 13.- Continued.

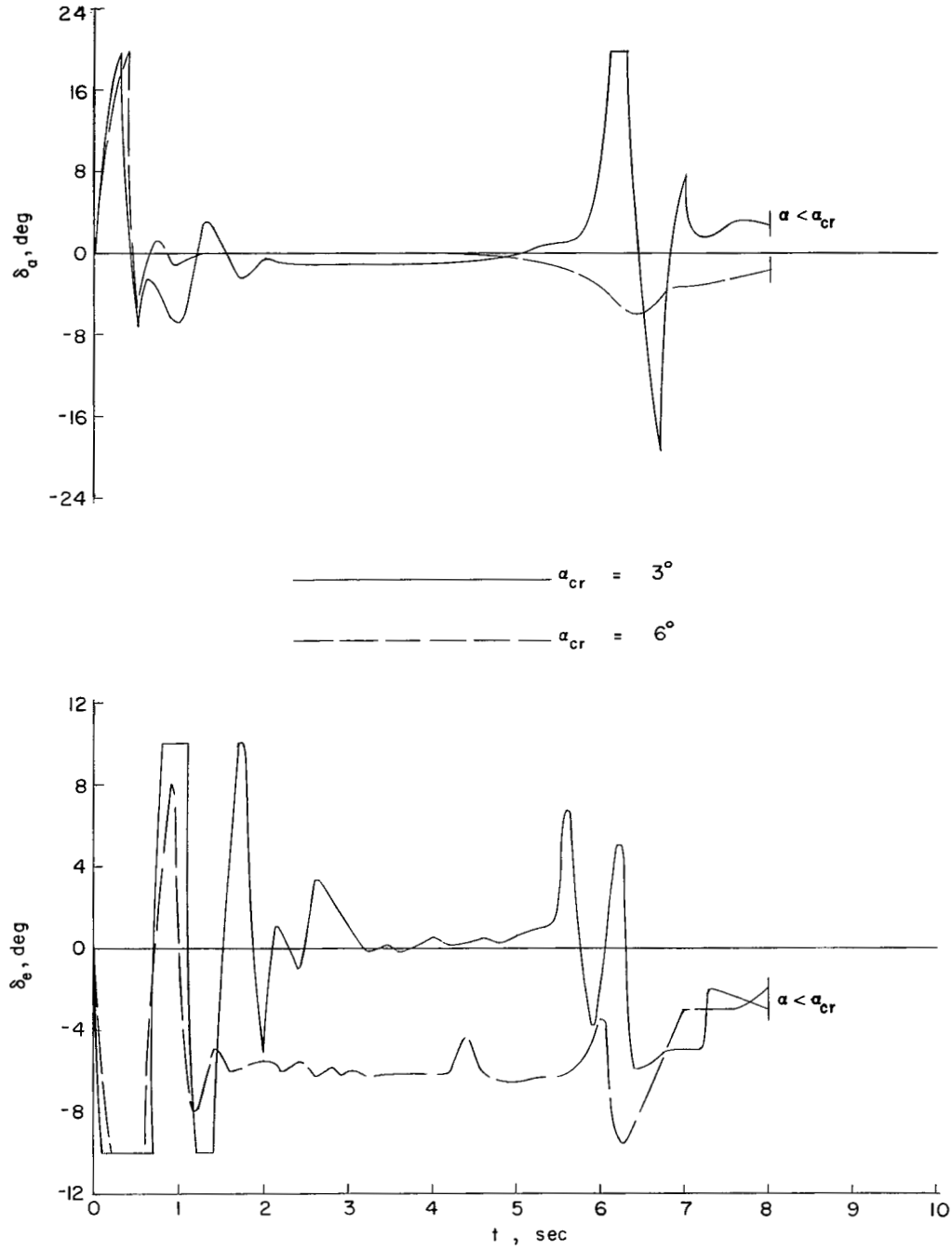

(d) Aileron and elevator motions.

Figure 13.- Concluded.

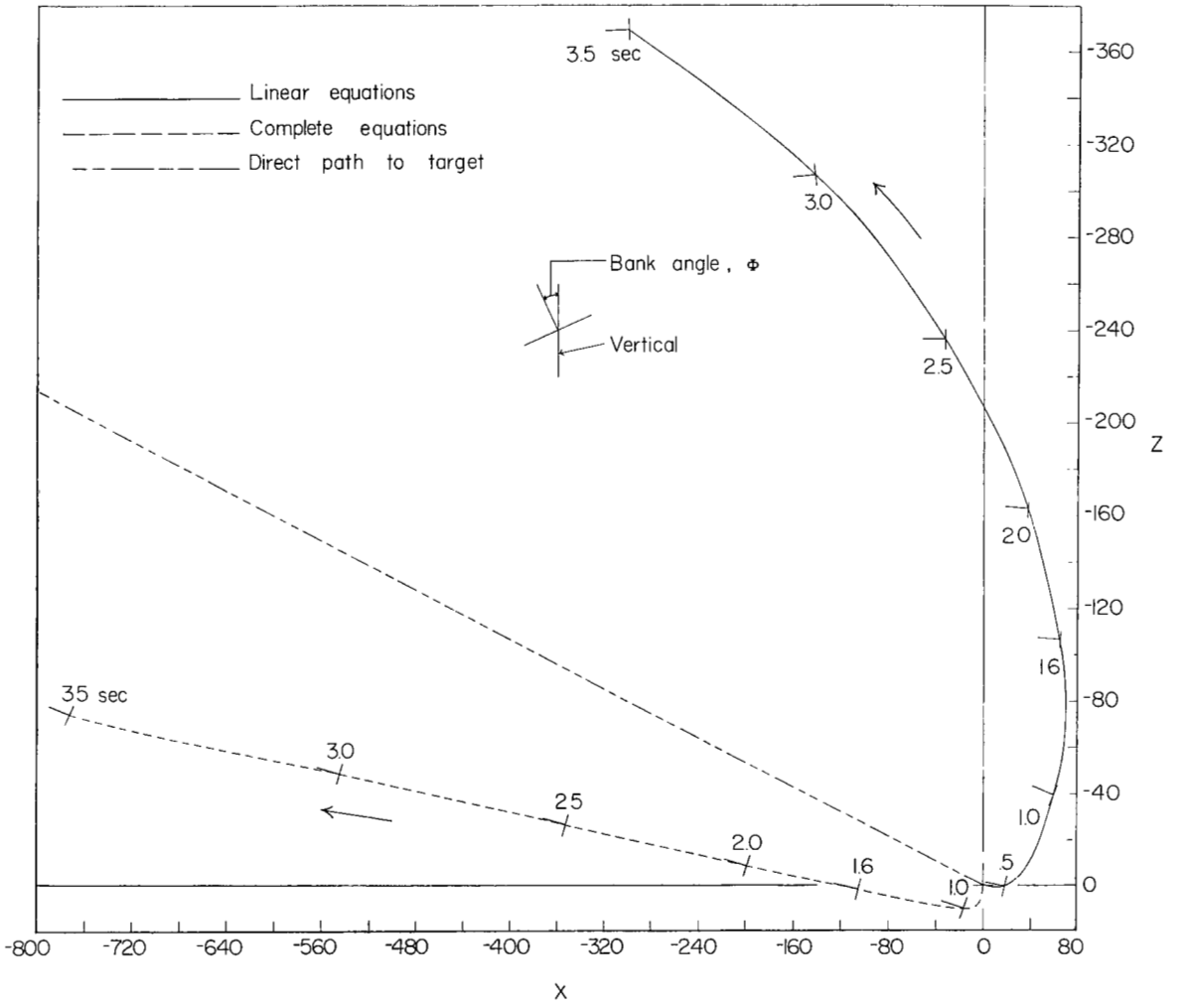

Figure 14.- Comparison of the path of the center of gravity of the interceptor in space for the complete and linear equations with the direct path in space to the target. Initial condition I; basic configurations 1 and 6.

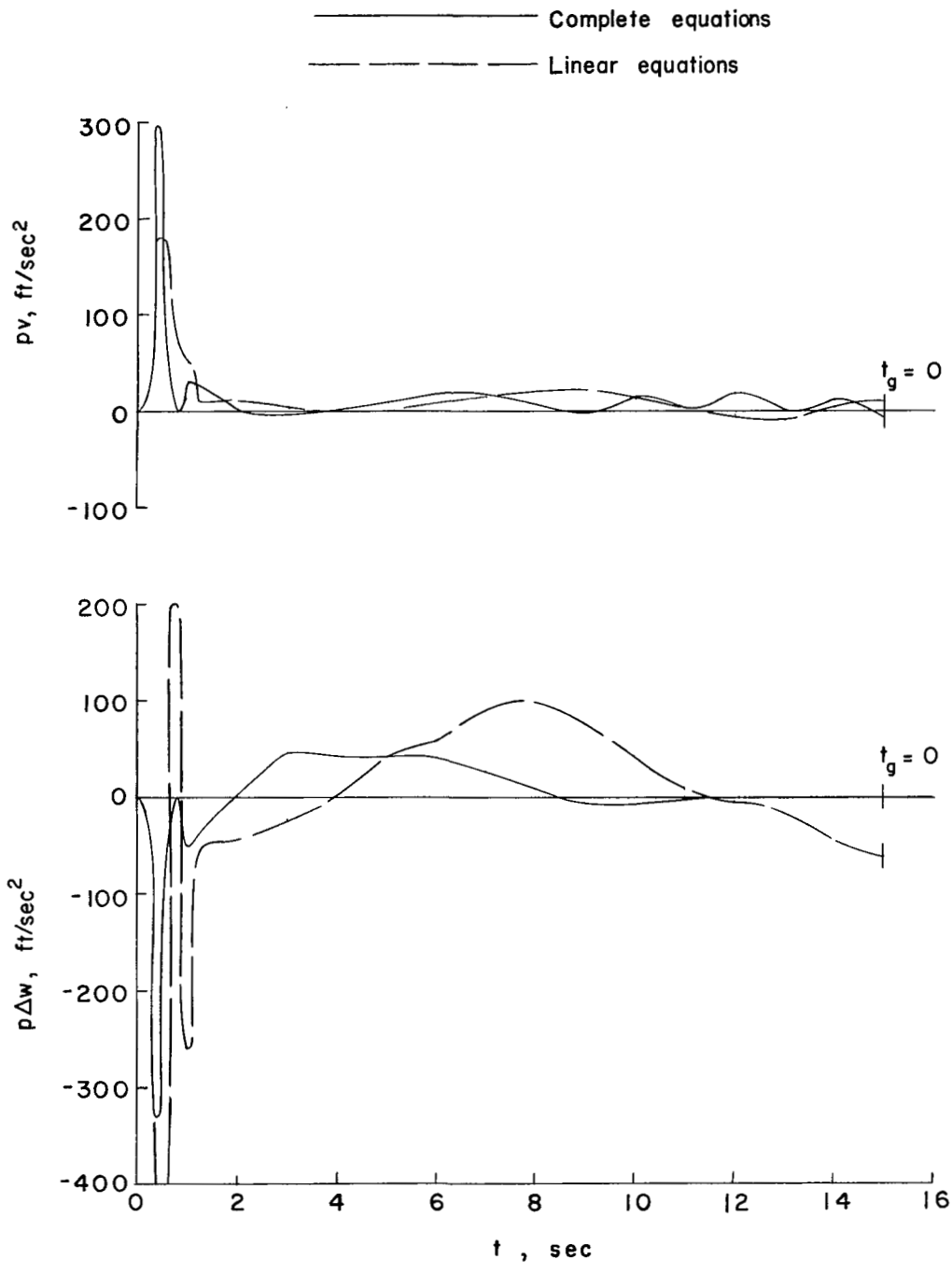

Figure 15.- Time histories of the important cross-product terms of the complete and linear equations of motion. Initial condition I with constant aerodynamics; basic configurations 1 and 6.

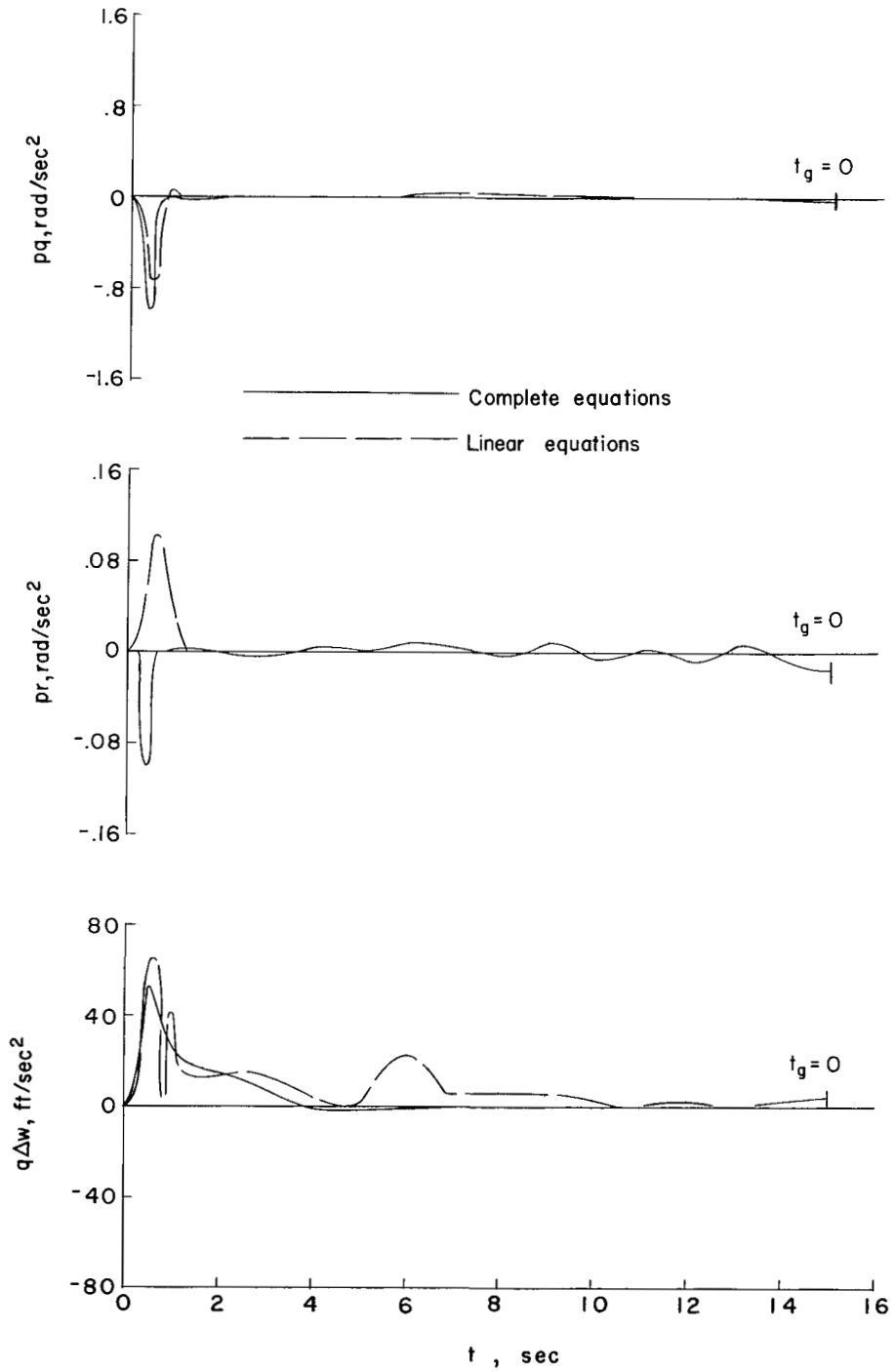

Figure 15.- Concluded.

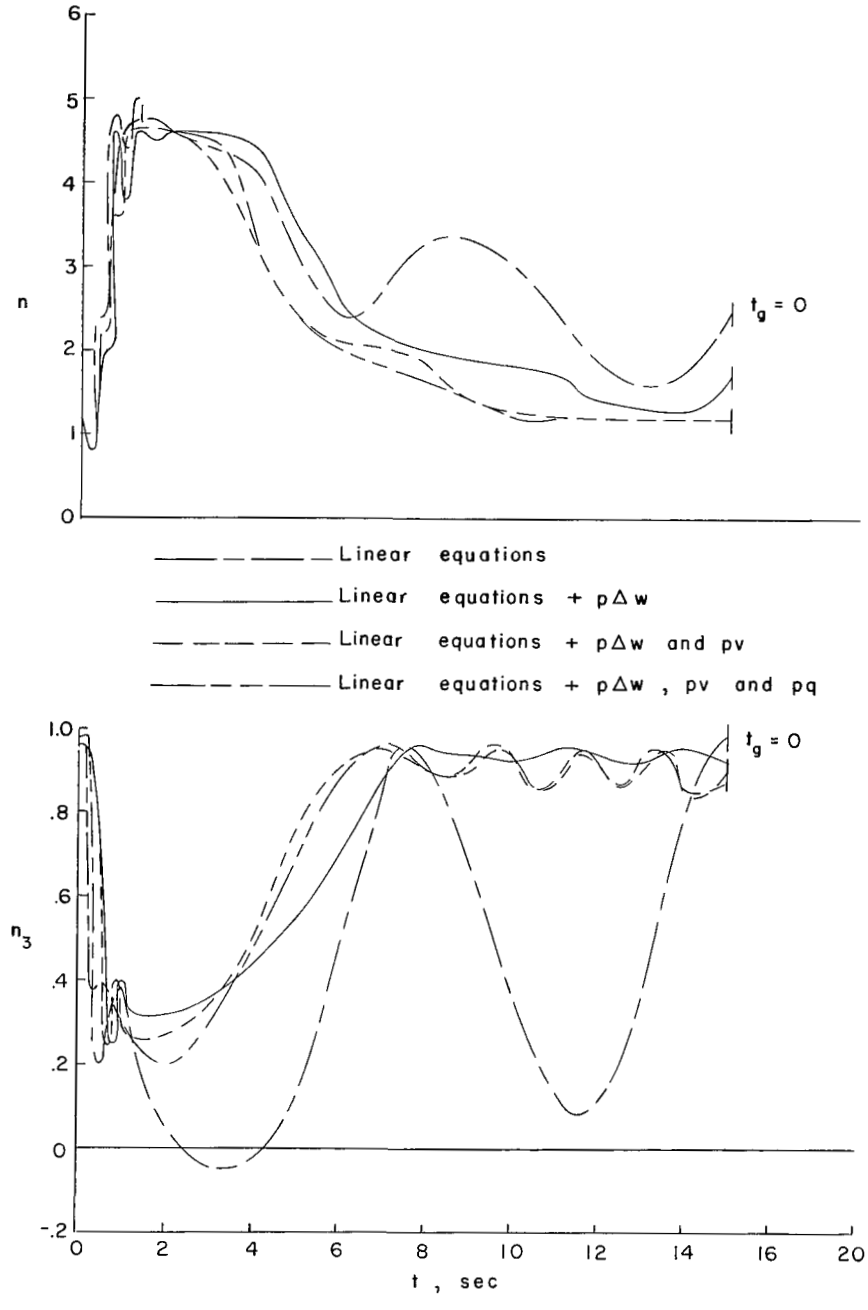

(a) Normal acceleration and the direction cosine n_3.

Figure 16.- Effect of the cross-product terms p Δw, pv, and pq on the interceptor response. Initial condition I, constant aerodynamics; basic configurations 1 and 6.

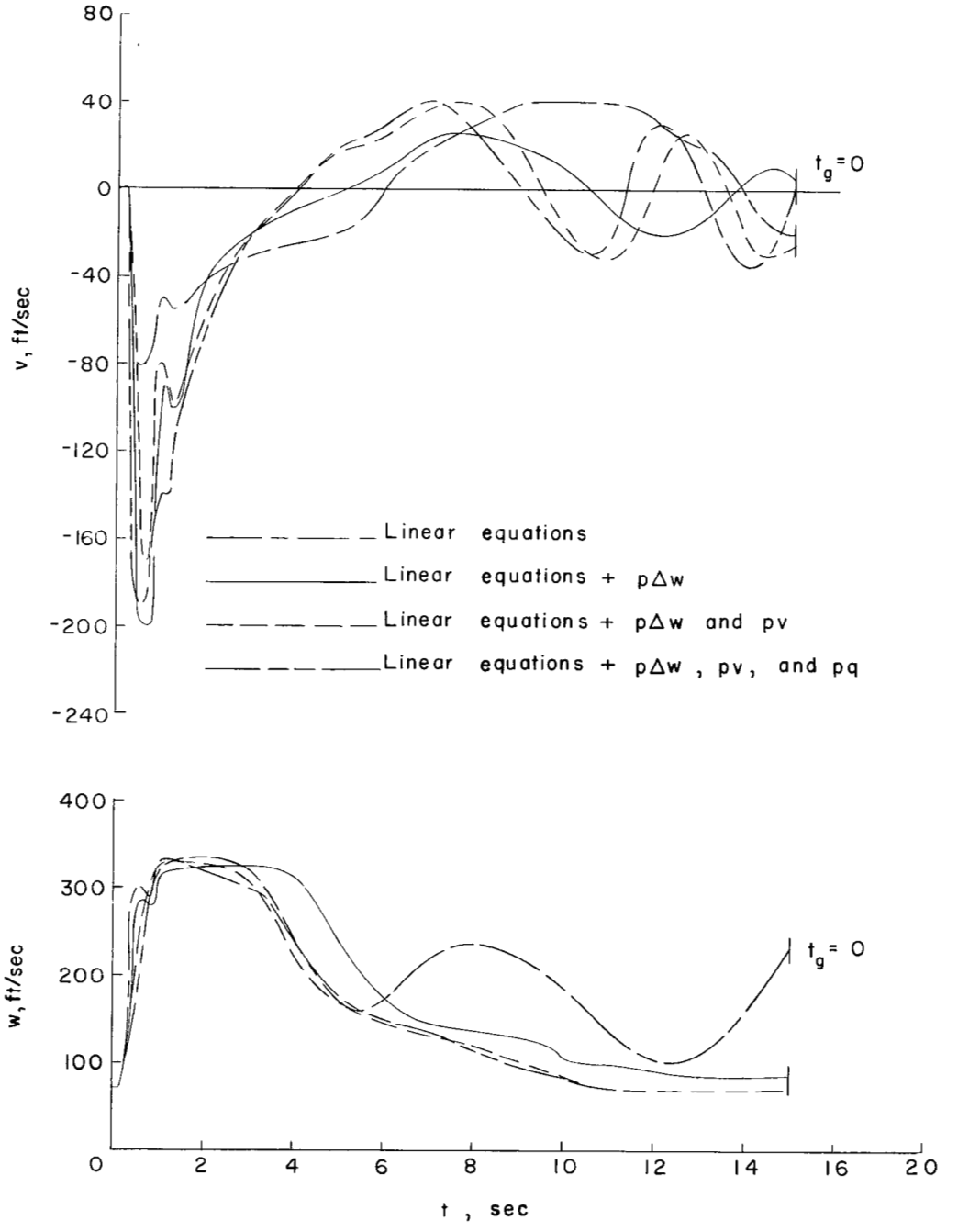

(b) Velocities v and w.

Figure 16.- Continued.

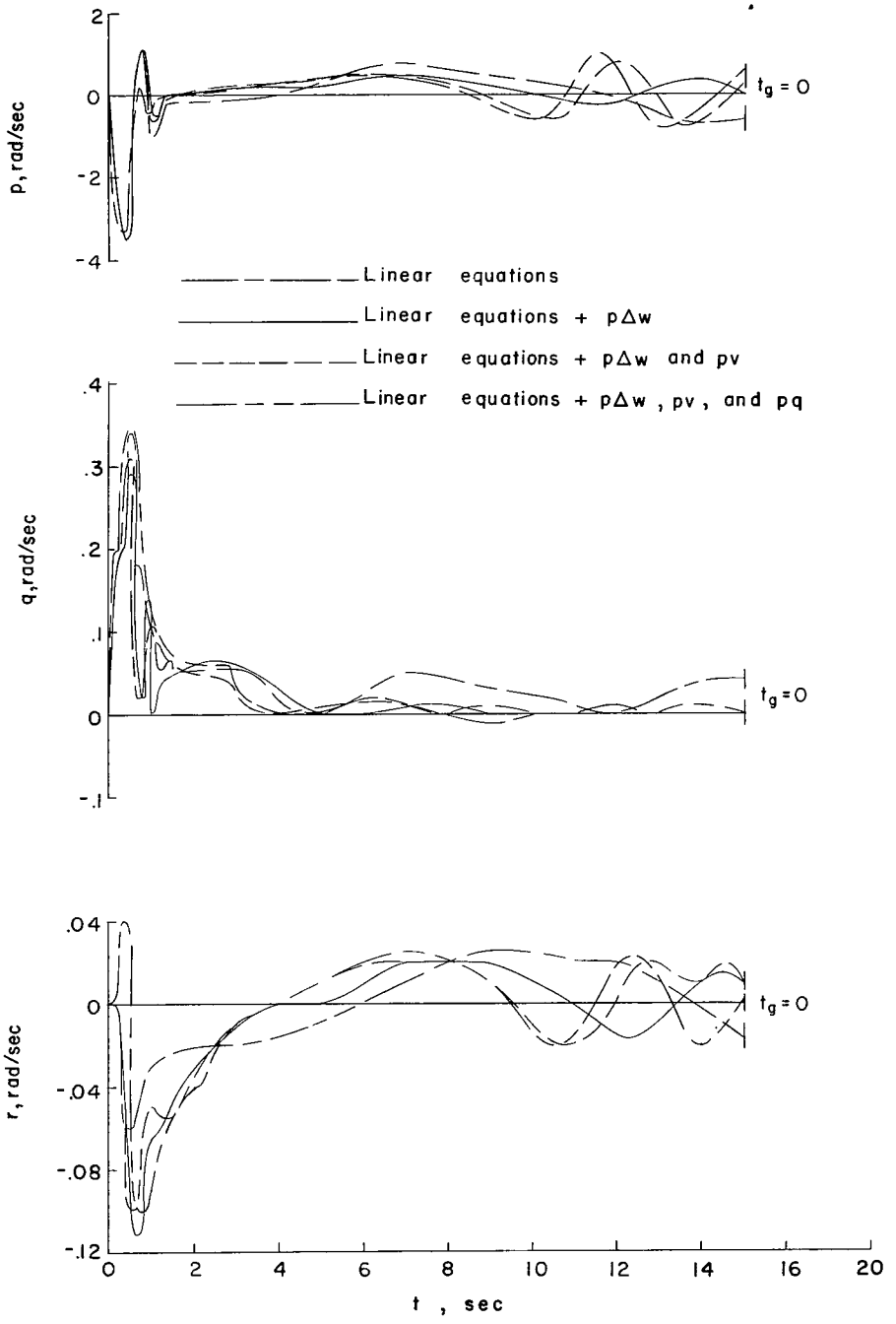

(c) Angular velocities.

Figure 16.- Concluded.

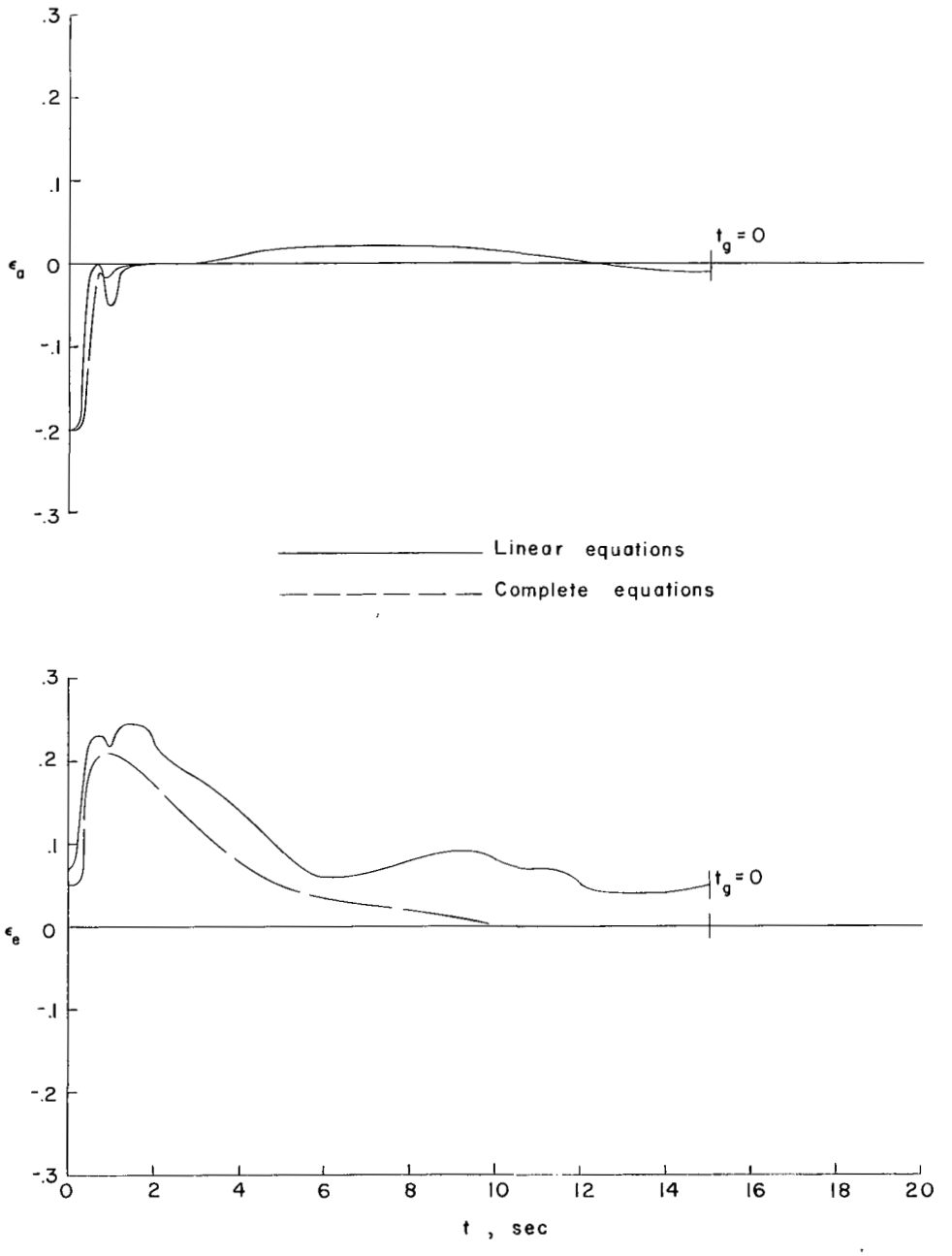

(a) Steering errors.

Figure 17.- Comparison of the steering errors, normal acceleration, and direction cosine n_3 for the complete and linear equations of motion. Initial condition I with constant aerodynamics, basic configurations 1 and 6.

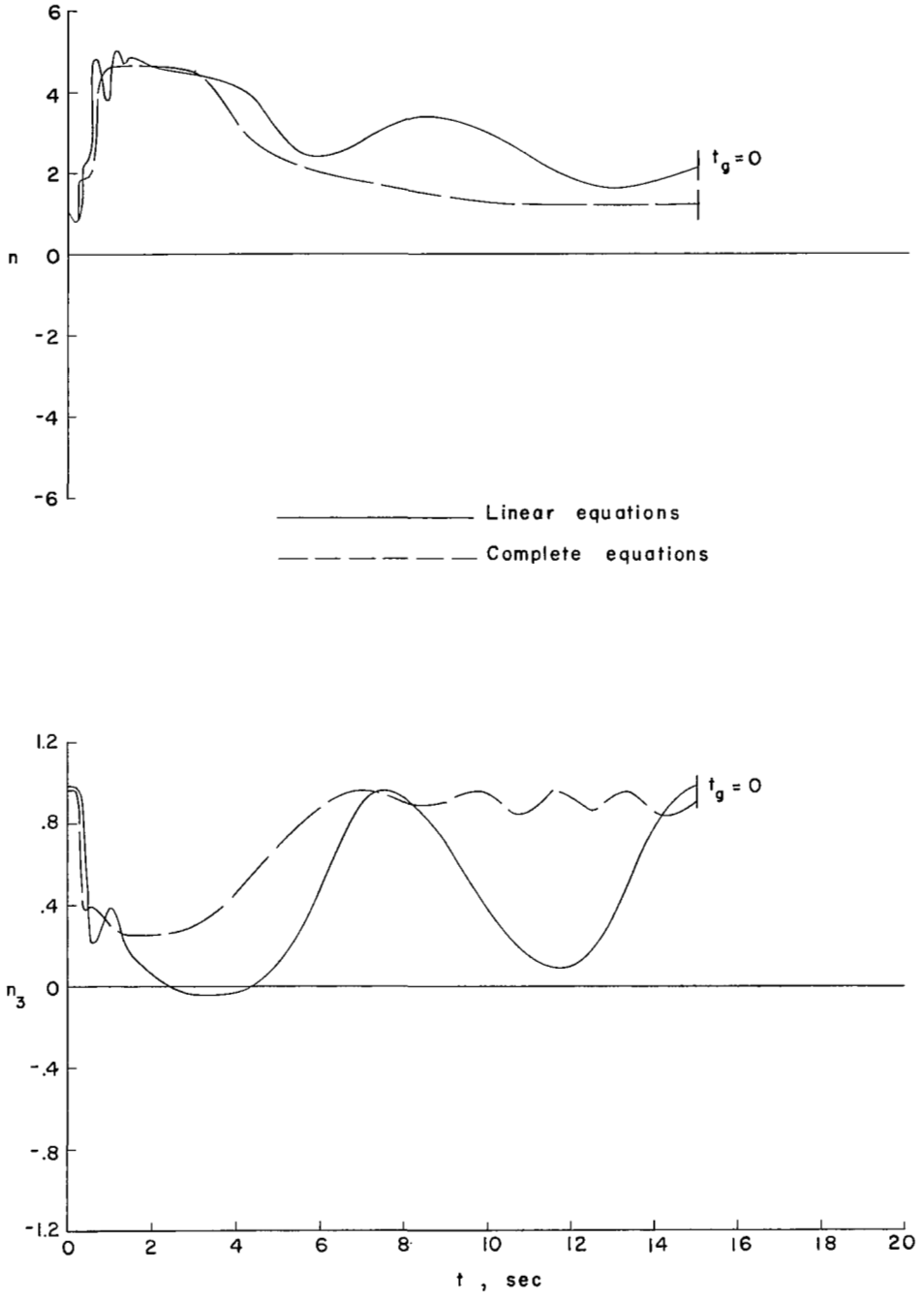

(b) Normal acceleration and direction cosine n_3.

Figure 17.- Concluded.

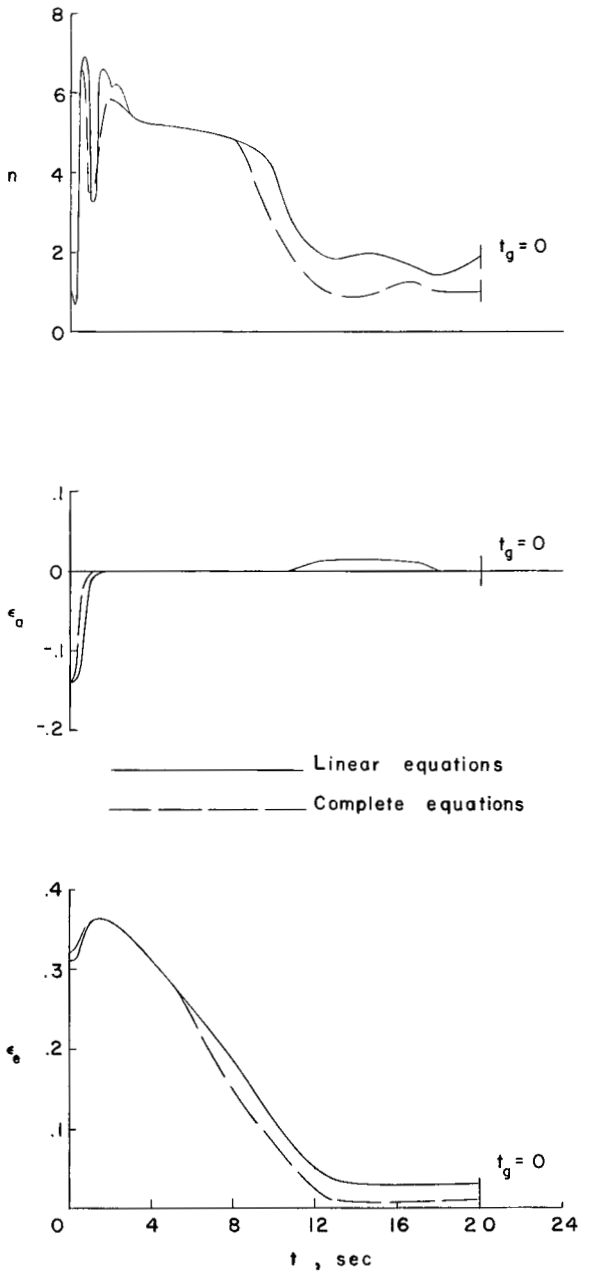

(a) Normal acceleration and steering errors.

Figure 18.- Comparison of the interceptor response for the complete and linear equations of motion. Low rolling velocity case; initial condition IV; constant aerodynamics; basic configurations 1 and 6.

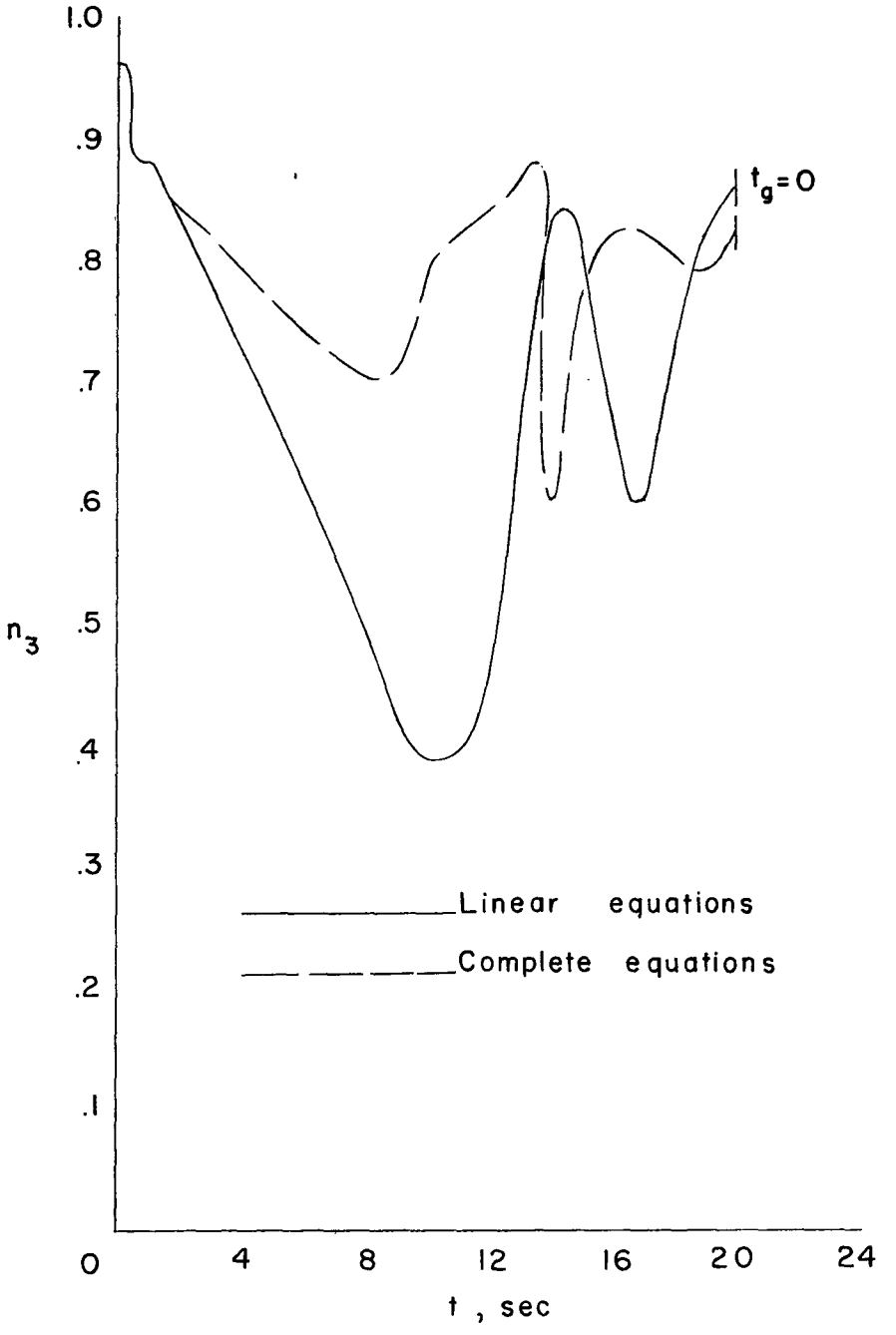

(b) Direction cosine n_3.

Figure 18.- Continued.

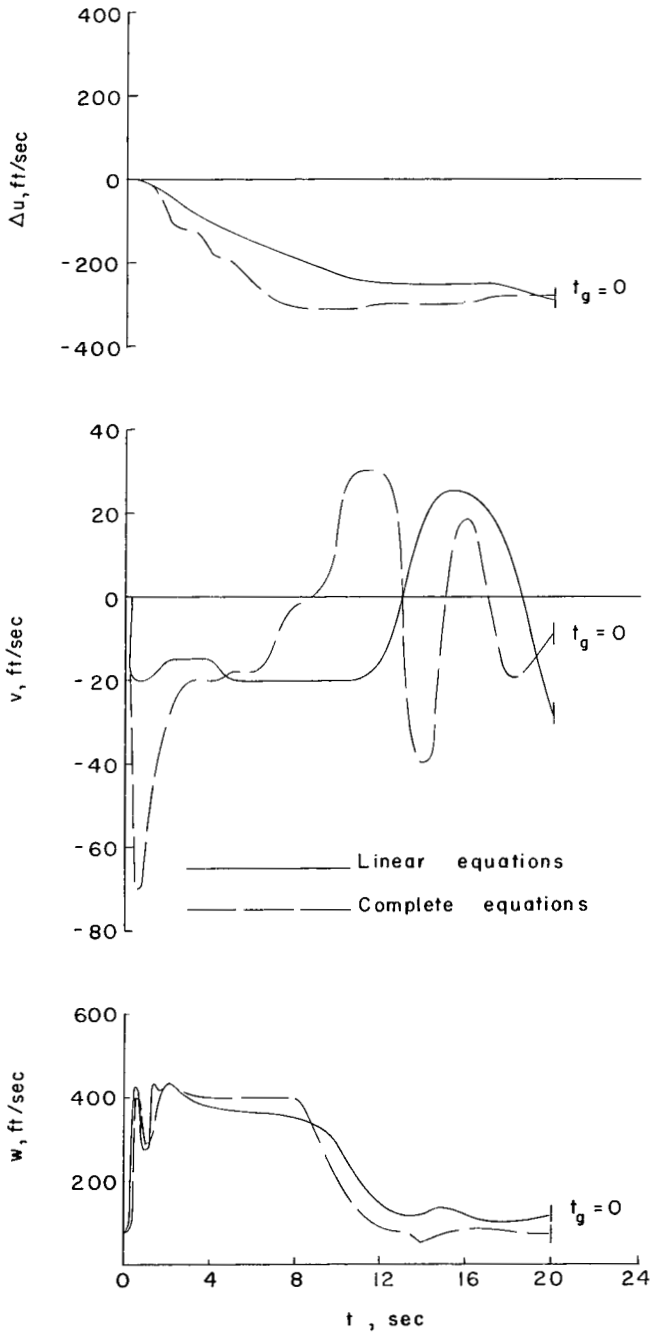

(c) Linear velocities.

Figure 18.- Continued.

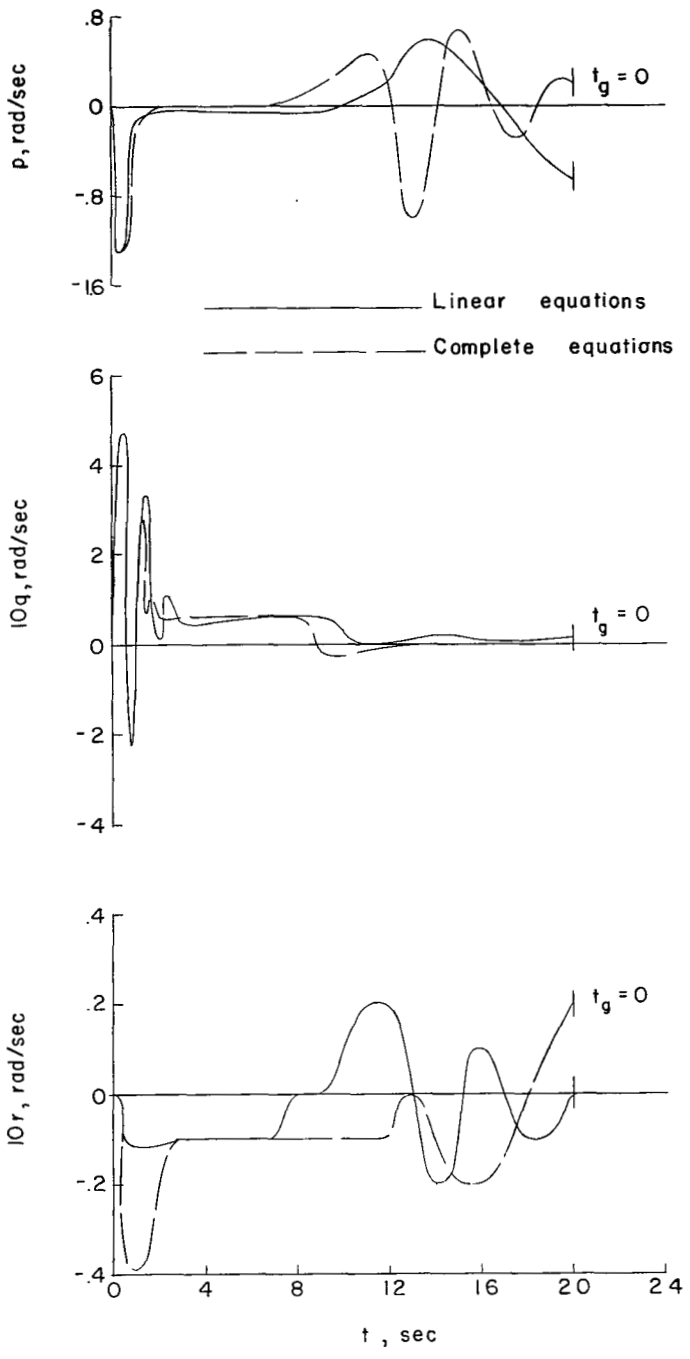

(d) Angular velocities.

Figure 18.- Concluded.

[redacted]

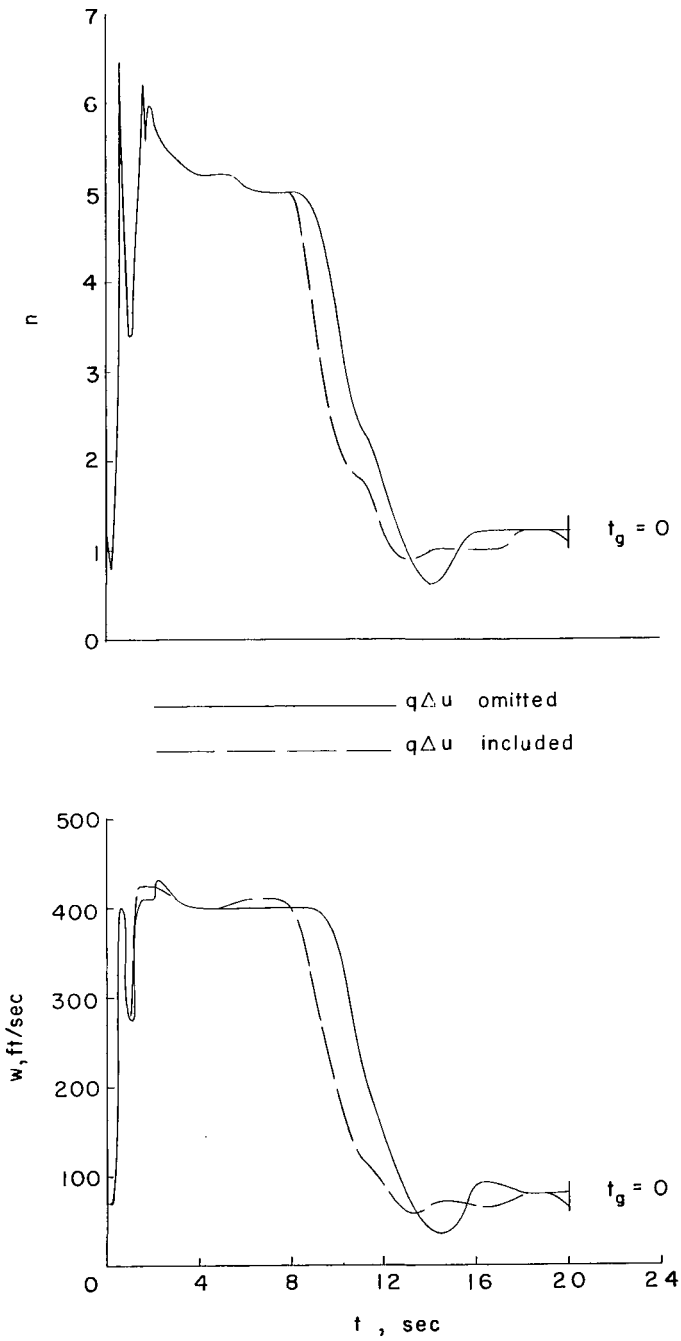

Figure 19.- Effect of $q\,\Delta u$ on the normal acceleration and w velocity responses of the interceptor. Initial condition IV; constant aerodynamics and $q\,\Delta w$ included; basic configuration 1.

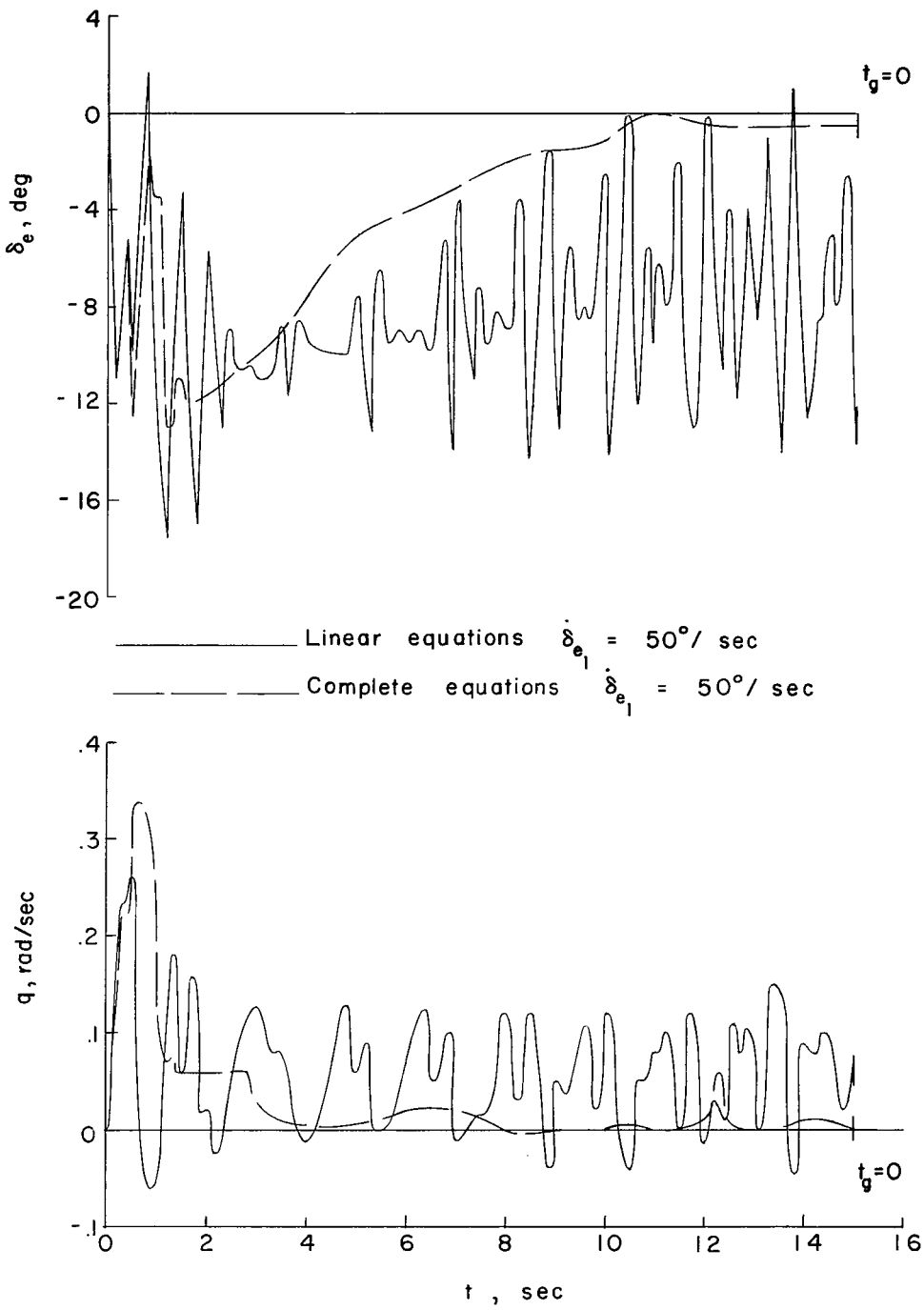

Figure 20.- The effect of the cross-product terms on the longitudinal rate-limiting oscillation. Initial condition I; constant aerodynamics; basic configurations 1 and 6.

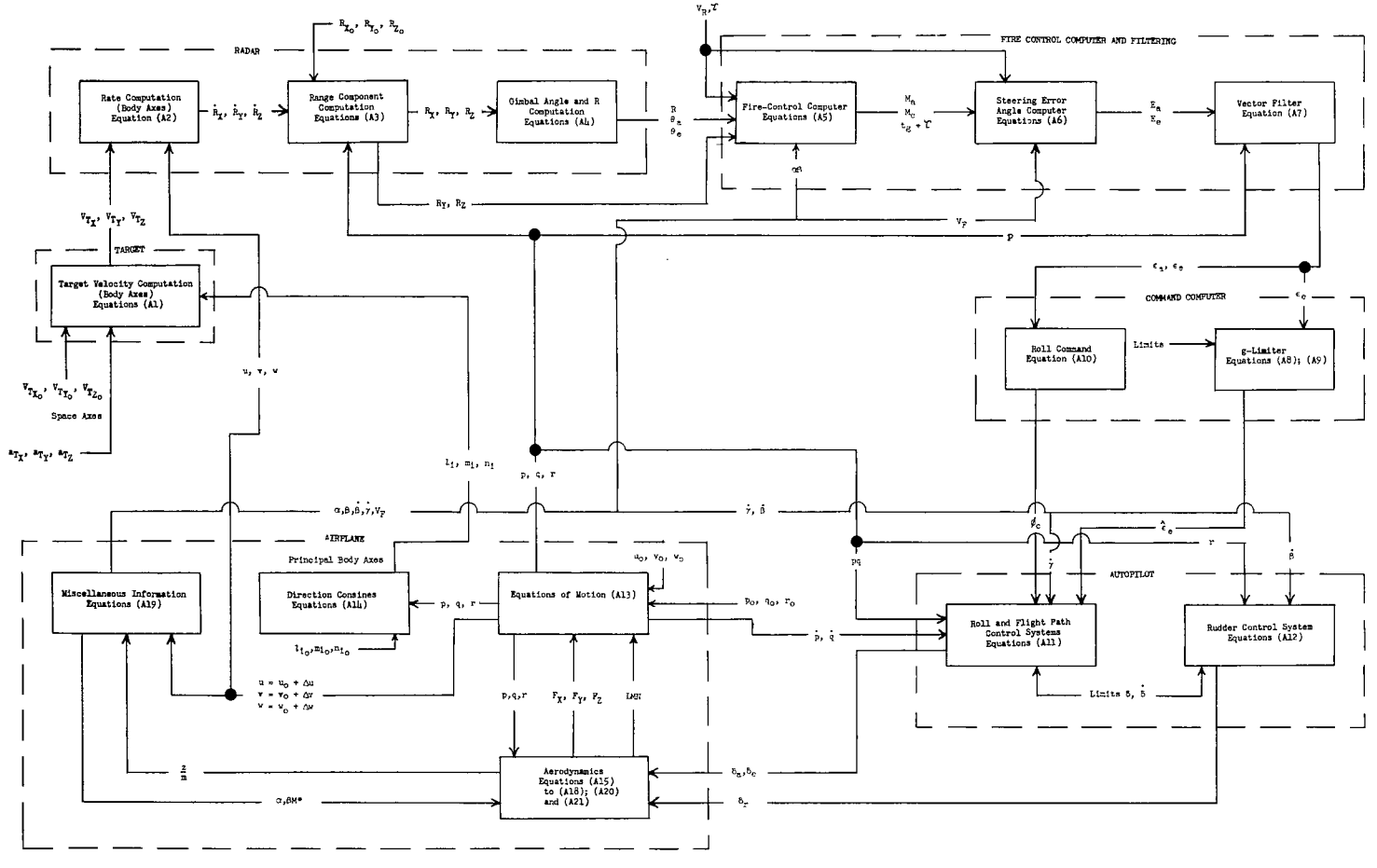

Figure 21.- Detailed block diagram of interceptor system simulated. Numbers in blocks refer to equations in Appendix A.